SURFACE MODIFICATION OF MAGNETIC NANOPARTICLES WITH CARBOXYMETHYL-BETA-CYCLODEXTRIN FOR REMOVAL OF DYES IN WASTEWATER

DEVITA CHRISTIANI CAHYADI

NATIONAL UNIVERSITY OF SINGAPORE

2012

SURFACE MODIFICATION OF MAGNETIC NANOPARTICLES WITH CARBOXYMETHYL-BETA-CYCLODEXTRIN FOR REMOVAL OF DYES IN WASTEWATER

DEVITA CHRISTIANI CAHYADI

(B.Eng, Diponegoro University, Indonesia)

A THESIS SUBMITTED

FOR THE DEGREE OF MASTER OF ENGINEERING

DEPARTMENT OF CHEMICAL & BIOMOLECULAR ENGINEERING

NATIONAL UNIVERSITY OF SINGAPORE

2012

Acknowledgements

First of all, I would like to take this opportunity to express my sincerest gratitude and appreciation to my supervisors, Associate Professor K. Hidajat and Associate Professor M. S. Uddin, who have supported and inspired me with their abundant patience, advice, effort and knowledge that enable me to overcome challenges as well as solve problems during this research.

I would also like to express my deepest thank to all the staff members in the Department of Chemical and Biomolecular Engineering and all my colleagues in the laboratory, especially Mr. Abu Zayed Md Badruddoza. Thanks for all suggestions, help and support for me during my experiment so this project can be completed successfully.

I also thank the lab staffs, especially Ms. Jamie Siew for her selfless assistance in supplying glass wares and also in purchasing chemicals during this work.

Special thankful gratitude goes to my beloved family members, especially my husband and sister. Thanks for all fervent love, and encouragement to pursue this Master degree.

Finally, I would also like to convey thanks to National University of Singapore and to the Department of Chemical and Biomolecular Engineering for providing the laboratory facilities throughout my research.

Devita Christiani Cahyadi

June 2012

Table of Contents

Acknowledgement		i
Table of contents		ii
Summary		vii
List of Tables		ix
List of Figures		xi
Nomenclature		xvi
Chapter 1	Introduction	1
	1.1. Background	1
	1.2. Research objectives	5
	1.3. Organization of thesis	7
Chapter 2	Literature Review	8
	2.1. Magnetic separation	8
	2.1.1. Principle of magnetic separation	8
	2.1.2. Driving force for dye adsorption on solid surface	9
	2.2. Magnetic particles	11
	2.2.1. Types of magnetic particles	12
	2.2.2. Properties of magnetic particles	13
	2.2.3. Preparation of magnetic particles	15
	2.2.4. Surface modification of magnetic particles	17
	2.2.5. Application of magnetic particles	19
	2.2.5.1. Biotechnology and biomedical	19

2.2.5.2. Biotechnology and bioengineering 19

2.2.5.3. Environmental protection 20

2.2.5.3.1. Heavy metals removal 20

2.2.5.3.2. Dyes removal 21

2.2.5.3.3. Organic pollutants removal 22

2.3. Cyclodextrin 22

2.3.1. Classification of CDs 23

2.3.2. CD inclusion complex 24

2.3.3. Applications of CDs 27

2.3.4. Advantages and disadvantages of coating MNPs with CDs for wastewater treatment (dyes removal) 27

2.4. Dyes (Rhodamine B and Acid Blue 25) 28

2.4.1. Rhodamine B (RhB) 28

2.4.2. Acid Blue 25 (AB25) 29

2.5. Adsorption and Desorption 30

2.5.1. Adsorption 30

2.5.1.1. Adsorption Equilibrium 31

2.5.1.1.1. Langmuir Isotherm 31

2.5.1.1.2. Freundlich Isotherm 33

2.5.1.1.3. Redlich-Peterson Isotherm 34

2.5.1.2. Adsorption Kinetic 35

2.5.1.2.1. Pseudo-first-order model 35

2.5.1.2.2. Pseudo-second-order model 36

2.5.2. Desorption 36

2.6. Scope of the thesis 37

Chapter 3 Materials and methods 40

3.1. Materials 40

3.2. Methods 41

3.2.1. Synthesis of carboxymethyl-beta-cyclodextrin (CM-β-CD) 41

3.2.2. Synthesis of uncoated magnetic nanoparticles (bare MNPs) 42

3.2.3. Coating CM-β-CD on the surface of magnetic nanoparticles 43

3.3. Adsorption experiments 43

3.3.1. Batch adsorption studies 44

3.3.1.1. The effect of pH on dye adsorption 46

3.3.1.2. The effect of temperature on dye adsorption 47

3.3.2. Adsorption equilibrium isotherm 47

3.3.3. Kinetics study 48

3.3.4. Desorption experiments 48

3.3.5. Recovery experiment 49

3.3.6. Error analysis 50

3.4. Analytical methods 51

3.4.1. Fourier Transform Infrared Spectroscopy (FTIR) 51

3.4.2. Transmission Electronic Microscopy (TEM) 51

3.4.3. Vibrating Sample Magnetometer (VSM) 52

3.4.4. Zeta Potential 52

3.4.5. X-ray Diffraction Analysis (XRD) 52

	3.4.6. Thermogravimetric Analysis (TGA)	53
	3.4.7. X-ray Photoelectron Spectroscopy (XPS)	53
Chapter 4	Characterization of magnetic nanoparticles, uncoated and surface modified with carboxymethyl-beta-cyclodextrin	54
	4.1. Introduction	54
	4.2. Results and discussion	56
	4.2.1. Fourier Transform Infrared Spectroscopy (FTIR)	56
	4.2.2. Transmission Electronic Microscopy (TEM)	57
	4.2.3. Vibrating Sample Magnetometer (VSM)	58
	4.2.4. Zeta Potential	59
	4.2.5. X-ray Diffraction Analysis (XRD)	60
	4.2.6. Thermogravimetric Analysis (TGA)	61
	4.2.7. X-ray Photoelectron Spectroscopy (XPS)	62
	4.3. Conclusions	64
Chapter 5	Adsorption, desorption and regeneration experiments of a basic dye (Rhodamine B) using CMCD-MNPs	66
	5.1. Introduction	66
	5.2. Results and discussion	69
	5.2.1. Adsorption at different pHs	69
	5.2.2. Adsorption equilibrium	71
	5.2.3. Adsorption kinetic	78
	5.2.4. Adsorption mechanism	83
	5.2.5. Desorption and regeneration experiments	84
	5.3. Conclusions	89

Chapter 6	Adsorption, desorption and regeneration studies of an acid dye (Acid Blue 25) using CMCD-MNPs	90
	6.1. Introduction	90
	6.2. Results and discussion	92
	6.2.1. Adsorption at different pHs	92
	6.2.2. Adsorption equilibrium	94
	6.2.3. Adsorption kinetic	101
	6.2.4. Adsorption mechanism	106
	6.2.5. Desorption and regeneration experiments	108
	6.3. Conclusions	113
Chapter 7	Conclusions and Recommendations	115
	7.1. Conclusions	115
	7.2. Limitations	119
	7.3. Recommendations for future work	120
References		123

Summary

Magnetic nanoparticles (MNPs) have shown their potential applications in bioseparation and environmental protection. They exhibit superparamagnetic property, large specific surface area per unit volume, versatility and biocompatibility. However, MNPs can be easily aggregated through hydrophobic, magnetic dipole–dipole and Van der Waals interactions. To maintain mainly the stability and magnetic properties of MNPs, their surfaces are coated with nontoxic and biocompatible materials such as zeolite, activated carbon, and polysaccharides like cyclodextrin.

Cyclodextrins (CDs) are a family of compound made of sugar (starch) molecules bound together in a cyclic ring. They comprise 6 to 8 glucose monomers in one ring which refer to α-, β- and γ-CDs, respectively. All types of CDs are toroidal, hollow truncate cones with external hydrophilic rims and internal hydrophobic cavity which can form inclusion with guest molecules in aqueous medium. The ability to form complexes of CDs has been explored for more than 30 years, so CDs and CDs based materials are widely applied in pharmaceuticals, environment protection and drug delivery.

The interests of this work are to synthesize of Fe_3O_4 nanoparticles, uncoated and coated with carboxymethyl-beta-cyclodextrin (CM-β-CD) and then use them to remove cationic and anionic dyes from waste. The MNPs are prepared by a chemical precipitation method using Fe^{2+} and Fe^{3+} salts in the molar ratio of 1:2 under vigorous stirring, inert and alkaline environment. During the reaction, the surfaces of the nanoparticles are modified

by CM-β-CD. The attachment of CM-β-CD on MNPs is characterized by Fourier Transform Spectroscopy (FTIR), Thermogravimetric Analysis (TGA), Zeta Potential and X-ray Photoelectron Spectroscopy (XPS). The size and superparamagnetism property of the magnetic nanoparticles resulted is determined by Transmission Electron Microscopy (TEM) and Vibrating Sample Magnetometer (VSM), respectively. Rhodamine B and Acid Blue 25 are used as targeted molecules for cationic and anionic dyes for adsorption studies at different pHs and temperatures. At 298 K, the optimum pHs for RhB and AB25 adsorption using CMCD-MNPs are found to be 5 and 3, respectively. Using CMCD-MNPs as adsorbent, the maximum adsorption capacities for RhB and AB25 are 55.6 and 476.2 mg/g, respectively, at 298 K. Compared to uncoated MNPs, grafting MNPs with CM-β-CD enhances adsorption capacities by twice and 1.3 times for removal of RhB and Acid Blue 25 from waste, respectively. Langmuir isotherm equation can fit well the experimental data, while pseudo-second-order kinetic model can describe well the adsorption kinetic data. Desorption studies are carried out using various chemicals such as organic solvents, acidic and alkaline solutions and it is found that pure methanol and ethanol in water (90% v/v) can desorb about 90% of RhB and all of AB25 from the adsorbent. The recyclability of CMCD-MNPs experiments are also investigated and results show that they can be reused for three and four cycles of RhB and AB25 adsorptions, respectively.

In summary, nano-sized magnetic particles have been successfully synthesized and functionalized with CM-β-CD. They offer a promising tool for treatment of cationic and anionic dyes in wastewater.

List of Tables

Table 2-1	Properties of α-, β- and γ-CDs	24
Table 2-2	Advantages and disadvantages of the use of CMCD-MNPs as adsorbent to treat dyes in aqueous solution	27
Table 3-1	Lists of chemicals used	40
Table 3-2	Physical-chemical properties of Rhodamine B and Acid Blue 25	40
Table 5-1	Adsorption isotherm parameters for RhB adsorbed onto CMCD-MNPs and uncoated MNPs at pH 5, initial concentrations = 100 to 1500 mg/L, adsorbent mass = ~120 mg, agitation time = 5 hours, volume = 10 ml, agitation speed = 200 rpm, three different temperatures (298, 313 and 328 K)	74
Table 5-2	Thermodynamic parameters for the uptake of RhB onto CMCD-MNPs at pH 5 and temperatures from 298 to 328 K	77
Table 5-3	Maximum adsorption capacities (q_m, mg/g) for the uptake of RhB using some other adsorbents reported in literatures	78
Table 5-4	Adsorption kinetic parameters of RhB adsorbed on the surface of CM-β-CD modified on magnetic nanoparticles adsorbent. Conditions: initial concentration 250 mg/L, pH 5, temperatures 298, 313 and 328 K	82
Table 5-5	Percentage of RhB removed from the CMCD-MNPs adsorbent using different desorbing agents	85
Table 5-6	The spectra of CMCD-MNPs before and after RhB adsorption, after desorption with methanol and after three times recycled	88
Table 6-1	Adsorption isotherm parameters for AB25 onto CMCD-MNPs and uncoated MNPs at pH 3 and three different temperatures Adsorption isotherm parameters for AB25 onto CMCD-MNPs and uncoated MNPs at pH 3, initial concentrations 100-3000 mg/L, agitation time 5 hours, and three different temperatures (298, 313 and 328 K)	97
Table 6-2	Thermodynamic parameters for adsorption of AB25 onto CMCD-MNPs at pH 3 and temperatures from 298 to 328 K	100

Table 6-3	Reported maximum adsorption capacities (q_{max} in $mg.g^{-1}$) in the literatures for AB25 obtained on some adsorbents	101
Table 6-4	Adsorption kinetic parameters of AB25 on the surface of CM-β-CD modified on magnetic nanoparticles adsorbent (conditions: initial concentration 250 mg/L, pH 3, temperatures 298, 313 and 328 K)	105
Table 6-5	Percentage of AB25 removed from the CMCD-MNPs adsorbent using different desorbing agents	109
Table 6-6	The spectra of CMCD-MNPs before and after AB25 adsorption, after desorption with ethanol-water (90% v/v) and after four times recycled	112

List of Figures

Figure 2-1	Schematic diagram for separation of non-magnetic materials	9
Figure 2-2	Superparamagnetic particles under the absence of an external magnetic field	14
Figure 2-3	Superparamagnetic particles under the influence of an external magnetic field	14
Figure 2-4	Structure and properties of CDs	24
Figure 2-5	Dimensions and hydrophilic/hydrophobic regions of the CD molecules	24
Figure 2-6	The formation of CD inclusion complex	25
Figure 2-7	Molecular structures of RhB, (a). Monomeric form/Cationic form and (b). Dimer form/Zwitterionic form	29
Figure 2-8	Molecular structure of AB25	30
Figure 3-1	Carboxymethylation on beta-cyclodextrin	41
Figure 3-2	The equipment setup for the preparation of magnetic nanoparticles	42
Figure 3-3	An illustration of surface modification of iron oxide nanoparticles with CM-β-CD	43
Figure 3-4	Schematic illustration of Fe_3O_4-CMCD interaction and isolation of targeted molecules by magnetic separation	45
Figure 3-5	An illustration of dyes removal using CMCD-MNPs, (a) RhB and (b) AB25	46
Figure 4-1	FTIR spectra of (a) Uncoated MNPs, (b) CMCD-MNPs and (c) CM-β-CD	57
Figure 4-2	TEM micrographs (a) Bare MNPs and (b) CMCD-MNPs	58
Figure 4-3	Magnetization curve of bare MNPs and CMCD coated MNPs at room temperature	59
Figure 4-4	Zeta potential of uncoated MNPs and CM-β-CD coated MNPs	60

Figure 4-5	XRD pattern of (a) Uncoated MNPs and (b) CMCD-MNPs	61
Figure 4-6	TGA curve of (a) Uncoated MNPs and (b) CMCD coated MNPs	62
Figure 4-7	XPS wide scan spectra of (a) Uncoated MNPs and (b) CMCD MNPs	63
Figure 4-8	XPS C 1s spectrum of CMCD-MNPs	64
Figure 5-1	RhB adsorption on CMCD-MNPs at different pHs (condition: initial concentrations = 100 to 1500 mg/L, adsorbent mass = ~120 mg, pH = 2 to 11, agitation time = 5 hours, volume = 10 ml, agitation speed = 200 rpm and room temperature)	71
Figure 5-2	Equilibrium isotherm for the adsorption of RhB onto CMCD-MNPs and uncoated MNPs (conditions: initial concentrations = 100 to 1500 mg/L, adsorbent mass = ~ 120 mg, pH 5, agitation time = 5 hours, volume = 10 ml, agitation speed = 200 rpm, temperatures 298, 313 and 328 K)	72
Figure 5-3	Langmuir isotherm plots for the adsorption of RhB onto CMCD-MNPs and uncoated MNPs (conditions: initial concentrations = 100 to 1500 mg/L, adsorbent mass = ~120 mg, pH 5, agitation time = 5 hours, volume = 10 ml, agitation speed = 200 rpm, temperatures 298, 313 and 328 K)	73
Figure 5-4	Freundlich isotherm plots for the adsorption of RhB onto CMCD-MNPs and uncoated MNPs (conditions: initial concentrations = 100 to 1500 mg/L, adsorbent mass = ~120 mg, pH 5, agitation time = 5 hours, volume = 10 ml, agitation speed = 200 rpm, temperatures 298, 313 and 328 K)	73
Figure 5-5	Redlich-Peterson isotherm plots for the adsorption of RhB onto CMCD-MNPs and uncoated MNPs (conditions: initial concentrations = 100 to 1500 mg/L, adsorbent mass = ~120 mg, pH 5, agitation time = 5 hours, volume = 10 ml, agitation speed = 200 rpm, temperatures 298, 313 and 328 K)	74
Figure 5-6	Van't Hoff plot for the adsorption of RhB on CMCD-MNPs at pH 5 and three different temperatures (298 K to 328 K)	76
Figure 5-7	The uptake of RhB onto CM-β-CD coated on MNPs versus time at three different temperatures (condition: initial concentration = 250 mg/L, adsorbent mass = ~120 mg, pH 5, volume = 10 ml, agitation speed = 200 rpm, temperatures 298, 313 and 328 K)	80

Figure 5-8	Pseudo-first-order kinetic plots of the adsorption of RhB onto CMCD-MNPs at three different temperatures (condition: initial concentration = 250 mg/L, adsorbent mass = ~120 mg, pH 5, volume = 10 ml, agitation speed = 200 rpm, temperatures 298, 313 and 328 K)	81
Figure 5-9	Pseudo-second-order kinetic plots of the adsorption of RhB onto CMCD-MNPs at three different temperatures (condition: initial concentration = 250 mg/L, adsorbent mass = ~120 mg, pH 5, volume = 10 ml, agitation speed = 200 rpm, temperatures 298, 313 and 328 K)	82
Figure 5-10	FTIR spectra of (a) CMCD-MNPs before adsorption, (b) after adsorption with Rhodamine B and (c) Rhodamine B. FTIR spectra of the samples were analyzed using Bio-Rad spectrometer at 64 scans at 4.0 cm^{-1} resolution in the range of 400 to 4000 cm^{-1}	84
Figure 5-11	Performance of CMCD-MNPs adsorbent for the adsorption of RhB after three cycles of regeneration (conditions: initial concentration = 250 mg/L, adsorbent mass = ~120 mg, pH 5, volume = 10 ml, agitation speed = 200 rpm, temperature 298 K)	87
Figure 5-12	FTIR spectra of CMCD-MNPs (a) and (b) before and after adsorption of RhB, (c) after desorption with pure methanol and (d) after regeneration three times recycled	88
Figure 6-1	AB25 adsorption on CMCD-MNPs at different pHs (condition: initial concentrations = 100 to 1500 mg/L, adsorbent mass = ~120 mg, pH 2 to 11, agitation time = 5 hours, volume = 10 ml, agitation speed = 200 rpm and room temperature)	93
Figure 6-2	Equilibrium isotherm for the adsorption of AB25 onto CMCD-MNPs and uncoated MNPs at three different temperatures (conditions: initial concentrations = 100 to 3000 mg/L, adsorbent mass = ~120 mg, pH 3, agitation time = 5 hours, volume = 10 ml, agitation speed = 200 rpm, temperatures 298, 313 and 328 K)	95
Figure 6-3	Langmuir isotherm plots for the adsorption of AB25 onto CMCD-MNPs and uncoated MNPs (conditions: initial concentrations = 100 to 3000 mg/L, adsorbent = ~120 mg, pH 3, agitation time = 5 hours, volume = 10 ml, agitation speed = 200 rpm, temperatures 298, 313 and 328 K)	96

Figure 6-4 Freundlich isotherm plots for the adsorption of AB25 onto CMCD-MNPs and uncoated MNPs (conditions: initial concentrations = 100 to 3000 mg/L, adsorbent = ~120 mg, pH 3, agitation time = 5 hours, volume = 10 ml, agitation speed = 200 rpm, temperatures 298, 313 and 328 K) 96

Figure 6-5 Redlich-Peterson isotherm plots for the adsorption of AB25 onto CMCD-MNPs and uncoated MNPs (conditions: initial concentrations = 100 to 3000 mg/L, adsorbent = 120 mg, pH 3, agitation time = 5 hours, volume = 10 ml, agitation speed = 200 rpm, temperatures 298, 313 and 328 K) 97

Figure 6-6 Van't Hoff plot for the adsorption of AB25 on CMCD-MNPs at pH 3 and three different temperatures (298 to 328 K) 99

Figure 6-7 The amount of AB25 adsorbed onto CM-β-CD coated on MNPs versus time at three different temperatures (conditions: initial concentrations = 250 mg/L, adsorbent mass = ~120 mg, pH 3, volume = 10 ml, agitation speed = 200 rpm, temperatures 298, 313 and 328 K) 103

Figure 6-8 Pseudo-first-order kinetic plots of the adsorption of AB25 onto CMCD-MNPs at three different temperatures (conditions: initial concentrations = 250 mg/L, adsorbent mass = ~120 mg, pH 3, volume = 10 ml, agitation speed = 200 rpm, temperatures 298, 313 and 328 K) 104

Figure 6-9 Pseudo-second-order kinetic plot of the adsorption of AB25 onto CMCD-MNPs at three different temperatures (conditions: initial concentrations = 250 mg/L, adsorbent mass = ~120 mg, pH 3, volume = 10 ml, agitation speed = 200 rpm, temperatures 298, 313 and 328 K) 105

Figure 6-10 FTIR spectra of (a) CMCD-MNPs before adsorption, (b) after adsorption with Acid Blue 25 and (c) Acid Blue 25. FTIR spectra of the samples were analyzed using Bio-Rad spectrometer at 64 scans at 4.0 cm^{-1} resolution in the range of 400 to 4000 cm^{-1} 107

Figure 6-11 Performance of CMCD-MNPs for the adsorption of AB25 after four cycles of regeneration (conditions: initial concentrations = 250 mg/L, adsorbent mass = ~120 mg, pH 3, volume = 10 ml, agitation speed = 200 rpm, temperature 298 K) 111

Figure 6-12 FTIR spectra of CMCD-MNPs (a) and (b) before and after AB25 adsorption, (c) after desorption with ethanol in water 90% (v/v) and (d) after four times recycled 112

Nomenclature

Symbols	Description
B	Magnetic flux density or magnetic induction strength, (T)
C	Concentration of targeted molecules, (mg/L)
C_0	Initial concentration, (mg/L)
C_e	Equilibrium concentration, (mg/L)
D_0	Mean diameter (average diameter) of magnetic particles, (nm)
D_{hkl}	Mean diameter of magnetic particles by XRD, (nm)
F_{obj}	Relative difference between the experimental and theoretical data, (dimensionless)
H	Magnetic field strength, (Am^{-1})
K_F	Freundlich constant ($mg/g(mg/L)^{n}_{F}$)
K_L	Langmuir constant, (L/g)
k_1	Equilibrium rate constant for pseudo-first-order kinetic model, (min^{-1})
k_2	Equilibrium rate constant for pseudo-second-order kinetic model, (g/mg min)
n	Total number of experimental data, (dimensionless)
n_F	Heterogeinity constant, (dimensionless)
q	Adsorption capacity, (mg/g solid)
q_e	Equilibrium adsorption capacity, (mg/g solid)
q_e^{exp}	Experimental adsorption capacity at equilibrium, (mg/g solid)
q_e^{cal}	Predicted adsorption capacity at equilibrium, (mg/g solid)
q_m	Maximum adsorption capacity, (mg/g solid)

q_t	Adsorption capacity at any time, (mg/g solid)
R_L	Separation factor, (dimensionless)
R^2	Correlation coefficient, (dimensionless)
S	Mass of nano-sized magnetic particles added, (g)
t	Time, (s, min)
V	Volume of dye solution, (mL)
x	Mass of targeted molecules adsorbed, (mg)
ΔG	Change of free energy, (kJ/mol)
ΔH	Change of enthalpy, (kJ/mol)
ΔS	Change of entropy, (J/mol K)

Greek letters

β	Half width of XRD diffraction lines, (rad)
β	Redlich-Peterson constant, (dimensionless)
λ	Wavelength of X-ray, (nm)
μ	Permeability of particle, (Hm^{-1} or NA^{-2})
θ	Half diffraction angle, (deg)

Abbreviations

AB25	Acid Blue 25
CD	Cyclodextrin
β-CD	Beta-cyclodextrin
BEs	Binding energies
CM-β-CD	Carboxymethyl-beta-cyclodextrin

CMCD-MNPs	Carboxymethyl-beta-cyclodextrin coated on magnetic nanoparticles
FTIR	Fourier Transform Infrared Spectroscopy
pI	Isoelectric point
pH_{ZPC}	pH at zero point charge
MNPs	Magnetic nanoparticles
RhB	Rhodamine B
TEM	Transmission Electronic Microscopy
TGA	Thermogravimetry Analysis
XRD	X-ray Diffraction
XPS	X-ray Photoelectron Spectroscopy
VSM	Vibrating Sample Magnetometer

Chapter 1 Introduction

1.1. Background

Separation plays an important role in the field of chemistry and chemical engineering. The process is a heat and/or mass transfer process and used to either obtain distinct products to meet a specification or remove undesirable impurities in a mixture. Some of common separation processes are distillation, membrane, adsorption and chromatography which have been employed in past decades. Since each technique has pros and, moreover, more than 50% of the capital of a chemical plant is invested in separation, a choice of separation process must be considered carefully.

In recent decades, there is an increasing attention toward separation process applying nano-sized particle magnetic for adsorption process, an exothermic process based on the difference in affinity in which adsorbates are accumulated on the surface of adsorbents and the separation process is done either by physical means through intermolecular interaction forces or by chemical bonds. The nano-sized magnetic particles have been developed due to their high adsorption capacity, ability to separate targeted molecules (magnetic and non magnetic molecules) and large affinity toward particular targeted molecules [1]. The interaction between magnet and guest molecules is able to separate contaminants even in a concentrated feed. It also reduces internal diffusion resistance and it has a great ratio of surface area per unit volume [2, 3]. Furthermore, the nano-magnetic particles adsorbent is easy to be prepared and isolated from feed solution by applying external magnetic field as well as having high adsorption capacity [1]. Besides these,

separation applying nano-sized magnetic particle can be used to isolate and purify diverse chemical and biologically active compounds on both laboratory and industrial scales [4].

Separation using nano-sized magnetic particle relates to particles, solution as a carrier and targeted molecules. The technique is applied to isolate and purify chemicals like metals ions and organic molecules or biologically active compounds such as proteins, amino acids and drugs from their mixture [4]. The principle of separation can be briefly described in the following. First of all, adsorbent magnetic particles and adsorbate targeted molecules make an interaction by electrostatic, hydrophobic and/or specific ligand interactions [5]. This interaction results complexes with magnetic properties. Second, separation of the complexes and bulk solution is done by applying external magnetic field. Third, separation of adsorbate and adsorbent uses desorbing agents.

However, nano-sized particles tend to aggregate to minimize their surface energy due to their large ratio of surface area per unit volume. Therefore, to achieve its stability, nanoparticles are usually functionalized with specific groups, for instance surfactants and hydroxyl groups. The coating method can also hamper the aggregation of the particles at a distance where the attraction energy between the particles is larger than the disordering energy of thermal motion [6].

To increase the adsorption ability of the nano-sized magnetic particles adsorbent, a modification of its surface has been developed. Various materials such as zeolites [7], activated carbon [8], cyclodextrin [9] and natural or synthetic polymers like chitosan [10]

can be applied in the functionalization of magnetic nanoparticles. These materials have been proven to remove effectively both organic and inorganic wastewater contaminants as well as to make separation easy and recover the adsorbents. Nowadays, there is an interest in using low-cost adsorbents from natural polymers, for instance polysaccharide and their derivatives including cyclodextrins. The adsorbents are used to remove pollutants from wastewater due to their particular structure, low toxicity, high chemical stability, biodegradable compounds, cost-effective, wide availability many countries as it is a part of starch, environmentally friendly, high chemical stability, high reactivity and selectivity toward organic compounds and metals [2, 11].

Cyclodextrins (CDs) are a family of compound made of sugar (starch) molecules bound together in a cyclic ring. They compose of five or more α (1-4) linked D-glucopyranoside units linked one as those in amylose. Particularly, they contain 6 to 8 glucose monomers in one ring [12]. There are three classes of CDs, α, β and γ, which have 6, 7 and 8 members of sugar-sing molecules, respectively. All types of CDs are toroidal, hollow truncate cones with external hydrophilic rims and internal hydrophobic cavity. The hydrophobic cavity can form inclusion with guest molecule(s) in aqueous medium, whereas the hydroxyl groups of the molecules have the ability to form cross linking with coupling agents [13]. The formation of the inclusion complexes uses physiochemical of guest molecules so they can be temporarily locked or caged within the host cavity of CDs [12]. The properties are solubility enhancement of highly insoluble guest, stabilization of labile guests against the degradative effects of oxidation, visible or UV light and heat, control of volatility and sublimation, physical isolation of incompatible compounds,

chromatographic separations, taste modification by masking off flavours, unpleasant odours and controlled release of drugs and flavours [14]. The molecular encapsulation in CDs is due to weak interactions, for example hydrophobic effects, Van der Waals interaction and hydrogen bonding [15]. In general, CDs, including β-CD, are able to form stable inclusion complexes with a various range of organic compounds such as straight or branched chain aliphatics, aldehydes, ketones, alcohols, organic acids, organic compounds including dye, fatty acids, aromatics, gases, and polar compounds such as halogens, oxyacids and amines [14]. The ability to form inclusion complexes of CDs has been developed for more than 30 years [16]. Consequently, this ability makes CDs and CDs based materials are applied in food, pharmaceuticals, cosmetics, environment protection, bioconversion, packing and the textile industry [12, 16, 17].

One class of CDs, beta-cyclodextrin (β-CD), is the most useful type of CDs because it is the most accessible, available commercially in lower cost. Moreover, it has a rather rigid structure compared to other CDs [14, 16]. Therefore, β-CD based polymers are commonly used in many fields like wastewater treatment. Many types of water insoluble β-CD based polymer have been used for pollutants removal in wastewater [9, 11, 16]. To increase the capability to absorb dyes, particularly cationic (basic) and anionic (acid) dyes, chemical coating of carboxyl group onto β-CD has been carried out [11, 16].

Studies on separation by adsorption using nano-sized magnetic particles coated with carboxymethyl-beta-cyclodextrin (CM-β-CD) have been applied in the removal of heavy metals [15] and organic contaminants such as some amino acids [18] and bisphenol-A

(BPA) [19, 20]. Attempts to extend the application of CMCD-MNPs as adsorbent for the treatment of dyes in wastewater would be studied. A quantitative analysis of maximum adsorption capacities of bare and CM-β-CD coated on MNPs is also necessary. These would provide a better comprehension of advantages in surface modification of magnetic nanoparticles and further broaden the other possibility of their application for environmental protection.

This work presents preparation and characterizations of nano-sized magnetic particle coated with CM-β-CD, application of these nanomagnetic particle for dye removal from aqueous solution and comparison in their performances to uncoated magnetic nanoparticles. First of all, carboxymethylation of β-CD was conducted, and then the CM-β-CD was grafted on the surface of nano-sized magnetic particles by chemical precipitation method. These magnetic nanoparticles were utilized to treat dye dissolved in liquid phase by adsorption technique. Surface functionalization of magnetic particle with CM-β-CD exhibiting inherent magnetic properties and complexation ability has shown as an effective tool for the removal of dye pollutants from wastewater.

1.2. Research objectives

The objectives of this research are to study the application of nano-sized magnetic particles adsorbent in the separation of anionic and cationic dyes and to determine their effectiveness. The aims can be classified into these scopes:

1. ***Coating CM-β-CD onto the surface of magnetic nanoparticles***
   a. Synthesis iron oxide magnetic nanoparticles (Fe_3O_4) with chemical precipitation method
   b. Synthesis of carboxymethyl-beta-cyclodextrin (CM-β-CD)
   c. Synthesis magnetic nanoparticles modified with CM-β-CD through reaction between magnetite nanoparticles and CM-β-CD.
2. ***Characterizations of the structure of magnetite nanoparticles coated by CM-β-CD using Fourier Transform Infrared Spectroscopy (FTIR), Transmission Electronic Microscopy (TEM), Vibrating Sample Magnetometer (VSM), Zeta Potential, X-ray Diffraction (XRD), Thermogravimetric Analysis (TGA) and X-ray Photoelectron Spectroscopy (XPS)***
3. ***Study on batch adsorption between dye solutions and nano-sized magnetic particles***
   a. Determine effects of pH and temperature, adsorption equilibrium and adsorption kinetic between acid and basic dyes using CMCD-MNPs adsorbent
   b. Compare the efficiency of adsorbing process using magnetic nanoparticles coated with CM-β-CD (CMCD-MNPs) and bare MNPs by evaluating the maximum adsorption capacity at equilibrium.
4. ***Study on desorption of the adsorbed targeted molecules with different desorbing agents***
5. ***Study on the recyclability of the CM-β-CD coated magnetic nanoparticles adsorbent***

1.3. Organization of thesis

The present thesis will be organized into seven chapters. Chapter 1 gives a brief introduction of background of magnetic separation, the objective of this research and the structural organization of the whole thesis. Chapter 2 presents the detailed information on the theoretical background. Chapter 3 describes the materials and methods of this experiment. Chapter 4 covers the characterizations of the uncoated and CM-β-CD coated magnetic nanoparticles. Chapters 5 and 6 present the adsorption, desorption and regeneration studies of a cationic and an anionic dyes using magnetic nanoparticles adsorbents, respectively. The last chapter, Chapter 7 gives the overall conclusions of the work and recommendations for future work.

Chapter 2 Literature Review

A literature review on separation of acid and basic dyes using magnetic particles is presented in this chapter. It includes background of magnetic separation, preparation of magnetic particles, surface modification and applications of magnetic particles, cyclodextrin, and adsorption.

2.1. Magnetic separation

2.1.1. Principle of magnetic separation

Magnetic separation is the process by which particles are separated from mixture using a magnetic force. The separation is based on difference in magnetic properties. The technique has been developed to separate both magnetic and non-magnetic materials. In separation of magnetic materials, the targeted molecules can be isolated without any modification of magnetic particles, such as in metal recovery [21]. On the other hand, to separate non-magnetic materials such as biomolecules and organic pollutants, usually uses a formation of complex of guest molecules with magnetic particles, as can be seen in Figure 2-1. Initially, the targeted molecules interact with intermediates such as surfactants, polymer or ligand modified on the surface on magnetic particles, and then they form a complex. The interaction between guest molecules and intermediates can be electrostatic interaction, hydrophobic interaction, inclusion complex formation or ligand-specific interaction. Finally, the complex is separated from the bulk solution using external or electromagnetic fields [5].

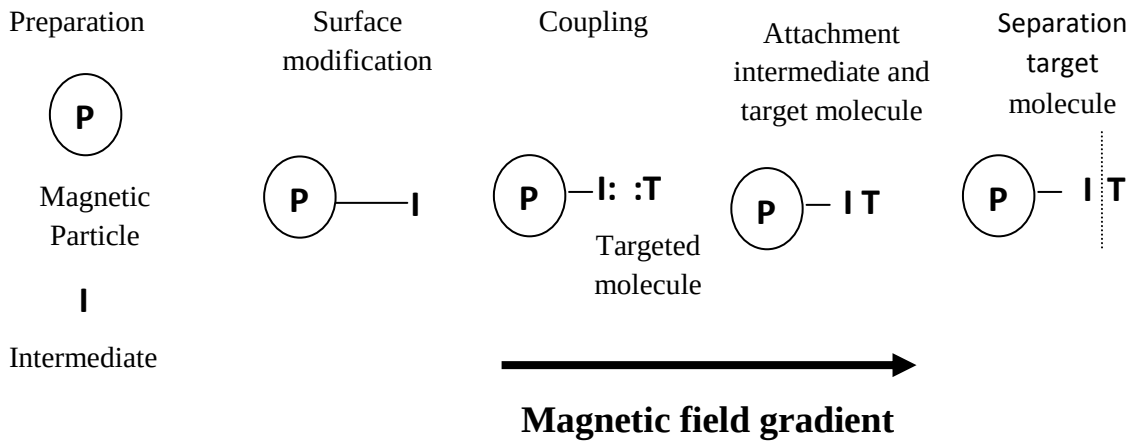

Figure 2-1 Schematic diagram for separation of non-magnetic materials

2.1.2. Driving force for dye adsorption on solid surface

The uptake of dye onto the adsorbent surface depends on several factors such as interaction between dyes and intermediates which may be hydrophobic interaction, electrostatic interaction or inclusion complex formation. Other factors like pH and temperature also have effects on the adsorption. Moreover, hydrogen bonding and Van der Waals forces may also involve in the adsorption of dye onto the surface of adsorbents.

Rhodamine B/ RhB (Basic Violet 10) is a basic dye and the most important class of xanthene dyes. It has different forms at different pHs, for example, at pHs lower than 5, it exists in monomers. However, as pH rises from 5 to 8, it agglomerates and forms dimers. Therefore, in this case, at neutral pHs, electrostatic interaction and charged surface effects cannot facilitate the adsorption [22, 23]. Whereas, the second dye, Acid Blue 25 (AB25) has negative charges for all pHs. Thus, electrostatic interaction influences the amount of the uptake of AB25 [24].

The interaction forces/mechanisms associated with dye adsorption are presented in the following:

1. Electrostatic interaction

In some dyes adsorption, electrostatic interaction may promote a dye to be placed with oppositely charged surface of magnetic nanoparticles adsorbent. Consequently, the dye can be removed by interaction of oppositely charged surface. Some works [24, 25] mentioned that dye removal is controlled by electrostatic interaction.

2. Inclusion complex formation

The three types of CDs, α, β and γ, are toroidal, hollow truncate cones with external hydrophilic rims and internal hydrophobic cavity. The internal hydrophobic cavity, the key structural feature of the CDs, can form inclusion with guest molecule(s) in aqueous medium [13]. Several interactions may involve in the targeted molecules and CD cavity, the guest adsorbate and other introduced group or crosslinked materials [16]. The major interaction in complexation processes are dipole-dipole, Van der Waals, hydrophobic interactions which induce the apolar group of a molecule to preferentially enter the CD cavity, hydrogen bonding between guest molecule and hydroxyl groups at the rim of the cavity (these contributions increase with polar molecules), solvent effects (release of high-energy water), as well as steric effects [26, 27]. Among the factors, hydrophobic interactions had been mainly considered as the major factor in complexation.

3. Hydrogen bonds

Although they are not found in large numbers in all interfaces, they make an important contribution to the binding energy of association. Hydrogen bonds can also provide attractive forces between molecules. In addition, they are probably thought to confer

specificity to interactions due to their dependence on the precise location of participating atoms. In dye adsorption, the bonds may be formed between hydroxyl-carbonyl and hydroxyl-hydroxyl.

4. Van der Waals interaction

Besides hydrogen bonds, Van der Waals interaction also assists interaction forces between molecules. The interaction force occurs among all neighbouring atoms in structures and interfaces as well as between atoms and solvent molecules. The force operates over small distances with no presence of water and the two non-polar groups become close each other. However, in adsorption process, the Van der Waals interaction is negligible compared to hydrophobic interactions [28].

Generally, in adsorption of guest molecules on magnetic particle, more than one interactions are involved either individually or mutually. Therefore, it is important to consider the interactions between adsorbate and adsorbent in order to get insight of mechanism taking place in the adsorption process.

2.2. Magnetic particles

Solid-liquid phase separation has been developed for long time for the removal and purification of chemical and biochemical targeted molecules. Magnetic separation is one of the solid-liquid phase separation processes and is applied in many fields such as industrial technology, biological, medical, environmental protection and waste management.

2.2.1. Types of magnetic particles

Ferrofluids, originally discovered in the 1960s, are stable colloidal dispersion of single domain ferro magnetic particles (Fe_3O_4) suspended in suitable aqueous carrier medium, so they have the fluid properties of a liquid and the magnetic properties of a solid [29]. In general, the ferrofluids consist of tiny particles (~10 nm in diameter). Their advantages were immediately obvious, (i). The location of the fluid could be precisely controlled through the application of a magnetic field, and (ii) by varying the strength of the field, the fluids could be forced to flow. In addition, modification the surface of ferrofluids with biocompatible, water soluble and nontoxic polymers or surfactants through chemical bonds or electrostatic interaction was carried out to increase their performance as well as to prevent aggregation. Researchers have prepared ferrofluids containing small particles of ferromagnetic metals, such as cobalt and iron, and magnetic compounds like manganese zinc ferrite, $Zn_xMn_{1-x}Fe_2O_4$. ($0 < x < 1$; this is a family of solid solutions). Nevertheless, by far, the most work has been conducted on ferrofluids containing small particles of magnetite, Fe_3O_4 [29].

Magnetite, a common type of ferromagnetic material which is usually black, has the chemical formula Fe_3O_4. However, it is also known as ferrous-ferric oxide ($FeO.Fe_2O_3$). Besides magnetic, the most common used magnetic particles is maghemite (γ-Fe_2O_3). Other types of magnetic particles are various types of ferrites ($MeO.Fe_2O_3$, where Me = Ni, Co, Mg, Zn, Fe or Mn) as magnetic moieties [30].

2.2.2. Properties of magnetic particles

In most materials, the relation between magnetic induction strength (*B*) and the magnetic field strength (*H*) is linear. Therefore, the magnetic properties of the materials can be expressed by an equation of the dependence between *B* and *H*, which can be shown as:

$$B = \mu.H \qquad [2\text{-}1]$$

Where, μ is the permeability of the particles.

Iron oxide particles respond in different ways when exposed to an external magnetic field because they have different values of μ. For instance the values of the permeability of iron oxide particles can be <1, 1, or > 1. At vacuum, their value of μ is 1. When μ<1, they can be diamagnetism and paramagnetism if μ>1. Consequently, iron oxide particles can exhibit superparamagnetism, ferromagnetism, paramagnetism or diamagnetism [31, 32].

In this thesis, we are interested in superparamagnetic materials which are suitable for all separation. The materials show non-magnetic moment in the absence of an external magnetic field but still can respond to the external magnetic field. On the other hand, in the presence external magnetic field, they do develop a mean magnetic moment [33]. It also has a zero intrinsic coercivity, high saturation magnetization, no hysteresis like ferromagnetic and no remanence magnetism. Generally, superparamagnetism takes place when the material is composed of very small crystallites (less than 30 nm) [34]. Since the particles are very small, no permanent magnetization remains after the magnetic particles are removed from a magnetic field as demonstrated in Figure 2-2. This is due to randomization of their spins as a result of the sufficient thermal energy to change the

direction of magnetization of the entire crystallites. Therefore, the magnetic field changes to average to zero and they do not interact each other. Nevertheless, the superparamagnetic materials still exhibit strong magnetic properties with very large susceptibility and still can respond to an external magnetic field [33]. They do not have remanence or coercivity, the shape of the hysteresis loop is thus thin [35].

Some advantages of the superparamagnetic particles are easy resuspension, large surface area, slow sedimentation, the stability and dispersion of magnetic force, no remanence magnetic force upon removal from the external force and uniform distribution of the particles in the suspension media. Figure 2-3 shows the particles behave like small permanent magnets when magnetized, so that they form aggregates or lattice due to magnetic interaction [33]. Consequently, these gains make iron oxide used in many applications such as separation, purification, drug delivery device, cancer treatments through hyperthermia, and as a contrast agent in Magnetic Resonance Imaging (MRI).

Fig. 2-2

Fig. 2-3

Figure 2-2 Superparamagnetic particles under the absence of an external magnetic field; it shows monodisperse particle distribution [33]

Figure 2-3 Superparamagnetic particles under the influence of an external magnetic field [33]

2.2.3. Preparation of magnetic particles

To prepare nano-sized magnetic particles some types of iron oxides have been first investigated, among which magnetite (Fe_3O_4) is the most feasible candidate due to its biocompatibility [36]. Another reason is the ability of electrons to move between Fe^{2+} and Fe^{3+} ions in the octahedral sites at room temperature [37].

First, nano-sized magnetic particles were prepared by size reduction. A larger coarse-grained ferromagnetic powder was ground in a ball mill [38]. The disadvantages of this method were time consuming and energy-costing, so many techniques were developed to prepare magnetic colloidal particles such as decomposition of metal carbonyls, electrodeposition techniques, and disruption of magnetotactic bacteria [4, 38].

Since size and shape became important factors in preparation nano-sized magnetic particles, numerous physical and wet chemical methods have been employed and developed such as (1). Physical methods like gas phase deposition and electron beam lithography, and (2). The wet chemical method is straightforward and more efficient with controllability of size, composition and even shapes [39].

One of the most common wet chemical methods is the chemical precipitation method or co-precipitation method [5]. This technique involves a reaction of ferric, ferrous and other ions in alkaline conditions under an inert atmosphere. The advantages of this method are that it is fast and simple to obtain narrow size distribution in nano-sized magnetic particles, and diverse surface modification can be carried out at the same time

during the preparation. There are two main methods for the synthesis of both Fe_3O_4 and γ-Fe_2O_3 nanoparticles in solution. First, ferrous hydroxide suspensions are partially oxidized with different oxidizing agents, such as aqueous hydrogen peroxide solution "spontaneously" in an open atmosphere or else in an inert atmosphere [40]. Second, the co-precipitation of Fe^{2+} to Fe^{3+} aqueous salt solutions by addition of a base [41]. The production of large quantities of magnetic nanoparticles with narrow size distribution remains a significant challenge for these methods [39].

Therefore, to precipitate Fe_3O_4 completely, alkaline solution is added to an aqueous mixture of Fe^{2+} and Fe^{3+} salts at a 1:2 molar ratio. The yield is black precipitated magnetite which is either well dispersed in a liquid or form composites with polymer or inorganic matrices (called magnetic microspheres or beads). The product is based on the following chemical reaction [42]:

$$FeCl_2 \cdot 4H_2O + 2FeCl_3 \cdot 6H_2O + 8NH_4OH = Fe_3O_4(s) + 8NH_4Cl + 20H_2O \qquad [2\text{-}2]$$

The reaction above must be carried out under a non-oxidizing oxygen free environment so a complete precipitation of Fe_3O_4 can be obtained and oxidation of Fe_3O_4 as shown in the following reaction can be avoided [32]:

$$Fe_3O_4 + 0.25O_2 + 4.5H_2O \longrightarrow 3\ Fe\ (OH)_3 \qquad [2\text{-}3]$$

Moreover, the oxygen-free condition is created by passing N_2 gas to the system. Besides protecting Fe_3O_4 from oxidation, passing N_2 gas also assists the size reduction to nano scale [36].

Since pH plays an important role in the composition and stability of magnetic particles, the reaction must be carried out in the alkaline media. In acidic media, Fe_3O_4 is not stable and will decompose to maghemite (Fe_2O_3 that is stable in acidic environment) based on this reaction [43]:

$$Fe_3O_4 \xrightarrow{H^+} Fe_2O_3 + Fe^{2+} + H_2O \qquad [2\text{-}4]$$

Some new methods with better control of size distribution of magnetic nanoparticles have recently been developed, including the microemulsion method [44] and high-temperature decomposition of organic precursors [45]. The advantages of these methods are that they produced good size control, narrow size distribution and good crystallinity and dispersibility of magnetic nano-sized particles. On the other hands, the disadvantages are that these methods cannot be applied to large scale and economic production, because they usually use expensive and toxic reagents, complicated synthetic steps, and high reaction temperature [39].

2.2.4. Surface modification of magnetic particles

In the absence of any surface modification, magnetic nano-sized particles exhibit hydrophobic surfaces with a large surface area to volume ratio. The hydrophobic interactions between particles cause the agglomeration of the particles through hydrophobic, magnetic dipole-dipole and Van der Waals interactions [46]. The aggregation of particles leads to form large clusters. As a result, the particle size will increase and thus sometimes lose the superparamagnetic properties. Next consequence,

the high capacity or selectivity for separation may decrease or even loss. If aggregated magnetic particles are used for in vivo applications, a rapid clearance from circulation and unexpected responses can occur [47]. In almost all applications, the preparation and surface functionalization of nano-sized magnetic particles contribute significant challenges in determining the particle size and shape, the stabilization, the size distribution, the surface chemistry and consequently the magnetic properties of the particles [39]. Coating also can increase surface area to volume ratio of nano-sized magnetic particles.

Therefore, surface modification of magnetic nanoparticles is an important factor for different applications and can be generally accomplished by physical/chemical adsorption of organic compounds by four major techniques methods, organic vapour condensation, polymer coating, surfactant adsorption and direct silanation with silane coupling agents [48]. To effectively stabilize of nano-sized magnetic particles in solution (ferrofluids), a formation of few atomic layers on their surfaces or a coating method is desirable. Basically, coating leads to the creation of more hydrophilic nanostructures via endgrafting, encapsulation, hyperbranching, or hydrophobic interactions [49].

Moreover, the coating also renders the nanoparticles water-soluble or oil-soluble that will be critical requirement for the conjugation of biomolecules and facilitates in binding some targeted molecules such as biological ligands. Therefore, numerous techniques have studied and developed to graft magnetic nanoparticles such as in situ coating and post-synthesis coating [50].

For wastewater treatment, the common surface functionalizations of nano-sized magnetic particles are inorganic materials such as bentonite [51], silica [52] and clay [53], carbon [54], surfactants [55], synthetic polymers such as poly acrylic acid (PAA) [56], poly ethylene and poly propylene (PE and PP) [57], and biopolymer like poly ethylene glycol (PGA) [58], polysaccharides [47] for example chitosan [59], and cyclodextrin (CD) [2, 15, 20].

2.2.5. Application of magnetic particles

Separation processes using MNPs have been explored and they have shown as an efficient tool to remove both chemical and biochemical contaminants. The uses of MNPs for separation a variety of targeted molecules are presented in the following:

2.2.5.1. Biotechnology and biomedical

The use of magnetic separation in the two fields has dramatically increased over the last couple of years. The application can be classified as *in vitro* and *in vivo*. For *in vitro* applications, the main application is in diagnostic and separation/labelling of bio molecules, such as protein, cell, enzyme, DNA/RNA, microorganism, whereas *in vivo* applications can be classified into diagnostic applications (magnetic resonance imaging/MRI) [39, 47] and therapeutic (drug delivery [47] and hyperthermia [60]).

2.2.5.2. Biotechnology and bioengineering

In these fields, MNPs are used as biosensor [61], biocatalyst and bioremediation [47], and bioseparation [47, 62].

2.2.5.3. Environmental protection

Water resources become critical important to living things, but there is a major environmental concern due to an increasing pollution from industrial wastewater. Numerous industries, for example pulp, paper, textile, plastics consume chemicals and dyes to process their products and also require a large amount of water. Consequently, water becomes contaminated by heavy metals, organic compounds and other hazardous materials. The contaminants make deleterious impacts the aquatic and terrestrial ecosystems. To remove contaminants in wastewater by adsorption, MNPs coated with polysaccharides show promising help.

2.2.5.3.1. Heavy metals removal

Copper is commonly found in municipal wastewater and its effects are dangerous to living things. Some techniques have been applied for its removal like ion extraction, coagulation or adsorption but they posses drawback due to low sensitivity and cross-reactivity. Currently, polysaccharide-coated MNPs provide an option for in bioremediation processes, for example S. cerevisiae was immobilized on chitosan coated MNPs and applied in the removal of Cu (II) from water by adsorption [63]. Besides copper, arsenic is another important contaminant in water. Recently, adsorption is one of particular interests for arsenic removal such as alginate-MNPs were developed as adsorbents for arsenic removal from wastewater, yielding higher arsenic uptake than bare alginate beads or bare MNPs [64].

2.2.5.3.2. Dyes removal

Textiles industry has been condemned as the most polluted industry in the world, since it requires a great amount of two main components, chemicals and water. Approximately, as many as 2000 different chemicals mostly are dyes and transfer agents, are used in textiles industry [9, 16]. Natural and synthetic dyes are used in textiles industry. However, the last group becomes commonly used due to economical and efficiency reasons. It will create problems because many synthetic dyes are designed as highly stable molecules, recalcitrant to be degraded by light, chemical and biological treatment. Some commercial synthetic dyes usually have unreported large complex structures [65]. Therefore, the discharge of dye wastewater can be one of industry's major problem since it contains numerous pollutants such as acid or caustic, dissolved solid, toxic compound like heavy metals, and colour. Among them, colour is very visible in wastewater; therefore, it can be easily recognized. Furthermore, these coloured effluents will cause major hazards to the environment. The presence of small amount of synthetic dyes is highly visible and undesirable. Most synthetic dyes are also resistant to detergent, very soluble in water, toxic, non-degradable, recalcitrant/stable, and even carcinogenic. Hence, they can be a serious threat to natural ecosystem and human beings. It also can cause the death of aquatic organisms that are important for humans and a lack of clean water resources. Therefore, we need to treat the wastewaters with toxic dyes before they are discharged into the water streams.

Recently, magnetic loaded adsorbent materials have gained special attention in water purification [66] due to various advantages such as high separation efficiency, simple

manipulation process, fast processing speed, economic and environmental friendly, able to handle concentrated feed, selectivity to particular guest molecules and easy specifically functional modifications. For dye removal, MNPs adsorbent modified with polysaccharides have become gain an interest such as chitosan coated on MNPs was applied to remove dyes [59, 67], cyclodextrin modified on MNPs was explored to treat basic (Methylene Blue [2] and Rhodamine B) and acidic (Acid Blue 25) dyes. MNPs modified with cyclodextrin have high uptake to the dyes and also exhibit an ability to be regenerated with almost constant adsorption capacity [15].

2.2.5.3.3. Organic pollutants removal

One of the organic contaminants that can be adsorbed with iron oxide nanoparticles coated polysaccharides is Bisphenol-A (BPA). Bisphenol A (BPA) is an important industrial chemical used primarily to make polycarbonate plastic and several types of resins, both of which are used in a wide variety of application such as baby bottles, food cans lining and flame retardants [19]. Cyclodextrin grafted on MNPs surface has shown a promising solution to remove BPA from wastewater [20].

2.3. Cyclodextrin

Cyclodextrins (CDs) are a family of compound made of sugar (starch) molecules bound together in a cyclic ring. They compose of five or more α (1-4) linked D-glucopyranoside units linked one as those in amylose. They are also known as cycloamyloses, cyclomaltoses and Schardinger dextrins [17]. Particularly, they contain 6 to 8 glucose monomers in one ring [12]. There are three types of CDs, α, β and γ, which have 6, 7 and

8 membered of sugar-sing molecules, respectively. All types of CDs are toroidal, hollow truncate cones with external hydrophilic rims and internal hydrophobic cavity. The hydrophobic cavity can form inclusion with guest molecule(s) in aqueous medium, whereas the hydroxyl groups of the molecules have the ability to form cross linking with coupling agents [13]. CDs are produced by an intramolecular transglycosylation reaction by degrading starch with cyclodextrin glucanotransferase (CGTase) enzyme [12].

2.3.1. Classification of CDs

CDs can be classified into three types, alpha-, beta- and gamma-cyclodextrins whose structures and properties can be seen in Figure 2-4 (a) and Table 2-1. They are crystalline, homogeneous, non-hygroscopic substances, and torus-like macro-rings built up from monomers, glucopyranose units. CDs are specifically constituted by 6-8 glucopyranoside units, and can be visualized as toroids with larger and smaller openings as shown in Figure 2-4 (b). The interior part is not hydrophobic, but it is considered to less hydrophilic than the aqueous environment. Therefore, it is able to be host to other hydrophobic molecules as illustrated in Figure 2-4 (c). On the other hand, the exterior part is sufficiently hydrophilic functioning to impart either CDs or their complexes water solubility [12]. Dimensions and hydrophilic/hydrophobic regions of α-, β- and γ-CD molecules are demonstrated in Figure 2-5.

The number of glucose units of the three types of CDs, can be presents as:

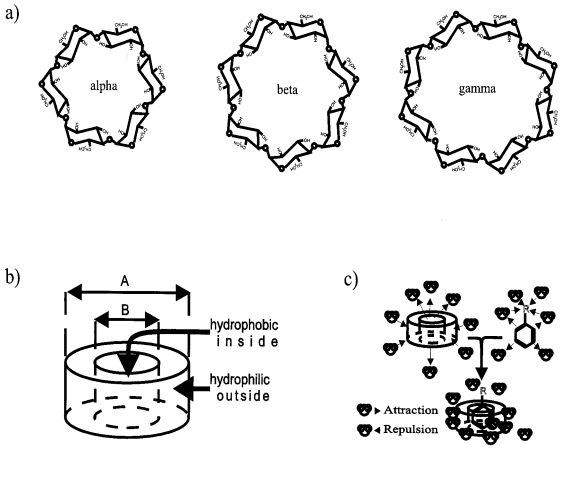

Fig. 2-4

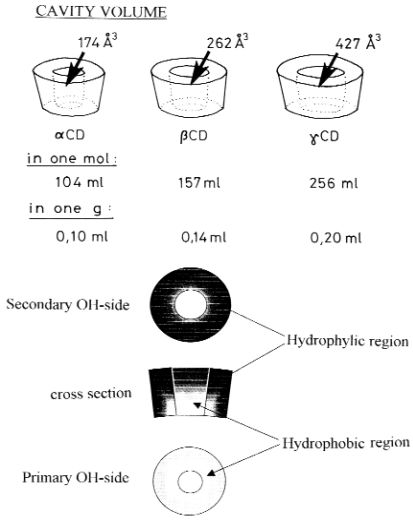

Fig. 2-5

Figure 2-4 Structure and properties of CDs [17], (a) apha-, beta-, and gamma-CDs; (b) three-dimensional form and properties of CDs; (c) formation of inclusion complex of a CD with a hydrophobic molecule

Figure 2-5 Dimensions and hydrophilic/hydrophobic regions of the CD molecules [12]

Table 2-1 Properties of α-, β- and γ-CDs [17]:

Properties	α-CD	β-CD	γ-CD
Number of glucopyranose units	6	7	8
Molecular weight (g/mol)	972	1135	1297
Solubility in water at 25^0C (%w/v)	14.5	1.85	23.2
Outer diameter (A) (Å)	14.6	15.4	17.5
Inner diameter (B) (Å)	4.7-5.3	6.0-6.5	7.5-8.3
Height of torus (Å)	7.9	7.9	7.9
Approx. cavity volume ($Å^3$)	174	262	427

2.3.2. CD inclusion complex

In aqueous solution, the CD cavity is slightly occupied by water molecules based on polar-apolar interaction or by appropriate guest molecules which are less polar than water. The dissolved CD is the 'host molecules' and several factors contribute as the driving force of the complexes formation [68], for instance (i). hydrophobic interactions

between hydrophobic "guest" molecules and the CD cavity, (ii) hydrogen bond links between polar functional groups of "guest" molecules and CD hydroxyl groups, (iii) Van der Waals interactions between hydrophobic "guest" molecules and the CD cavity, (iv) the substitution of the high enthalpy water molecules by an appropriate guest molecules in the cavity, (v) release of energy by conformational changes, (vi) dipole and dispersive interactions, (vii) charge transfer interaction and (viii) electrostatic interactions. The formation of the inclusion complexes also uses physiochemical of guest molecules so they can be temporarily locked or caged within the host cavity of CDs [16]. Among the factors, hydrophobic interactions had been mainly considered as the major factor in complexation [26], even though the nature of the substrate included determines the contributions of each of those forces. The association of the CD and guest molecules and the dissociation of the CD or guest complexes formed are governed by the thermodynamic equilibrium [12]. One or two or three CD molecules contain one or more encapsulated guest molecules, commonly, the host guest ratio is 1:1, as shown in Figure 2-6. This is the essence of "molecular encapsulation" and the simplest and also the most frequent case. However, 2:1, 1:2 and 2:2 or even more complicated associations and higher order equilibria exist and almost simultaneously [12].

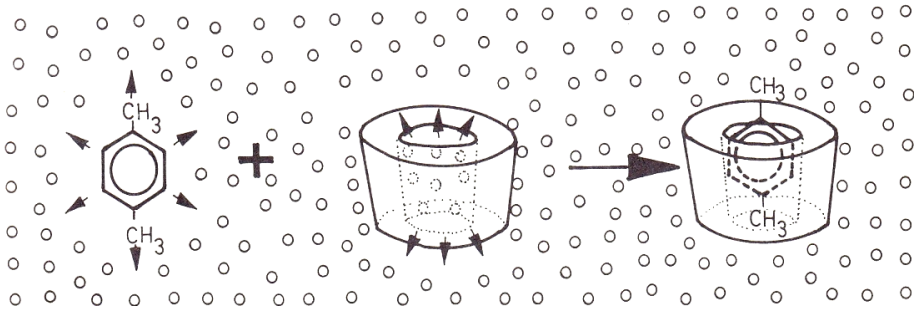

Figure 2-6 The formation of CD inclusion complex [12], small circles are water molecules

The properties of complexation are solubility enhancement of highly insoluble guest, stabilization of labile guests against the degradative effects of oxidation, visible or UV light and heat, control of volatility and sublimation, physical isolation of incompatible compounds, chromatographic separations, taste modification by masking off flavours, unpleasant odours and controlled release of drugs and flavours [14]. In general, CDs, including β-CD, are able to form stable inclusion complexes with a various range of organic compounds such as straight or branched chain aliphatics, aldehydes, ketones, alcohols, organic acids, organic compounds including dye, fatty acids, aromatics, gases, and polar compounds such as halogens, oxyacids and amines [14]. The structure and stability of inclusion complexes depends on two key parameters [14]; first, substrate polarity. The stability of inclusion complexes depends on the hydrophobicity of the substrate. Only compounds less polar than water are able to form inclusion complexes with CD. Reversely, hydrophilic molecules and strongly hydrated and ionized groups are not, or weakly form inclusion complexes with CD. The second factor is geometric compatibility. Second, the size and geometry of the guest substrate with respect to the dimensions of the cavity of CDs. A wrong sized guest will not fit properly into the CD cavity, for instance the bulky anthracene can only fit into γ-CD [19].

The ability to form inclusion complexes of CDs has been developed for more than 30 years [16]. Consequently, this ability makes CDs and CDs based materials are applied in food, pharmaceuticals, cosmetics, environment protection, bioconversion, packing and the textile industry [12, 16, 17].

2.3.3. Applications of CDs

CDs have supramolecular structures that can conduct chemical reactions known as 'host–guest' reactions or complexation. These reactions are intramolecular interactions between interacting molecules, ions or radicals without yielding covalent bonds. In addition, the formation of inclusion complex in CDs can be modified easily. Consequetly, they are widely used in many industrial products such as food, drugs and pharmaceutical industries, technologies and analytical methods, wastewater treatment, environment protection and as carriers (solubilizers, stabilizers) for biological active substances, enzyme models, separating agents, as a result of their stability, non toxic or negligible cytotoxic effects [12, 69].

2.3.4. Advantages and disadvantages of coating MNPs with CDs for wastewater treatment (dye removal)

Table 2-2 list the general gains and drawbacks of surface coating of MNPs with natural polymers such as CDs:

Table 2-2 Advantages and disadvantages of the use of CMCD-MNPs as adsorbent to treat dye in aqueous solution

Advantages	Disadvantages
• Cost-effective materials • Abundant materials and widely available in many countries as it is a part of starch • Renewable materials • Low toxicity • High chemical stability • Environmentally friendly • Good capacity in wastewater treatment such as the removal of heavy metals, various dyes and organic pollutants	• The performance of CM-β-CD relates to the origin of β-CD and the steps in carboxymethylation process • Requires chemical derivatization to improve its performance • The performance of the magnetic nano-adsorbent depends on pH • Generally, it is a non-destructive process

• Fast kinetic in dye removal • High ability to treat either dilute of concentrated aqueous feed • High selectivity towards organic compounds and heavy metals • Recyclable • Biocompatible	

2.4. Dyes (Rhodamine B and Acid Blue 25)

Generally, dyes are chemical compounds used to impart colour by attaching themselves to the materials. Many industries use natural as well as synthetic dyes. However, the last class becomes commonly used due to economical and efficiency reasons. Anthraquinone, phthalocyanine, triarylmethane and azo dyes are quantitatively the most important groups of synthetic dyes. The azo dyes characterized by an azo group consisting of two nitrogen atoms, are the largest class of dyes used in textile industry. Within the azo dyes, many dyes such as acid, reactive, disperse, vat, metal complex, mordant, direct, basic and sulphur dyes, can be derived [70].

2.4.1. Rhodamine B (RhB)

Among the various classes of dyes, basic dyes are the brightest class of soluble dyes used by the textile industries. Due to their high tintorial value, they are often considered as the most problematic classes of dye [71]. In general, basic dyes, often called as cationic dyes are dyes having cationic properties due to the chromophore as a part of positive charged ion which is probably delocalized on the nitrogen atoms [65]. They have affinity to act upon materials with negatively charged ions. One class of basic dyes is Rhodamine B (RhB) or Basic Violet 10, the most important xanthene dye. The dye is used as dye laser,

water tracing agent, biological stain, in the pharmaceutical and cosmetic industries, and even, in food stuff [72]. In this work, RhB has been chosen as the model of adsorbate, because (i) it is toxic, (ii) the tintorial value is high, since it is very visible at a very low concentration, (iii) it has good solubility in water and some organic solvent like methanol and ethanol, (iv) it has been widely used as a colorant in textiles due to its more rigid structure than other organic dyes [73], and (v) it is used commercially without further purification and (vi). It is present in the in the wastewaters of several industries, for instance textile, leather, jute and food industries [74]. Figure 2-7 shows the molecular structures of RhB which depend on pH solution, i.e. monomeric at low and high pHs and dimeric at neutral pHs.

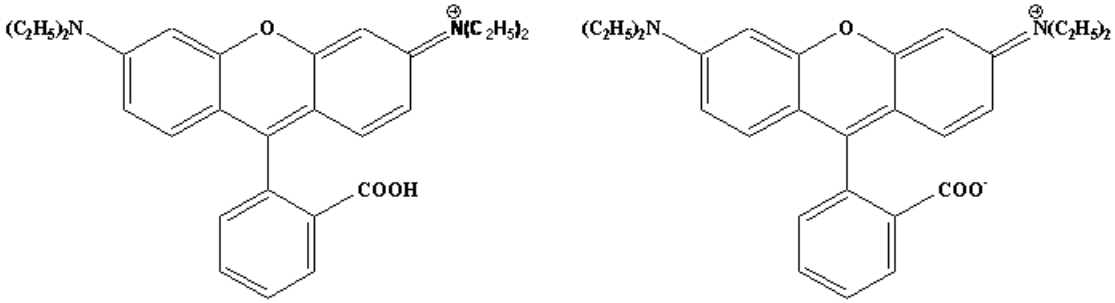

(a) (b)

Figure 2-7 Molecular structure of RhB, (a). Monomeric form/Cationic form and (b). Dimer form/Zwitterionic form

2.4.2. Acid Blue 25 (AB25)

Anthraquinonic dyes represent the second most important class of commercial dyes after azo-compounds [75]. Acid Blue 25 (AB25) is one type of anthraquinone dyes whose structure is depicted in Figure 2-8, and used mainly used for dying wool, polyamide, nylon, silk, paper, ink, aluminum, detergent, wood, fur, cosmetics, and leather. It is chosen since (i) it is known strong adsorption onto solids [24], (ii) it often serves as

model compound for removing organic contaminants from aqueous solutions [24], (iii) it is used commercially and without purification [24], (iv) it is used extensively and commercially in many fields such as for wool, nylon, silk, other protein fibers, paper, ink, aluminium, detergent, wood, fur, cosmetics, and biological stain [76], (v) it often serves as model compound for removing anthraquinonic dyes from aqueous solutions [76], (vi) particularly, anthraquinone dyes like Acid Blue 25 have been considered carcinogenic [77, 86].

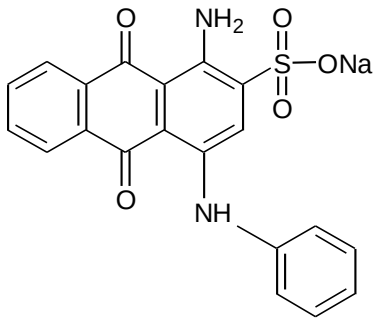

Figure 2-8 Molecular structure of AB25

2.5. Adsorption and Desorption

2.5.1. Adsorption

Adsorption is an exothermic process based on the difference in affinity where adsorbates are accumulated on the surface of adsorbents and the separation process is done either by physical means through intermolecular interaction forces or by chemical bonds. Therefore, the process can be classified as physisorption and chemisorptions.

Physisorption (physical adsorption) is a reversible exothermic process due to weak intermolecular forces of attraction and low heat of adsorption, usually between -20 and 0 kJ/mol [24]. With an increase in temperature, the amount of molecules adsorbed

decreases rapidly and is generally very small above the critical temperature of the adsorbate. Whereas, chemisorption (chemical adsorption) is an irreversible exothermic process required forces much stronger than in physical adsorption. The change of the activation energy is relatively high, generally -80 to 400 kJ/mol [24].

2.5.1.1. Adsorption Equilibrium

Equilibrium study shows the distribution of adsorbate in solid and liquid at fixed temperature equilibrium [12]. It illustrates an interaction between adsorbate (dye) and adsorbent to get information about the affinity of the adsorbent. Furthermore, we can estimate the amount of adsorbent taken to remove pollutant from solution and it also shows the adsorbent's capacity. Many models have been developed to analyze equilibrium in adsorption, for instance Langmuir, Freundlich and Redlich-Peterson.

2.5.1.1.1. Langmuir Isotherm

Langmuir isotherm is the simplest and the most widely used isotherm model for the adsorption of contaminant from a liquid solution [16]. The model was proposed in 1916. Several assumptions are applied such as [9, 16, 22, 65]:

(i) The model is based on monolayer adsorption taking place on specific homogeneous surfaces, therefore enthalpy is assumed to be same at everywhere. Although for heterogeneous surface, Langmuir isotherm model still can be used with a limitation not go beyond experimental data.

(ii) The adsorption process is carried out at well-defined localized site.

(iii) All adsorption sites are identical and energetically equivalent or the structure of the adsorbent is homogeneous.

(iv) Only one adsorbate molecule is placed at each site and once an adsorbate occupies a site, there is no further adsorption occurs at the site.

(v) The adsorbent has finite capacity for the adsorbate molecules (no adsorption takes place at equilibrium).

The general formula of Langmuir isotherm for adsorption can be expressed as [65]:

$$\frac{C_e}{q_e} = \frac{1}{q_m} C_e + \frac{1}{q_m K_L} \qquad [2\text{-}5]$$

where *Ce* (mg/L) is the equilibrium concentration of the aqueous solution and q_e (mg/g) is the amount of targeted molecules adsorbed on the solid at equilibrium. q_m (mg/g) is the maximum uptake of the adsorbate and K_L (L/g) is Langmuir constant.

To validate this model, a plot of C_e/q_e vs C_e must be linear. The value of parameters, q_m and K_L can be obtained from calculation of the slope and the intercept. In general, the model is well applied for low concentrations of adsorbates [78]. The essential feature of the model can be stated in a dimensionless constant. The constant is known as separation factor or equilibrium parameter (R_L) which is calculated by the following equation [79]:

$$R_L = \frac{1}{1 + K_L C_0} \qquad [2\text{-}6]$$

where C_0 (mg/L) is initial concentration of targeted molecules in solution and K_L (L/g) is Langmuir constant related to the energy of adsorption. The equilibrium parameter R_L reflects the shape of isotherm as:

Value of R_L	Shape of isotherm
$R_L > 1$	Unfavorable
$R_L = 1$	Linear
$0 < R_L < 1$	Favourable
$R_L = 0$	Irreversible

2.5.1.1.2. Freundlich Isotherm

Freundlich isotherm model was proposed in 1906, earlier than Langmuir model. It applies assumptions [16]:

i. Adsorption takes place on more than monolayer coverage surface or on heterogeneous surface, so each site has different sorption energy.
ii. The sorption energy is considered as a function of surface coverage
iii. The amount of adsorbed material is the total of adsorption on all sites.

Freundlich isotherm model can be expressed as:

$$\ln q_e = \frac{1}{n_F} \ln C_e + \ln K_F \qquad [2\text{-}7]$$

where q_e (mg/g) is the amount of the material adsorbed at equilibrium; C_e (mg/L) is the equilibrium adsorbate concentration in liquid solution; K_F (mg/g(mg/L)$^{n}_{F}$) is Freundlich constant associated with the bonding energy and n_F is the heterogeneity factor, shown how deviate the adsorption process from linearity is [16]. If the magnitude of $1/n_F$ is equal to 1, the adsorption is linear. If the value is either less or more than unity, the adsorption is a chemical or physical mechanism, respectively. The exponent $1/n_F$ also indicates the adsorption intensity and it is usually less than 1 due to first utilization of the highest binding energy then followed by the weaker sites, and so on [65]. The parameters of Freundlich model, n_F and K_F are calculated from the slope and intercept of a plot of ln q_e versus ln C_e.

2.5.1.1.3. Redlich-Peterson Isotherm

To compromise between Langmuir and Freundlich model, in 1959, Redlich and Peterson developed an empirical isotherm formula by combining three parameters. Here, the adsorption mechanism is a hybrid unique and does not follow ideal monolayer adsorption. The equation is also applied for further applications such as in kinetic or mass transport isotherm models [78]. Since the equation combined elements from Langmuir and Freundlich model, it can be converted to Freundlich isotherm model at low surface coverage and to Langmuir model at high concentration of adsorbate. Redlich-Peterson model can be represented in the following:

$$\log\left(K_r . {}^{C_e}\!/_{q_e} - 1\right) = \beta \log C_e + \log a_r \qquad [2\text{-}8]$$

here, K_r is assumed to be equal to K_L [65].

Adsorption equilibrium also gives information of thermodynamic parameters such as the free energy change (ΔG), enthalpy (ΔH) and entropy (ΔS). They are calculated using the following equations:

$$\Delta G = -RT \ln K_p \qquad [2\text{-}9]$$

$$\Delta G = \Delta H - T\,\Delta S \qquad [2\text{-}10]$$

$$\ln K_p = -\frac{\Delta H}{RT} + \frac{\Delta S}{R} \qquad [2\text{-}11]$$

Where Kp is the thermodynamic equilibrium constant, i.e. the ratio of equilibrium dye concentration in adsorbent and in solution. The method of Khan and Singh was applied to determine the constant Kp, by drawing a plot ln (q_e/C_e) versus q_e and extrapolating to zero q_e [80]. The slope and the intercept of the plot of ln Kp versus $1/T$ are used to determine ΔH and ΔS respectively.

2.5.1.2. Adsorption Kinetic

Adsorption kinetic indicates the rate of solute uptake which leads to determine residence time. It is also important to get information of the efficiency and characteristics of adsorbent [22]. Furthermore, it has significant importance to design the volume of the reactor to obtain high adsorption efficiency and low cost. Many kinetic models such as Lagergren pseudo-first-order and Ho and McKay pseudo-second-order models were applied to determine what mechanism controls or rate-limitting steps of the adsorption. The controlling mechanisms may be adsorption surface, mass transfer and external diffusion [16]. In general, the adsorption process includes two diffusions, mass transfer from bulk solution to the adsorbent surface across the boundary layer and diffusion in the adsorbent surface.

2.5.1.2.1. Pseudo-first-order model

Lagergren pseudo-first-order model is a common equation for the kinetic adsorption of solute from aqueous solution based on the capacity of the solid. The model can be written in the following [81]:

$$\log(q_e - q_t) = \log q_e - \frac{k_1}{2.303} t \qquad [2\text{-}12]$$

where q_e and q_t (mg/g) are the amount of targeted molecules adsorbed at equilibrium and at time t respectively and k_1 (min^{-1}) is the equilibrium rate constant for pseudo-first-order adsorption process. The plot of log (q_e-q_t) versus t produces a straight line. The slope of the straight line gives the value of the first-order-rate constant, k_1. If the adsorption follow Lagergren pseudo-first order model, the plot must have a high correlation coefficient (R^2~1) and the intercept equals log q_e. If a high R^2 is obtained, but the intercept is not

equal to log q_e, the adsorption process does not seem to follow pseudo-first-order kinetic model [81]. Moreover, if experimental data are well fitted with equation [2-12], the adsorption process is controlled by diffusion through a boundary. On the other hand, if the magnitude of the coefficient correlation (R^2) is low, it indicates that the adsorption is not controlled mainly by diffusion and some other mechanisms may involve [81].

2.5.1.2.2. Pseudo-second-order model

Pseudo-second-order kinetic model involves steps of adsorption such as external film diffusion, internal particle diffusion, and surface adsorption. The experimentally observed adsorption rate is also the overall rate of the whole process. The kinetic model is expressed by the following equation [82]:

$$\frac{t}{qt} = \frac{1}{k_2 q_e^2} + \frac{1}{qe} t \qquad [2\text{-}13]$$

where q_e and q_t (mg/g) are the amount of the uptake of adsorbate at equilibrium and at time t respectively and k_2 (g/mg min) is the equilibrium rate constant for pseudo-second-order adsorption process. If the experimental results are well fitted to the equation [2-13], pseudo-second-order kinetic model can be applied. The slope and intercept of the plot of t/q_t versus t were used directly to calculate the kinetic parameters, q_e and k_2.

However, pseudo-first and second-order kinetic models only determine the behaviour of overall adsorption process based on the solid adsorption capacity [19].

2.5.2. Desorption

Desorption study helps to understand adsorption mechanism and recyclability of the spent adsorbent as well as the adsorbent (dye). Various desorbing agents show the way of

the attachment between the dye and the adsorbent. For instance, if neutral pH water is used as desorbing agent, then the mechanism of the attachment is through the weak bonds. Acids such as sulphuric acid or alkaline water desorp the dye then the adsorption is through ion exchange. Organic acid like acetic acid or organic solvent is used as desorbing agent, so the attachment is chemisorptions. If a mineral acid like hydrochloric acid is used, then the dye is adsorbed through physisorption [22].

2.6. Scope of the thesis

The objective of this project is to synthesize CM-β-CD, graft the surface of iron oxide nanoparticles with CM-β-CD, use the adsorbent to uptake anionic and cationic dyes from solution, then compare the yields with those of uncoated MNPs, and carry out desorption as well as regeneration studies. Magnetic nanoparticles show a potential adsorbent for chemical and biomolecules separations, but only limited work has been published on the surface functionalization of MNPs with CM-β-CD as well as their application for wastewater treatment, especially dye removal. Based on the previous literature review, the scope of this project are:

1. *Synthesis and characterization of a derivative of cyclodextrin, carboxymethyl-beta-cyclodextrin (CM-β-CD)*

CM-β-CD is synthesized through a stirred reaction of beta-cyclodextrin, sodium hydroxide and chloroacetic acid, followed by filtration, precipitation and drying. Characterization is carried out with FTIR analysis.

2. Preparation and characterization of uncoated iron oxide nanoparticle (bare MNPs)

Synthesis of MNPs is carried out using chemical precipitation method by mixing $FeCl_3$ and $FeCl_2$ with a molar ratio of 2:1, under alkaline (ammonia), vigorous stirring and a nitrogen environment. Characterizations of the chemical, physical and magnetic properties of CMCD-MNPs are carried out using different tools, such as FTIR, TEM, VSM, Zeta Potential, XRD, TGA and XPS.

3. Preparation and characterization of iron oxide nano-sized particle grafted with CM-β-CD (CMCD-MNPs)

Synthesis of CMCD-MNPs is carried out using one step chemical precipitation method by mixing $FeCl_3$, $FeCl_2$ (with a molar ratio of 2:1) and CM-β-CD, under alkaline (ammonia), vigorous stirring and nitrogen environment. Characterizations of the chemical, physical and magnetic properties of CMCD MNPs are carried out using different tools, such as FTIR, TEM, VSM, Zeta Potential, XRD, TGA and XPS.

4. Application of both uncoated and CM-β-CD coated MNPs in anionic and cationic dyes removal

Separations of acid and basic dyes by both MNPs are carried out by determining RhB and Acid Blue 25 as model guests based on difference in their properties and their important presence in wastewater caused by industries. Adsorption studies of these dyes are performed in different parameters such as pH and temperature, in order to obtain the optimum conditions for adsorption. To get information about the affinity of the adsorbent and the adsorbent capacity, equilibrium study is explored. The rate and factors involving in the uptake of solute are achieved through kinetic study. The adsorption mechanism of the dyes is determined through FTIR analysis. How good the experimental data can be

fitted to the isotherm models is evaluated with error analysis. Moreover, the mechanism of adsorption and recyclability of the spent adsorbent are observed through desorption and regeneration studies.

Chapter 3 Materials and Methods

3.1. Materials

The chemicals used in this project are listed in Table 3-1. All the chemicals were used as received without further treatment. The physical and chemical properties of Rhodamine B and Acid Blue 25 are presented in Table 3-2.

Table 3-1 Lists of chemicals used

Name	**Chemical formula**	**Grade**	**Supplier company**
Acetic acid, glacial (99.7%)	CH_3COOH	GR	Alfa-Aesar
Acetone (99.5%)	$(CH_3)_2CO$	GR	Merck
Acid Blue 25	$C_{20}H_{13}N_2NaO_5S$	GR	Sigma Aldrich
Ammonium hydroxide (25%)	NH_4OH	GR	Merck
β-cyclodextrin hydrate (99%)	$C_{42}H_{70}O_{35}\cdot H_2O$	GR	Sinopharm Chemical
Chloroacetic acid (99%)	$ClCH_2CO_2H$	GR	Alfa Aesar
Di-sodium hydrogen phosphate (99%)	Na_2HPO_4	GR	Merck
Ethanol (99.5%)	C_2H_5OH	GR	Merck
Hydrochloric acid (37%)	HCl	GR	Merck
Iron (II) chloride tetrahydrate (98%)	$FeCl_2\cdot 4H_2O$	GR	Alfa-Aesar
Iron (III) chloride hexahydrate (98%)	$FeCl_3\cdot 6H_2O$	GR	Alfa-Aesar
Methanol (99.5%)	CH_3OH	GR	Merck
Milli-Q water	H_2O		NUS
Nitric acid (65%)	HNO_3	GR	Science Lab.
Potassium chloride	KCl	GR	Merck
Rhodamine B (95%)	$C_{28}H_{31}ClN_2O_3$	GR	Sigma Aldrich
Sodium acetate (99%)	CH_3COONa	GR	Merck
Sodium chloride	NaCl	GR	Merck
Sodium dihydrogen phosphate monohydrate (99%)	$NaH_2PO_4.H_2O$	GR	Merck
Sodium hydroxide	NaOH	GR	Merck
Trizma base	$NH_2C(CH_2OH)_3$	GR	Sigma Aldrich

Table 3-2 Physical-chemical properties of Rhodamine B and Acid Blue 25

Property	**Rhodamine B**	**Acid Blue 25**
CI name	Basic Violet 10	Acid Blue 25
CI number	45170	62055
Chemical class	Triarylmethane	Anthraquinone
Melting point	165°C (329°F)	Not established
Boiling point	Not applicable	Not applicable
Solubility in water	8 mg/mL	40 mg/mL
Solvent solubility	Soluble in alcohol (15 mg/mL)	Soluble in ethanol and acetone

Molecular weight	479.01	416.38
Chemical formula	$C_{28}H_{31}ClN_2O_3$	$C_{20}H_{13}N_2NaO_5S$
λmax (nm)	555	600
Dye content	95%	45%

3.2. Methods

3.2.1. Synthesis of carboxymethyl-beta-cyclodextrin (CM-β-CD)

Carboxymethyl-beta-cyclodextrin (CM-β-CD) was prepared by the following procedure [2]:

A mixture of beta-cyclodextrin (β-CD) (10 grams, 8.818 mmol) and NaOH (9.3 grams, 232.5 mmol) was treated with a-27-ml volume of monochloroacetic acid (16.5% w/w). The mixture was reacted at 50^0C for 5 hours. Then, the reaction product was cooled to room temperature and the pH was adjusted to neutral (6 to 7) using HCl. The neutral solution was filtered to separate salt containing in it. The solution was poured to a superfluous methanol solvent to produce a white precipitation. The solid precipitation was filtered and dried under vacuum. Then, it was crushed with an addition of acetone. Finally the mixture was dried under vacuum to produce carboxymethyl-β-cyclodextrin (CM-β-CD). IR (KBr): ν (cm^{-1}): 3140-3680 (-OH), 2923 (-CH), 1704 (C=O), 960-1200 (C-C, C-O-C). Figure 3-1 illustrates the carboxymethylation process on beta-cyclodextrin.

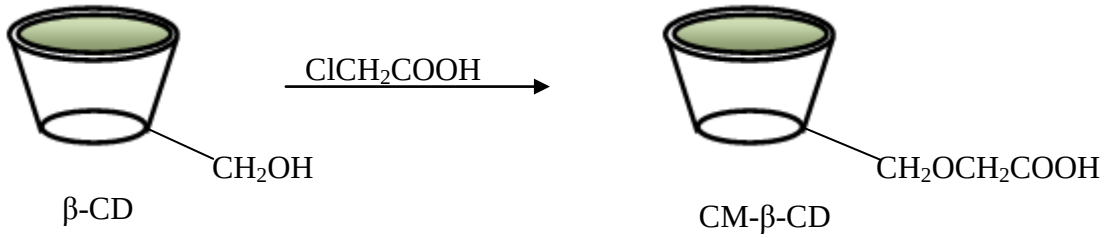

Figure 3-1 Carboxymethylation on beta-cyclodextrin

3.2.2. Synthesis of uncoated magnetic nanoparticles (bare MNPs)

MNPs were prepared by chemical precipitation method under inert (N_2) environment [83, 84]. For synthesis of bare MNPs, the equipment was first setup as demonstrated in Figure 3-2. Here, a complete precipitation of Fe_3O_4 was achieved under alkaline condition and N_2 bubbling while maintaining a molar ratio of Fe^{2+} and Fe^{3+} at 1:2. To obtain 1 g of Fe_3O_4 particle, a mixture of 0.86 g of $FeCl_2 \cdot 4H_2O$, 2.36 g of $FeCl_3 \cdot 6H_2O$ and 40 mL of ultrapure water was stirred vigorously at speed of 1000 rpm in N_2 atmosphere and heated to 80^0C. When the temperature reached 80°C, 5 mL of NH_4OH solution (25% v/v) was added and the reaction was continued for another 30 mins. The resulting suspension was cooled down to room temperature and then washed with ultrapure water approximately five times to remove any unreacted chemicals. Finally, the wet uncoated magnetic particles were separated from the solution by magnetic decantation. The reaction [2-2] occurred in the synthesis of MNPs.

Figure 3-2 The equipment setup for the preparation of magnetic nanoparticles

3.2.3. Coating CM-β-CD on the surface of magnetic nanoparticles

CMCD-MNPs were prepared by one-step co-precipitation method as described in the following [2]:

A mixture of 0.86 grams of $FeCl_2.4H_2O$, 2.36 grams of $FeCl_3.6H_2O$ was dissolved in 40 ml of de-aerated Milli-Q water. The mixture was heated to 90^0C under nitrogen environment with continuous stirring at 1200 rpm. When reaching 90^0C, 1.5 grams of CMCD and 5 ml of ammonia solution of 25% were added to the mixture. In this method, the carboxyl groups of CM-β-CD directly react with the surface OH groups on the magnetite to form Fe-carboxylate. The reaction was continued to an hour at 90^0C under vigorous stirring and inert environment. After that, the wet CMCD-MNPs were isolated from the solution by magnetic decantation. The precipitation was then washed several times with ultrapure water to remove any unreacted chemical, until the water was clean and had neutral pH. The reaction [2-2] also takes place during the synthesis of CMCD-MNPs and an illustration of coating the surface of MNPs is presented in Figure 3-3.

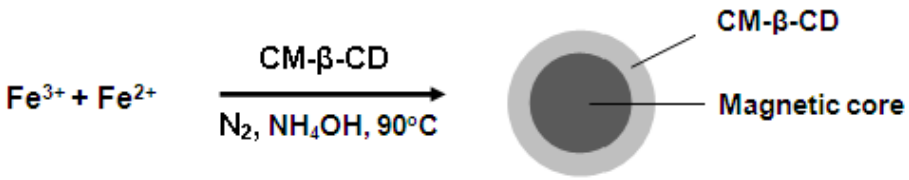

Figure 3-3 An illustration of surface modification of iron oxide particles with CM-β-CD

3.3. Adsorption experiments

The adsorption capacity was carried out using Basic Violet 10 (RhB) and Acid Blue 25 as model guest solutes. These dyes are produced commercially and used without further purification [22, 24]. In general, a 1500 mg/L stock solution of RhB while that of AB25

was 3000 mg/L, were prepared in 0.05 M buffer solutions at different pHs. From the stock solution, various initial concentrations of RhB solutions from 100 to 1500 mg/L were achieved by dilution while those of AB25 were 100 to 3000 mg/L. A calibration curve of each dye was obtained by plotting between absorbance and concentration of dye solution at a variation of initial concentrations with each wavelength by means of UV/vis spectrophotometer (model Shimadzu UV-1601). Each standard solution was prepared in 2 samples and each measurement was carried out twice for each sample under the same operational conditions to assure the reproducibility.

3.3.1. Batch adsorption studies

Batch mode adsorption studies for the two dyes were performed to investigate the effects of pH and temperature. The adsorptions of the dyes onto the surface of CM-β-CD magnetic nanoparticles adsorbent were observed in 0.05M buffer at predetermined initial concentrations, pHs and temperatures. After that, a 110 to 120 mg of wet magnetic nanoadsorbents was added to 10 ml of dye solutions and the mixtures were agitated in a shaker at 220 rpm at predetermined time intervals, at least 5 hours to reach equilibrium. After equilibrium was attained, the adsorbate was separated from the nano-sized adsorbent particles using a strong permanent magnet made of Nd-Fe-B. The supernatant was taken. The separation process for each solution was carried out in the same period. The amount of the dye adsorbed by the adsorbent was measured from the concentration change of RhB in supernatant using UV/vis spectrophotometer (model Shimadzu UV-1601). Each experiment was conducted in two samples and three times for each sample

under the same operational conditions. The equilibrium solid phase concentration was calculated by equation [3-1] based on a mass balance relationship.

$$q = (C_i - C_e).\frac{V}{m} \qquad [3\text{-}1]$$

where C_i and C_e (mg/L) are the initial and equilibrium concentrations of dye solution put in contact with the adsorbent, respectively; m (g) is the mass of the wet adsorbent and V (ml) is the volume of dye solution.

The illustration of the interaction between Fe_3O_4 nanoparticles and CMCD, and isolation of targeted molecules by magnetic separation are shown in Figure 3-4, while Figure 3-5 illustrates the separation of dyes (RhB and AB25) using CMCD-MNPs.

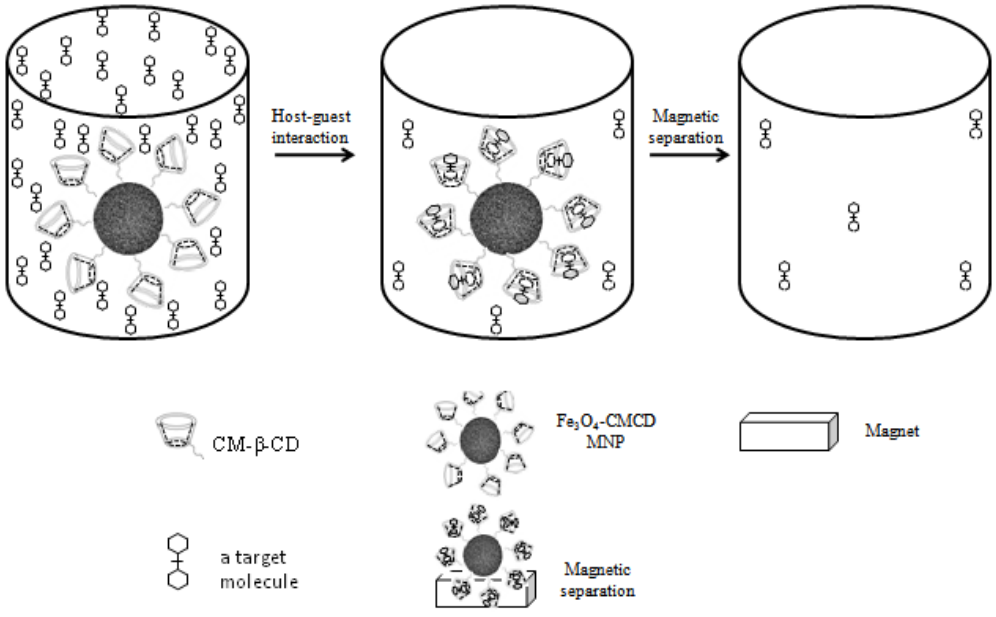

Figure 3-4 Schematic illustration of Fe_3O_4-CMCD interaction and isolation of targeted molecules by magnetic separation

(a) (b)

Figure 3-5 An illustration of dyes removal using CMCD-MNPs, (a) RhB and (b) AB25
In each Figure, *left vial*: before adsorption, *middle vial*: after adsorption by CMCD-MNPs and *right vial*: after desorption.

3.3.1.1. The effect of pH on dye adsorption

The uptake of RhB and AB25 using CMCD-MNPs adsorbent in both acidic and alkaline solution were investigated by conducting batch adsorption experiments with an initial concentration of the dyes solutions ranging from 100 to 1500 mg/L for RhB and those of AB25 were 100 to 3000 mg/L, at a pH range of 2 to 11. The range of the initial concentrations of AB25 was extended because for some pHs, the plateau part of the equilibrium adsorption capacities (q_e) could be achieved by increasing concentrations. The pHs were measured by a digital pHmeter (model: Hanna instrument 8417). The pHs of the solutions were prepared with 0.05 M buffer solutions and then adjusted by adding either 0.1 M HNO_3 or 0.1 M NaOH. Approximately 120 mg of the wet adsorbent (CMCD-MNPs) was brought into contact with 10 ml of the dye aqueous solution of each concentration at different pHs in sample vials. Then each sample vial was shaken (200 rpm) using Thermolyne Oscillator for at least 5 hours to attain the equilibrium condition. Upon equilibrium, nanoparticles were separated from supernatant by magnetic

decantation. Then, 20 μL of dye solution was diluted with 3 ml of buffer solution for each pH and analyzed the concentration and absorbance using UV/vis spectrophotometer (Shimadzu UV-1601).

3.3.1.2. The effect of temperature on dye adsorption

The effect of temperature was investigated by conducting equilibrium experiments using concentrations of RhB from 100 to 1,500 mg/L and AB25 from 100 to 3,000 mg/L, both were performed at their optimum pHs by varying the temperature of the shaker from 298 to 328 K. Each sample vial was mixed with 120 mg of wet adsorbent and agitated for 5 hours at 200 rpm. All other factors such as pH and adsorbent dosage were maintained constant. When reaching equilibrium, the same procedures to calculate the equilibrium solid phase concentration were repeated.

3.3.2. Adsorption equilibrium isotherm

The experiment was conducted in the CMCD-MNP adsorbent using RhB concentrations varied from 100 to 1500 mg/L and at pH 5 and a variation of temperatures of 298, 313 and 328 K. For AB25, the experiment was carried out at concentrations from 100 to 3000 mg/L, pH 3 and the same variation of temperatures as those of RhB. The mixture was agitated at 200 rpm for 5 hours to reach the equilibrium condition. Other factors such as adsorbent dose were maintained constant. When reaching equilibrium, the same procedures to calculate the equilibrium solid phase concentration were repeated.

3.3.3. Kinetics study

The rate of dye adsorbed was studied at regular intervals of time within 180 minutes using a concentration of 250 mg/L for both dyes, at their optimum pHs and temperatures varied from 298 to 328 K. The mixture was agitated at 200 rpm until the equilibrium condition was attained. Other factors were maintained constant. When reaching equilibrium, the same procedures to calculate the equilibrium solid phase concentration were carried out.

The experimental concentrations of the dye in kinetic and equilibrium studies were measured based on the calibration curve.

3.3.4. Desorption experiments

Desorption of RhB and AB25 from magnetic nanoparticles was studied by applying various desorbents, for example organic solvents (methanol and ethanol), organic acids (acetic acid) as well as acid and alkaline solutions. First of all, equilibrium experiments for the two dyes were conducted on the CMCD-MNPs adsorbent at their optimum pHs and at room temperature. After reaching 5 hours, desorbing agents (5 mL) were directly added to the solutions. Then, the agitation process was continued for another 5 hours. After reaching the second 5 hours, supernatants were collected using magnetic decantation. Then, 20 μL of supernatant was diluted with 3 ml of buffer solution and analyzed using UV/vis spectrophotometer (Shimadzu UV-1601). The experimental concentrations of the supernatants were measured based on the calibration curve. The percentage of dye desorbed was calculated with the following equation:

$$\%\ dye\ desorbed\ = \frac{\left((C_e)_2 - (C_e)_{2,0}\right).(V_1 + V_2)}{(q_e)_1.S}\ x\ 100\% \qquad [3\text{-}2]$$

$$\%\ dye\ desorbed\ = \frac{\left((C_e)_2 - (C_e)_{2,0}\right).(V_1 + V_2)}{(C_0\ -\ (Ce)_1).V_1}\ x\ 100\% \qquad [3\text{-}3]$$

$$(Ce)_{2,0} = \frac{(Ce)_1.V_1}{(V_1 + V_2)} \qquad [3\text{-}4]$$

where C_0 (mg/L) is the initial concentration of the dye; $(C_e)_1$ (mg/L) is the equilibrium concentration of the dye adsorbed by CMCD-MNPs; $(C_e)_{2,0}$ and $(C_e)_2$ (mg/L) are the equilibrium concentration of the dye without desorption and desorbed by desorbing agent, respectively; $(q_e)_1$ (mg/g) is the adsorption capacity at equilibrium; V_1 and V_2 (ml) are the volumes of dye solution and desorbing agent, respectively, and S (g) is the mass of magnetic nanoparticles added.

3.3.5. Recovery experiment

Long term stability and regeneration of the adsorbent are key factors for an adsorbent since they relate to the cost analysis. The cost of the adsorbent can be less if the adsorbent possesses high reproducibility of adsorption and desorption properties. Therefore, it is important to observe the recyclability of CM-β-CD functionalized on the surface of magnetic nanoparticles adsorbent. Recovery study was investigated by conducting adsorption and desorption experiments for several cycles. For each cycle, the adsorption capacity of the dye and the percentage of dye desorbed were calculated and tabulated. In each adsorption cycle, two samples of the 10 ml of dye solution with an initial concentration of 250 mg/L were added with 120 mg of wet adsorbent at each optimum pH and room temperature. In the desorption study, a-5-ml of desorbent was added as to

each sample. The desorbing agents were mixed to samples after they had attained the equilibrium (approximately 5 hours for adsorption). After reaching the desorption equilibrium, CMCP-MNPs were washed with water to remove the remaining dye and then the adsorbent was applied for additional dye separation.

3.3.6. Error analysis

Although the adsorption models seem to be simple mathematical structures and have relatively few adjustable parameters, the parameter estimation problems in the modelling of the adsorption data are usually non-linear and the solutions are non-convex. In general, a transformation of non-linear models to linear ones usually results in parameter estimation error and uncertainties [85]. The error function has to be determined to evaluate the fit the experimental data to the isotherm models. The isotherm parameters are generally obtained by a minimization the relative difference between the experimental and the theoretical data of adsorption capacities as presented [86]:

$$F_{obj} = \sum_{i=1}^{n} \left(\frac{q_e^{\exp} - q_e^{calc}}{q_e^{\exp}} \right)_i^2 \qquad [3\text{-}5]$$

Where q_e^{exp} and q_e^{cal} (mg/g) are the experimental and predicted adsorption capacity at equilibrium respectively, n is the total number of experimental data. If the data of the model are similar to those of experiment, F_{obj} is a small number, and vice versa.

3.4. Analytical methods

3.4.1. Fourier Transform Infrared Spectroscopy (FTIR)

FTIR is identification (qualitative analysis) used to determine organic and inorganic materials. Infrared light radiation having various wavelengths is passed through the target sample, therefore some is absorbed and some is transmitted. The spectrums obtained give insight of molecular components and structures in the sample. The FTIR measurement was carried out in a Bio-Rad, Model 400 with a KBr background. Approximately 2 mg of dry sample was mixed with 198 mg of KBr powder, and then the mixture was pressed to form a pellet which is used for the measurement. The spectrum in percent transmission was measured at various wavelengths from 400 to 4000 cm^{-1}. Absorption bands in the range of 1500 to 4000 wavenumbers are particularly caused by functional groups such as -OH, C=O, N-H, and $CH_{3,}$ while a range of 400 wavelength numbers is considered as the fingerprint region for each material.

3.4.2. Transmission Electronic Microscopy (TEM)

TEM is used to characterize the size and morphology of the as-synthesized nano-sized magnetic particles. For TEM analysis, a bright-field TEM (Model: JEM-2010) was used to determine the size of the MNPs. To prepare the sample for TEM measurement, a certain quantity of MNPs was diluted in ethanol, then the diluted sample was dropped on a copper film (200 mesh and covered with formvar/carbon) to form a thin layer. The copper film was dried at room temperature for 24 hours before TEM measurement.

3.4.3. Vibrating Sample Magnetometer (VSM)

The VSM is the basic instrument for characterization of magnetic property of materials as a function of magnetic field and temperature. Before used for VSM measurement (Model: 1600, DMS), a certain amount of wet magnetic particles were freeze-dried using Edwards freeze-dryer, ESM 1342 for 24 hours. A plastic cylinder cell containing the sample was attached on a rod in the applied magnetic field from -15,000 to 15,000 Oe, in which the rod was vibrating in a certain rate. The magnetization curve of the magnetic particles at room temperature was then plotted with the changes of magnetic field strength and its direction.

3.4.4. Zeta Potential

The measurement of zeta potential gives information of the pI (isoelectric point) or pH_{ZPC} (pH of zero point charged) of the magnetic particles which is significant in determining the magnitude of attraction or repulsion between particles in colloid system [5]. The zeta potentials of the synthesized nano-sized magnetic particles were measured at maximum 100 runs per analysis using a Brookhaven Zeta Plus 90 analyzer at different pHs from 2 to 12, and room temperature. Samples at different pH were prepared by diluting 5 mg of dry Fe_3O_4 magnetic particles either bare or CMCD coated MNPs in 100 ml of 10^{-3} M NaCl. The pHs of the aqueous solutions were adjusted by HCl or NaOH solutions.

3.4.5. X-ray Diffraction Analysis (XRD)

The crystallographic structure of the nano-sized the magnetic particles were observed by X-ray diffraction. The instrument used is a Shimadzu XRD-6000 Spectrometer, 40 kV,

30 mA, wavelength λ = 0.154 nm). It applied a monochromatized X-ray beam from nickel filtered Cu Kα radiation. The pattern obtained was plotted by intensity versus 2θ in the range of 20°-80°.

3.4.6. Thermogravimetric Analysis (TGA)

TGA is an analysis technique used to measure the amount and rate of weight change of a sample as a function of temperature and time in a specified pressure. The thermal analysis technique is applied to estimate the composition of the multi component samples, moisture content of samples and their thermal stability at temperatures up to 1000^0C. The technique can confirm the attachment of CM-β-CD onto the surface of magnetite nanoparticles, thus, it can give information of the binding efficiency of CM-β-CD on the surface of MNPs. TGA test is conducted with a thermal analysis instrument, TA 2050/winNT. The same amount of dry uncoated MNPs and CMCD-MNPs were loaded to the system under N_2 atmosphere at temperatures from 20^0C to 700^0C with a ramp rate of 10^0C per minute and then weight loss was observed at this range.

3.4.7. X-ray Photoelectron Spectroscopy (XPS)

XPS is a technique that utilizes soft x-ray and the emitted photoelectrons as a distribution of kinetic energy. The method is used to analyze the composition and electronic state of the surface region of a sample by observing the energy differences between x-ray and photoelectron as core level electrons' binding energies (BEs). The measurement of XPS was carried out on a VG ESCALAB Mk II spectrometer with a Mg Kα X-ray source (1253.6 eV photons) at a constant retard ratio of 40. The technique was applied to

determine elements such as C, O and Fe in the samples. The dry samples were mounted on the standard sample studs by means of double-sided adhesive tapes. The core-level binding energies were obtained at an angle of 75^0 between photoelectrons and samples surface. The X-ray source was operated at a reduced power of 120 W and at 7.5×10^{-9} Torr or lower during each measurement.

Chapter 4 Characterization of magnetic nanoparticles, uncoated and surface modified with carboxymethyl-beta-cyclodextrin

4.1. Introduction

Fe_3O_4 nanoparticles show an efficient tool for the separation in aqueous environments as they can be prepared easily and inexpensively, and modified with different polymeric materials to enhance their colloidal stability against gravitational force, morphology and functionality and to reduce interaction and aggregation of particles. The small sizes of the magnetic particles also exhibit a large surface area to unit volume ratio. However, there are still interactions between these small particles which mostly arise from the dipole-dipole interaction. The effects of the interactions have been explored extensively for the past few years [87].

Many efforts to modify the surface of magnetic particles have been studied and developed in order to minimize agglomeration between particles and to obtain organic-inorganic nano-sized magnetic particles. MNPs can be further functionalized with non-specific moieties (ionic, hydrophobic, hydrogen bond), group specific (dye ligand, immobilized metal affinity), and highly specific ligands (antigen-antibody, enzyme-inhibitor) [47]. Recently, there is an interest to explore the possibility of using polysaccharides and their derivatives to encapsulate MNPs for chemical and bioseparation processes. The most widely used ones are agarose and chitosan [47].

Some researchers have prepared and modified the surface of Fe_3O_4 nano-sized particles with chitosan and used them for bioseparation [59]. However, less work has been published for the use of CDs as the surface coating of magnetic particles. In fact, the surface modification of magnetic particles with CDs for dye removal possesses a variety of advantages, for instance cost-effective material, very abundant and widely available in many countries since it is derived from starch, environmentally friendly, good adsorption capacity to wide range of pollutants such as dyes, heavy metals and other organic pollutants either in diluted or concentrated feed, fast kinetics in dye adsorption, outstanding versatility and unique ability to encapsulate contaminants by forming complexes in their cavities. Therefore, in this project, nano-sized magnetic particles were prepared through surface functionalization of Fe_3O_4 as the core and carboxymethyl-beta-cyclodextrin (CM-β-CD) as the outer shell. The nanoadsorbent was synthesized via one step chemical co-precipitation method in vigorous mechanical stirring, alkaline environment and inert atmosphere. Before used as adsorbent for the removal of anionic and cationic dyes, the characteristics of magnetic nanoparticles were observed. The conformation of binding CM-β-CD to the iron oxide particles was investigated by FTIR, TGA and XPS. The superparamagnetic property of uncoated and CM-β-CD coated on magnetic particles was confirmed by VSM. The size and morphology of the resulted magnetic nanoparticles were analyzed by TEM. The domination of Fe_3O_4 phase in the as-synthesized nanoadsorbent was investigated by XRD. The pI and electrostatic dispersion of the nano adsorbent was observed by zeta potential analysis.

4.2. Results and discussion

4.2.1. Fourier Transform Infrared Spectroscopy (FTIR)

The FTIR spectra of uncoated MNPs, CMCD-MNPs and CM-β-CD in the 400-4000 cm^{-1} wavelength numbers are shown in Figure 4-1. The spectrums of uncoated MNPs have the characteristic adsorption band of Fe-O in the tetrahedral site and -OH stretching vibration of 579 and 3396 cm^{-1} respectively. Those of CMCD-MNPs are slightly different, 586 and 3387 cm^{-1}. In general, absorption bands with wavenumbers of 1500 to 4000 cm^{-1} typically represent functional groups (e.g. -OH, C=O, N-H, and CH_3). Therefore, these ranges are highly particular for each material (fingerprint region) [5]. The characteristic peaks of CM-β-CD spectrums were 947, 1030, 1057 and 1704 cm^{-1}. The peaks at 945, 1030, and 1057 cm^{-1} are attributed to the R-1,4-bond skeleton vibration of β-CD, antisymmetric glycosidic ν_a (C-O-C) vibrations and coupled ν (C-C/C-O) stretching vibrations respectively [2]. While the peak at 1704 cm^{-1} is corresponded to the attachment of the carboxymethyl group (-$COOCH_3$) on the β-CD molecule. These main peaks are in a range of 900 to 1200 cm^{-1} and slightly shifted to 945, 1026, and 1150 cm^{-1} in the spectrums of CMCD-MNPs as shown in Figure 4-1 (b). In addition, two significant characteristic peaks at 1620 and 1400 cm^{-1} are attributed to COOM (M is metal ions) groups which shows that the COOH groups of CM-β-CD were reacted with OH groups of Fe_3O_4 to form iron-carboxylates [2, 88]. Thus, it can be concluded that CM-β-CD has been successfully coated on the surface of Fe_3O_4 nanoparticles adsorbent.

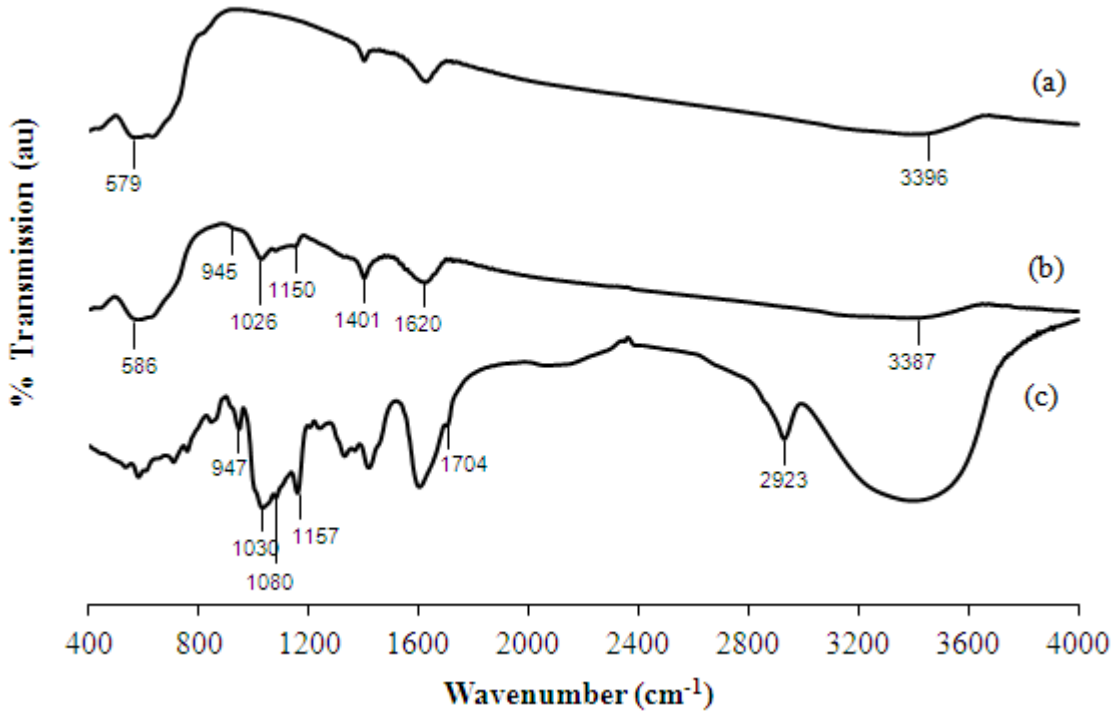

Figure 4-1 FTIR spectra of (a) uncoated MNPs, (b) CMCD-MNPs and (c) CM-β-CD

4.2.2. Transmission Electronic Microscopy (TEM)

Typical TEM morphology and size distribution of uncoated MNPs and CM-β-CD coated MNPs are shown in Figure 4-2. As observed from micrographs, the magnetic particles are specifically well shaped spherical or ellipsoidal. The mean diameter of CM-β-CD coated magnetic nanoparticles is about 11 nm which is slightly higher than that of uncoated magnetic nanoparticles (mean diameter is about 10 nm) [89]. This finding show that the binding process does not result in agglomeration and change in size of the nanoparticles. It is known that the magnetic particles with size less than 30 nm will exhibit superparamagnetism [2, 34]. Thus the resulted surface coating of MNPs coated with CM-β-CD shows superparamagnetic properties which are further evidenced by VSM studies.

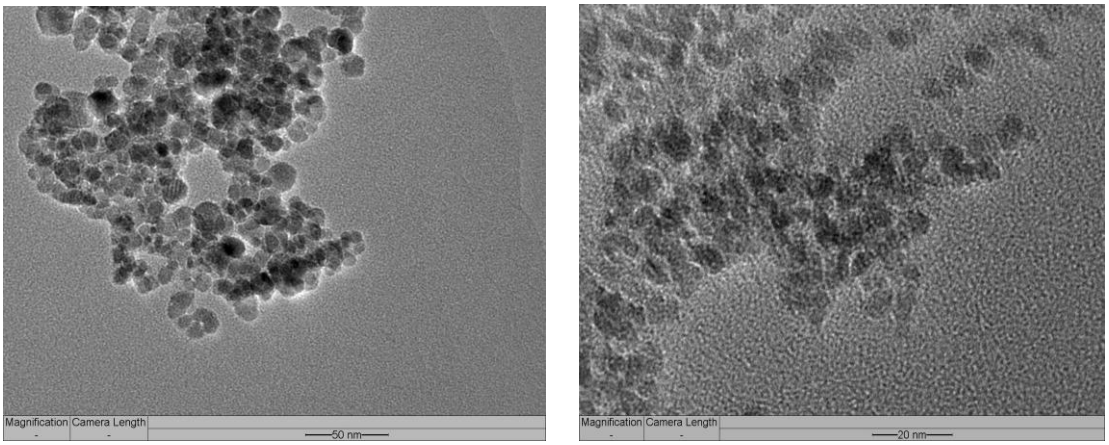

(a) (b)

Figure 4-2 TEM micrographs of (a) Bare MNPs and (b) CMCD-MNPs

4.2.3. Vibrating Sample Magnetometer (VSM)

The magnetic properties of both uncoated and CM-β-CD coated on magnetic manoparticles were measured by VSM at room temperature. In the absence of magnetic fields, these particles showed single domain magnetic dipoles which show no preferred directional ordering, due to the domination of the thermal forces towards the dispersion of these particles. While in the presence of sufficiently high external magnetic field, the particles exhibited a referential ordering in the direction of this field. The hysteresis loops, a particular characteristic of superparamagnetic particles can be seen in Figure 4-3. Both bare and CM-β-CD coated magnetic nanoparticles possess the hysteresis loops, it is thus indicated that both particles have superparamagnetic properties. From *M* versus *H* curve, the saturation magnetization value (*Ms*) of bare MNP was found to be 75 emu g^{-1} which is less than that of its bulk counterpart (92 emu g^{-1}) [90]. After coated with CM-β-CD, the saturation magnetization value of magnetic particles became 54 emu g^{-1}. A decrease of M_s might be attributed to the existence of non-magnetic materials (CM-β-CD layer) on the surface of MNPs leading to a formation of non-magnetic shell. This finding

indicates that surface coating with CM-β-CD possesses highly efficient magnetic manipulation when used as nanoadsorbents for the separation of dyes from aqueous solution under relatively low external magnetic field.

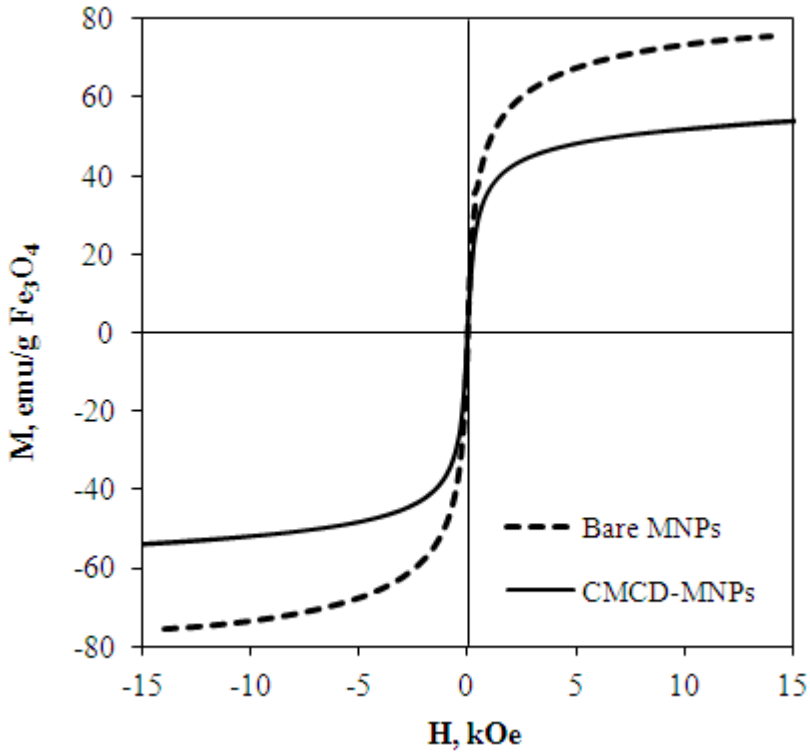

Figure 4-3 Magnetization curve of bare MNPs and CMCD coated MNPs at room temperature

4.2.4. Zeta Potential

As can be seen in Figure 4-4, the isoelectric point of uncoated MNPs was 6.7; it is consistent with the value reported in the literature [3]. After we had grafted with CM-β-CD, the point of zero charge occurred at pH 4.7. The finding indicates a successful surface coating of CM-β-CD onto the nano-sized magnetic particle adsorbent. Moreover MNPs modified with CM-β-CD yields acidic surface since pH_{pzc} is lower than that of

uncoated MNPs and this surface acidity is due to introduction of several oxygen containing functional groups [90].

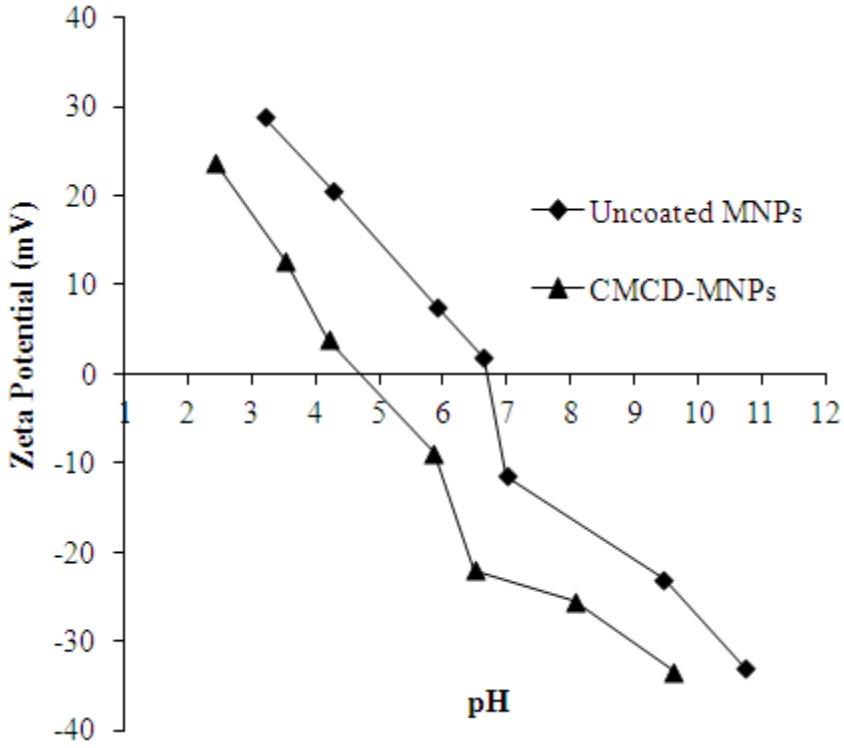

Figure 4-4 Zeta potential of uncoated MNPs and CM-β-CD coated MNPs

4.2.5. X-ray Diffraction Analysis (XRD)

Figure 4-5 shows the XRD pattern of both uncoated and CM-β-CD coated magnetite particles. There were six characteristic peaks [91, 92] occurred at 2θ of, 30.1^0, 35.6^0, 43.3^0, 53.3^0, 57.1^0 and 62.9^0 corresponded to their indices (220), (311), (400), (422), (511), and (440) respectively. The six characteristics peaks show that the nano-sized magnetic particles are pure Fe_3O_4 with spinel structure. Moreover, after being surface coated by CM-β-CD, the phase of Fe_3O_4 did not change which was proved by no other peaks detected which were related to impurities. The average crystal size of magnetic nanoparticles is calculated using Debye-Scherrer's equation, $D_{hkl} = 0.9\ \lambda / (\beta \cos\theta)$. Here,

λ is x-ray wavelength (0.154 nm), β is the half of XRD diffraction lines in radian and θ is half diffraction angle of 2θ. From the highest peak, 311, the diameter of bare MNPs and CMCD MNPs were 10 nm and 10.5 nm, respectively.

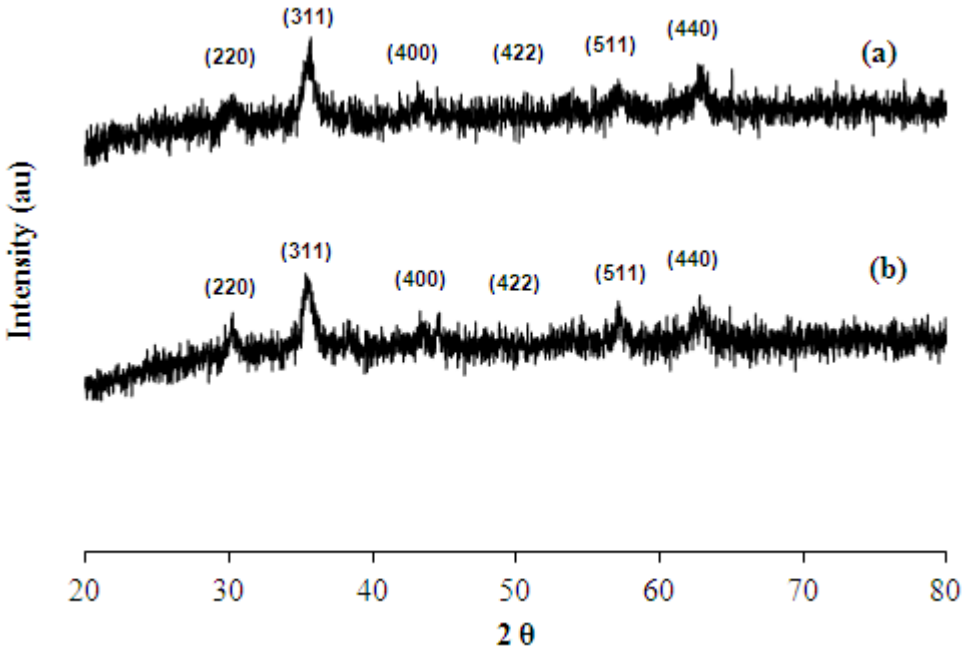

Figure 4-5 XRD pattern of (a) Uncoated MNPs and (b) CMCD-MNPs

4.2.6. Thermogravimetric Analysis (TGA)

The amount of CM-β-CD bound on the surface of iron oxide nanoparticle was observed by thermogravimetric analyses for uncoated and CM-β-CD coated MNPs. Figure 4-6 demonstrates that the weight loss of the uncoated MNP is 1.6% at temperatures below 140^0C which may be caused by the loss of water absorbed in the sample. From 20 to 700^0C, the total weight loss of bare MNP is 2.4% which may be due to the loss of the water absorbed and dehydration of -OH groups in the sample. The weight loss of CMCD coated on the surface of MNP can be seen in Figure 4-6 (b). At a temperature less than 200^0C, there was a slow weight loss due to the residual water released. Between 200 to

400^0C, the sample lost CM-β-CD due to its thermal decomposition of CM-β-CD moieties [2]. It is depicted from a sharp decrease in weight from 1.8% to 12.8%. Therefore, TGA curve gives insight about the attachment of CM-β-CD onto the surface of MNPs was successful.

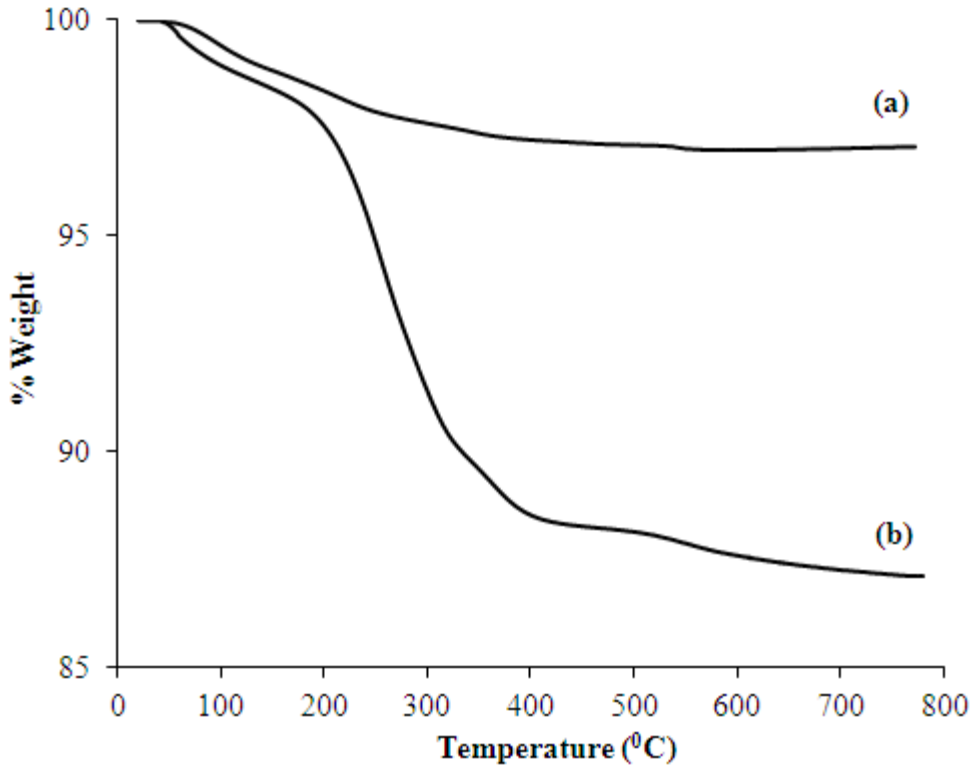

Figure 4-6 TGA curve of (a) Uncoated MNPs and (b) CMCD coated MNPs

4.2.7. X-ray Photoelectron Spectroscopy (XPS)

The XPS wide scan spectrum of bare MNPs and CMCD coated MNPs are shown in Figure 4-7. As can be seen, the spectrum (a) shows the C1s, O1s and Fe2p peaks of uncoated magnetic particles are at about 281.6, 527.1 and 707.8 eV respectively. The last two peaks were slightly shifted to 527.2 and 708 eV after CM-β-CD has been coated onto the surface of MNP whereas the first peak remained constant. The intensities of C1s were

increased from 8,020 to 12,230 cps and so were those of O1s, from 27,880 to 36,170 cps. They are attributed to the attachment of carboxyl and hydroxyl groups to the metal ion. Therefore, XPS analysis of the surface composition agreed with the FTIR analysis.

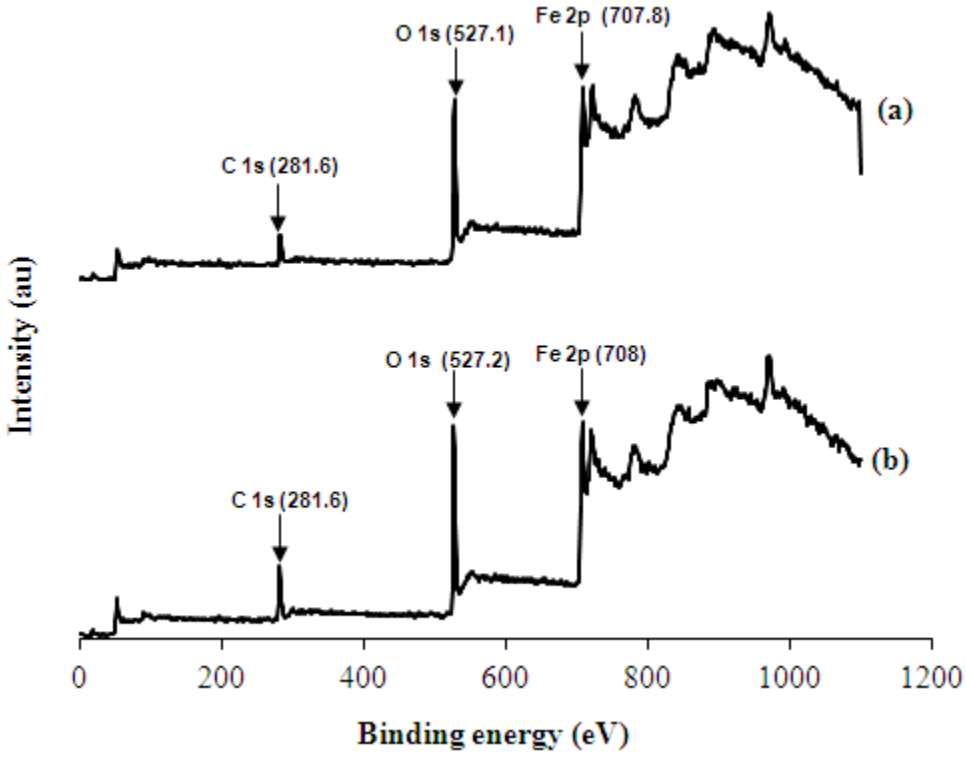

Figure 4-7 XPS wide scan spectra of (a) Uncoated MNPs and (b) CMCD-MNPs

The chemical binding in of CM-β-CD on the surface of MNPs is demonstrated by Figure 4-8. It shows the C 1s deconvoluted spectrum which can be curve-fitted into four peak components with binding energy of about 284.4, 286.4, 287.9 and 288.6 eV, attributable to the carbon atoms in the forms of C-C (aromatic), C-O (alcoholic hydroxyl and ether), C=O (carbonyl) and COO^- (carboxyl and ester) species, respectively. The C-O/C-O-C and C=O peaks are the characteristic of CM-β-CD. Moreover, the presence of COO^- peak at 288.6 eV indicates that the COOH functional groups on CM-β-CD reacted with surface OH groups to from metal-carboxylate (COOM). The findings shown by Figures 4-7 and 4-8 confirm a successful coating of CM-β-CD onto the surface of the nano-sized magnetic particles.

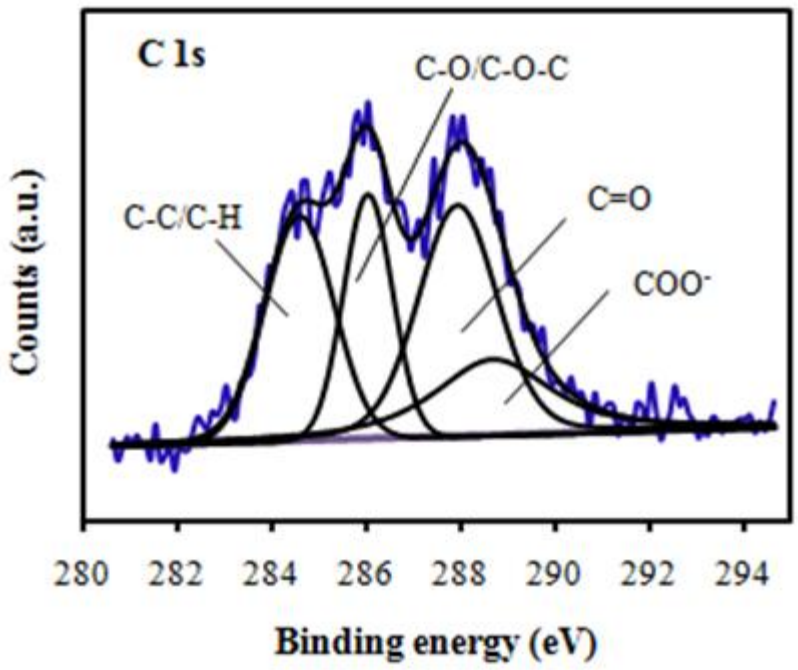

Figure 4-8 XPS C 1s spectrum of CMCD-MNPs

4.3. Conclusions

Surface modification of magnetic nanoparticles with carboxymethyl-beta-cyclodextrin was prepared by one step chemical co-precipitation method. Before coating on the surface of MNPs, carboxymethyl groups were attached to the surface of beta-cyclodextrin. In this coating, the carboxyl (COOH) groups of CM-β-CD directly react with the surface OH groups on the magnetite to form Fe-carboxylate (COOM, M=metal). The reaction was performed at vigorous stirring, alkaline condition, 90^0C and inert environment. Besides functionalizing the surface of MNPs, uncoated MNPs were also prepared with the same method in the absence of CM-β-CD and at 80^0C. The two particles, bare and coated magnetic particles were characterized using Transmission Electron Microscopy (TEM), X-ray Diffractometer (XRD) and Vibrating Sample

Magnetometer (VSM). TEM characterization indicated that the mean diameters of uncoated and CM-β-CD coated MNP were 10 and 11 nm, respectively. Both particles also exhibited superparamagnetic properties showed by VSM analysis. The confirmation of the grafting of CM-β-CD to the surface of Fe_3O_4 nanoparticles was analysis using Thermogravimetric Analysis (TGA), Fourier Transform Spectroscopy (FTIR) and X-ray Photoelectron Spectroscopy (XPS). The two types of magnetic particles were used as adsorbents for the separation of cationic and anionic dyes, Rhodamine B and Acid Blue 25, in aqueous solution.

Chapter 5 Adsorption, desorption and regeneration experiments of a basic dye (Rhodamine B) using CMCD-MNPs

5.1. Introduction

The development of the industry and growth of population require an intensive protection of water and soils from residues and contamination from chemicals, hazardous organic compounds, fuels and heavy metals. A variety of industries such as pulp, paper, textile, plastics consume chemicals and dyes in production processes and release a large amount of wastewater. Hence, clean water resources become finite and scarce.

The chemicals used in various industries, such as dyes generate a considerable polluted and coloured wastewater [9, 16]. In addition, dyeing process also relates to other materials such as particulates, processing assistants, salts, surfactants, acids and alkalis [93]. Therefore, the effluent of dye wastewater contains numerous pollutants such as acid or caustic, dissolved solid, toxic compound like heavy metals, and colour. In addition, most industries use synthetic dyes which are produced on a large scale as it is estimated that more than 100,000 commercially available dyes in the world [10]. Synthetic dyes are specifically designed as highly stable molecules, recalcitrant to be degraded by light, chemical and biological treatment. They are toxic, carcinogenic, and teratogenic compounds [94]. Most of them are resistant to detergent, photo degradation, biodegradation, oxidizing agents, very soluble in water and non-degradable [54]. Some commercial synthetic dyes usually have unreported large complex structures and they also a major class of recalcitrant organic compounds [65]. They are extensively applied in

many fields of up-to-date technology, such as textile and leather tanning industries, paper production, food technology, and agricultural research. Due to their wide use in industries, they are common water contaminants and difficult to remove as a result of their complex aromatic structure [10]. Thus, they can be a serious threat to aquatic ecosystem and living things.

The most important groups of synthetic dyes are anthraquinone, phthalocyanine, triarylmethane and azo dyes. The azo dyes characterized by an azo group consisting of two nitrogen atoms, are the largest class of dyes used in textile industry. Within the azo dyes, many dyes such as acid, reactive, disperse, vat, metal complex, mordant, direct, basic and sulphur dyes, can be derived [70]. Among the various classes of dyes, basic dyes are the brightest class of soluble dyes used by the textile industries. In general, basic dyes, often called as cationic dyes are dyes having cationic properties due to the chromophore as a part of positive charged ion which is probably delocalized on the nitrogen atoms [65]. They have affinity to act upon materials with negatively charged ions. They have high brilliance and intensity of colours so they are highly visible even in very low concentration and also classified as toxic colorant [95]. Consequently, they are often considered as the most problematic classes of dye [71]. Moreover, basic dyes are also low cost dyes. They are usually applied to wool, silk, cotton and modified acrylic fibres [9].

One class of basic dyes is Rhodamine B (RhB) or Basic Violet 10 (C.I. number 45170), the most important xanthene dye. The dye is used as dye laser, water tracing agent,

biological stain, in the pharmaceutical and cosmetic industries, and even, in food stuff [72]. Several reasons are considered before choosing RhB as a model of guest molecules, for example its toxicity, high tintorial value, soluble in water and some organic solvent like methanol and ethanol, its more rigid structure than other organic dyes [73], its commercial use without further purification and its widely present in the in the wastewaters of several industries, for instance textile, leather, jute and food industries [74].

Among various physical, chemical and biological methods applied to remove dye pollutant from wastewater, physical adsorption has increasingly received more attention due to its simplicity and efficiency for the removal of dyes from water stream, cost-effective and no adverse substances produced [96, 97] in comparison to other separation techniques such as coagulation, flocculation, precipitation and activated sludge [98]. Several works have been published on the uptake of dye in aqueous solution through adsorption, however, only limited work has been published on adsorption of dye contaminants using nano-sized surface functionalized magnetic particles. Therefore, in this project, magnetic nanoparticles, both uncoated and CM-β-CD coated on their surfaces, were prepared and characterized, as presented in Chapter 4. The nano-sized magnetic particles grafted with CM-β-CD were used as adsorbent for separation of RhB from aqueous solution at different adsorption parameters, pH and temperature. In general, pHs of solution affect the surface charges of adsorbents. Lower pHs provide more protons so the surface of the adsorbent can be more positive, and vice versa. While in adsorption separation, temperature has several effects in the solubility of the solute

molecules, the swelling capacity of the adsorbent and the equilibrium condition associated with the exothermicity of the adsorption process [24]. The enhancement of coating strategy in dye adsorption was also compared to uncoated MNPs performed at room temperature, optimum pH and under other similar conditions. To confirm the attachment of RhB onto the surface of CMCD-MNPs, FTIR analysis was carried out. The similarities between theoretical and experimental adsorption capacities were observed by error analysis. After performing dye adsorption, desorption of RhB was studied in different chemicals to determine the adsorption mechanism of the dye to the adsorbent and the possibility of the adsorbent recovery. The desorbing agents used in this study were organic solvents (methanol and ethanol), organic acids (acetic acid) as well as acid and alkaline solutions. All experiments were conducted in batch adsorption technique. Evaluation of structural changes of RhB in adsorption, desorption and recycle processes was also carried out by FTIR.

5.2. Results and discussion

5.2.1. Adsorption at different pHs

In this work, the effect of pH on the dye adsorption was studied in batch adsorptions at pHs 2 to 11. Here, adsorption equilibriums were run at specific pHs. The solutions were agitated at least 5 hours at room temperature to attain equilibrium condition. Here, the pH of the aqueous solution has a significant effect for the uptake of RhB by CMCD-MNPs adsorbent.

As can be seen in Figure 5-1, the maximum and minimum adsorption capacities of RhB are at pH 5 and 8, respectively. At lower pHs, the electrostatic repulsion between cationic RhB and positively charged CMCD-MNPs leads to the decreased percentage of adsorption. Therefore, when pH decreases from 5 to lower ones, the adsorption capacity reduces. However, as pH increases, from 5 to 8, RhB molecules change their forms from monomeric to dimeric/zwitterionic forms with Figure 2-7 as a reference. The aggregation of RhB molecules is due to the attractive electrostatic interactions between carboxyl (COO^-) and xanthane (N^+) groups of the dye [22, 23]. Consequently, the dye molecules become bigger and make them difficult to penetrate to the pores of the adsorbent. This phenomenon has also been observed by Ghanadzadeh et al [99] when they studied the aggregation of RhB in the microporous solid hosts. They found that when pHs are higher than 8, there were more hydroxyl (OH^-) ions present in the solution which give rise to a competition with COO^- to bind N^+. So in our case, at pHs higher than 8, the RhB molecules become less aggregates or the formation of dimers decreases, which causes the adsorption of RhB onto CMCD-MNPs begins to rise again [22, 23].

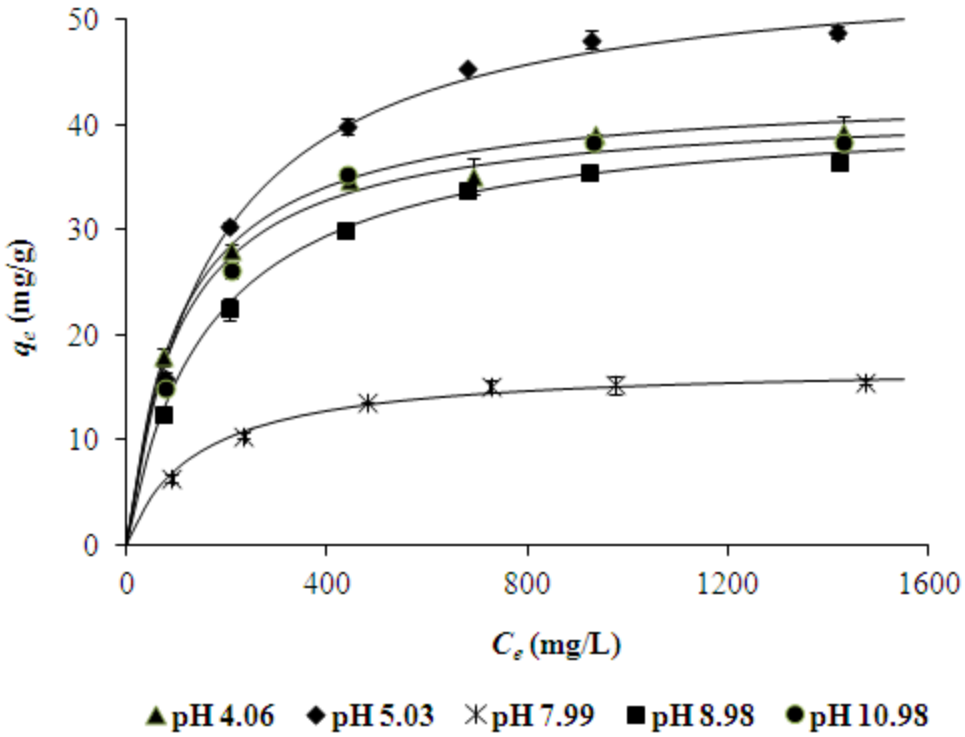

Figure 5-1 RhB adsorption on CMCD-MNPs at different pHs (condition: initial concentrations = 100 to 1500 mg/L, adsorbent mass = ~120 mg, pH = 2 to 11, agitation time = 5 hours, volume = 10 ml, agitation speed = 200 rpm and room temperature)

5.2.2. Adsorption equilibrium

The adsorption isotherms of RhB adsorbed onto uncoated and CM-β-CD grafted on the surface of magnetic nanoparticles (bare MNPs and CMCD-MNPs) were studied at the optimum pH (pH 5) with initial dye concentrations ranging from 100 to 1500 mg/L. The RhB adsorption on CMCD-MNPs was also explored at different temperatures from 298 to 328 K. Figure 5-2 shows the experimental adsorption data for RhB on uncoated and CM-β-CD coated MNPs adsorbents. It demonstrates that for adsorption with CMCD-MNPs at temperatures from 298 to 328 K and also with uncoated MNPs at 298 K, the equilibrium adsorption capacities increased with increasing RhB concentration from 100 to 1000 mg/L. However, with further increase in the dye concentration (>1000 mg/L), the

equilibrium adsorption capacities did not change much and it reached an asymptotic value. Therefore, uncoated and CM-β-CD modified on MNPs adsorbent effectively removes this dye at low initial concentrations; at higher concentrations the isotherms reach a maximum capacity as indicated by the plateau of the figure.

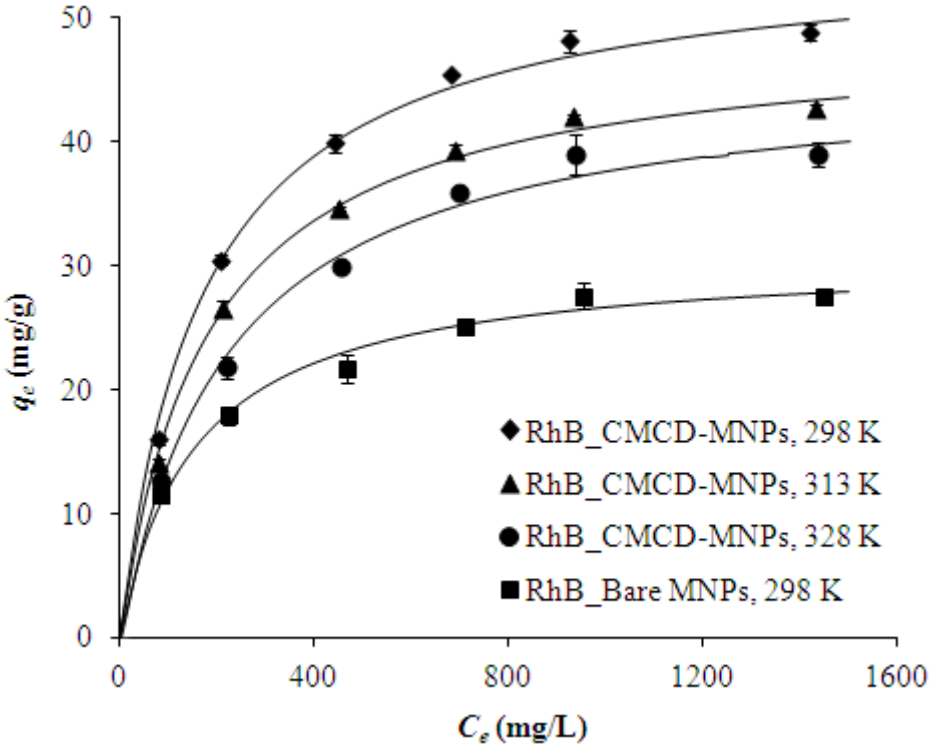

Figure 5-2 Equilibrium isotherm for the adsorption of RhB onto CMCD-MNPs and uncoated MNPs (conditions: initial concentrations = 100 to 1500 mg/L, adsorbent mass = ~ 120 mg, pH 5, agitation time = 5 hours, volume = 10 ml, agitation speed = 200 rpm, temperatures 298, 313 and 328 K)

Figures 5-3 to 5-5 show the fitting of isotherms based on Langmuir, Freundlich and Redlich-Peterson models, respectively. The fitting results, correlation coefficients (R^2) and the least square fittings (F_{obj}), are tabulated in Table 5-1. It can be seen that Langmuir isotherm model can fit better than the other two models. The values of β in Redlich-Peterson model for all temperatures are closed to unity; this shows that Redlich-Peterson model is indeed similar to Langmuir model.

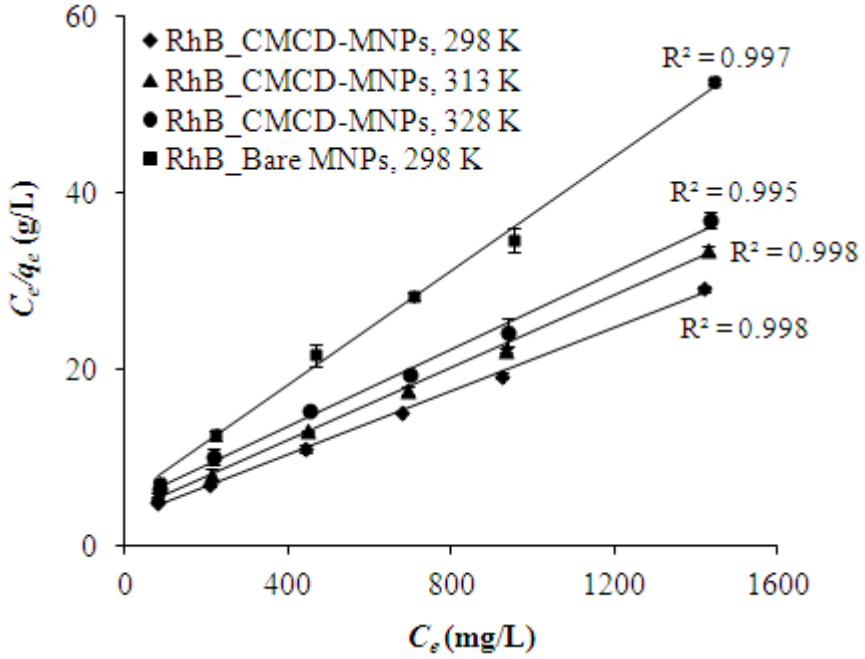

Figure 5-3 Langmuir isotherm plots for the adsorption of RhB onto CMCD-MNPs and uncoated MNPs (conditions: initial concentrations = 100 to 1500 mg/L, adsorbent mass = ~120 mg, pH 5, agitation time = 5 hours, volume = 10 ml, agitation speed = 200 rpm, temperatures 298, 313 and 328 K)

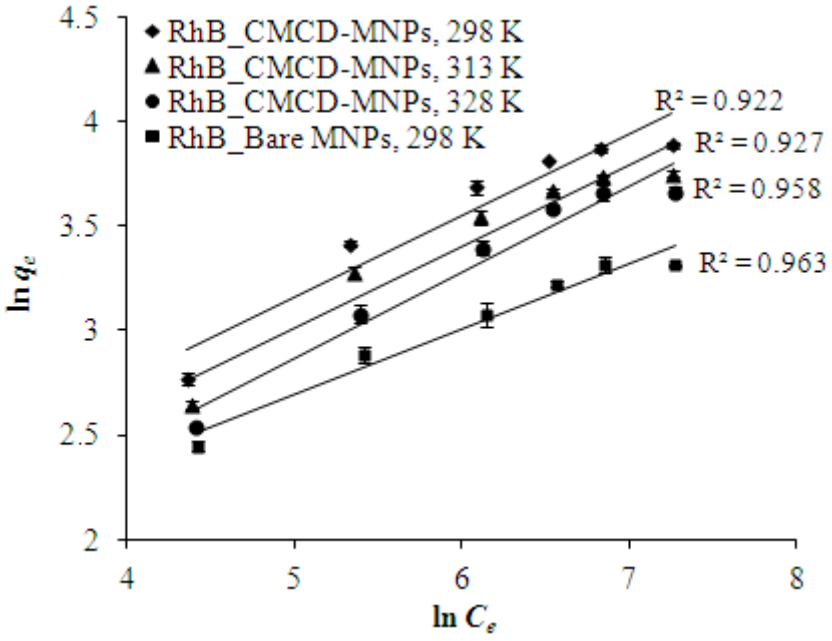

Figure 5-4 Freundlich isotherm plots for the adsorption of RhB onto CMCD-MNPs and uncoated MNPs (conditions: initial concentrations = 100 to 1500 mg/L, adsorbent mass = ~120 mg, pH 5, agitation time = 5 hours, volume = 10 ml, agitation speed = 200 rpm, temperatures 298, 313 and 328 K)

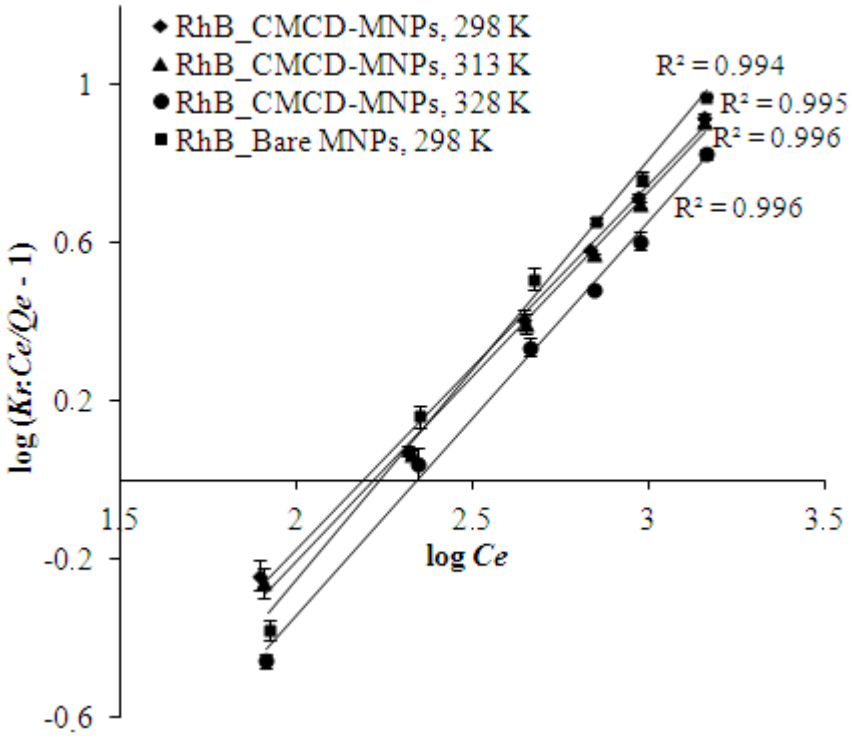

Figure 5-5 Redlich-Peterson isotherm plots for the adsorption of RhB onto CMCD-MNPs and uncoated MNPs (conditions: initial concentrations = 100 to 1500 mg/L, adsorbent mass = ~120 mg, pH 5, agitation time = 5 hours, volume = 10 ml, agitation speed = 200 rpm, temperatures 298, 313 and 328 K)

Table 5-1 Adsorption isotherm parameters for RhB adsorbed onto CMCD-MNPs and uncoated MNPs at pH 5, initial concentrations = 100 to 1500 mg/L, adsorbent mass = ~120 mg, agitation time = 5 hours, volume = 10 ml, agitation speed = 200 rpm, three different temperatures (298, 313 and 328 K)

Isotherm models	Parameters	CMCD-MNPs			Uncoated MNPs (298 K)
		298 K	313 K	328 K	
Langmuir	q_m (mg/g)	55.56±0.14	48.78±0.13	45.87±0.31	30.77±0.17
	K_L (L/g)	0.32±7.9x10^{-4}	0.27±7.1x10^{-4}	0.21±1.4x10^{-3}	0.20±1.1x10^{-3}
	R^2	0.998	0.998	0.995	0.997
	R_L	0.10-0.63	0.11-0.64	0.13-0.69	0.10-0.14
	Error (F_{obj})	0.013	0.029	0.076	0.063
Freundlich	n_F	2.57±7.7x10^{-3}	2.57±6.9x10^{-3}	2.42±4.6x10^{-3}	3.18±5.7x10^{-3}
	K_F (mg/g)/L/g)^n	3.36±0.01	2.92±7.9x10^{-3}	2.24±4.3x10^{-3}	3.07±5.5x10^{-3}
	R^2	0.922	0.927	0.958	0.963
	Error (F_{obj})	0.484	0.276	0.158	0.152
Redlich-Peterson	β	0.93±1.9x10^{-3}	0.94±1.4x10^{-3}	1.00±1.8x10^{-3}	1.07±3x10^{-3}
	R^2	0.995	0.996	0.996	0.994
	Error (F_{obj})	0.039	0.032	0.034	0.042

Table 5-1 shows that the maximum adsorption capacities for RhB adsorption on CMCD-MNPs and uncoated MNPs adsorbents (both were performed at 298 K) are 55.56 and 30.77 mg/g, respectively. It shows that CMCD-MNPs can adsorb RhB almost twice than uncoated MNPs at pH 5 and 298 K, due to the amount of CM-β-CD coated on the surface of the magnetic nanoparticles adsorbent, approximately 12.8%. The adsorption favourability of RhB which is measured in terms of separation factor (R_L) can be seen in Table 5-1. The separation factors are all between 0 and 1 which indicate that the adsorptions of RhB on MNPs are indeed favourable ones. Moreover, the value of Langmuir isotherm constant or K_L which relates to binding sites affinity is also shown in this table. For CMCD-MNPs used as adsorbent, the lower operating temperature performs better than the higher one.

Based on Table 5-1, all values of n_F (heterogeinity factor) for RhB adsorption on CMCD-MNPs at different temperatures and uncoated MNPs are more than one. They also indicate favourable adsorption. Another parameter $1/n_F$ (a deviation from linearity of the adsorption mechanism which is related to adsorption intensity) for all experiments range is less than 1 because the first utilization of sites with the highest binding energies followed by lower binding energy sites [65].

The effect of temperature on dye adsorption on CMCD-MNPs can be seen by plotting the van't Hoff plot (ln *Kp* versus 1/*T*) as shown in Figure 5-6.

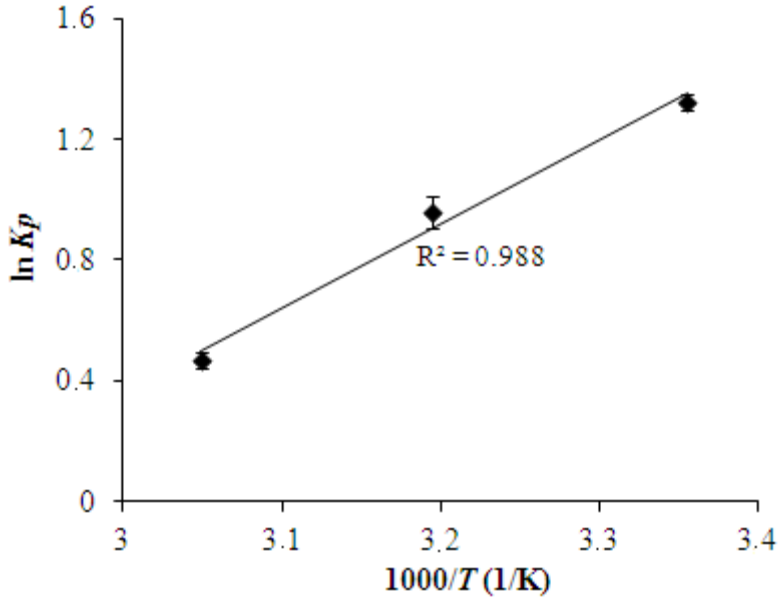

Figure 5-6 Van't Hoff plot for the adsorption of RhB on CMCD-MNPs at pH 5 and three different temperatures (298 K to 328 K)

The thermodynamic parameters for the adsorption of RhB using CMCD-MNPs are presented in Table 5-2. They are obtained from equations [2-9] to [2-11]. The free energy change (ΔG) values for adsorption of RhB onto CMCD-MNPs at 298, 313 and 328 K were -3.28, -2.42 and -1.30 kJ/mol, respectively. All negative values confirm the favourability and spontaneous nature of adsorption, and also show the affinity of the adsorbent for the dye molecules [2, 9]. Furthermore, the magnitude of ΔG of RhB adsorption on CMCD-MNPs decreases with increasing temperature confirming that the adsorption process performs better at lower temperature. Generally, in adsorption with biopolymer, temperature has negative effect in the amount of guest molecules adsorbed. Temperature has several effects in the solubility of the dyes, the swelling capacity of the adsorbent and the equilibrium condition associated with the exothermicity of the adsorption process [24]. At high temperature, the solubility of the dye molecules increases, so molecules will attach stronger to the solution than to the adsorbent.

Moreover, rising the temperature causes a decrease of surface activities of the sites of the adsorbent [100], so the uptake of the dye becomes low.

The heat of adsorption (*ΔH*) is found to be -23.13 kJ/mol which indicates the exothermic nature of adsorption. Whereas, the negative value of entropy (*ΔS*) shows a decrease in randomness at the solid-solution interface and no significant changes has occurred in the internal structure of the adsorbent through the adsorption of RhB onto CM-β-CD coated nanomagnetic adsorbent [101].

Table 5-2 Thermodynamic parameters for the uptake of RhB onto CMCD-MNPs at pH 5 and temperatures from 298 to 328 K

Thermodynamic parameter	298 K	313 K	328 K
ΔG (kJ/mol)	$-3.28\pm8.1\times10^{-3}$	$-2.42\pm6.3\times10^{-3}$	$-1.30\pm8.9\times10^{-3}$
ΔH (kJ/mol)	-23.13±0.08		
ΔS (J/mol K)	-66.39±0.23		

The comparison of the maximum adsorption capacities found from published work is presented in Table 5-3. It shows that the adsorption capacity of RhB on CMCD-MNPs found in this study is slightly higher than some of the functionalized nanoadsorbent. Therefore, the modification of CM-β-CD onto the surface of magnetic nanoparticles can be an effective adsorbent for removing basic dyes.

Table 5-3 Maximum adsorption capacities (q_m, mg/g) for the uptake of RhB using some other adsorbents reported in literatures

Adsorbent	Maximum adsorbed amount, q_m (mg/g)	Reference
A carbonaceous adsorbent from Thespusia populini bark	77.2	[102]
CM-β-CD coated on magnetic nanoparticle (CMCD-MNPs)	55.6	This work
Epichlorohydrine crosslinked cyclodexrin polymer	53.2	[9]
Coconut shell carbon	46.9	[103]
Tamarind husk	40.3	[104]
A carbonaceous adsorbent prepared from an indigenous waste	40.2	[22]
Turdal husk	26.1	[104]
Bengal gram husk	24.4	[104]
Banana peel	20.6	[105]
Walnut shell charcoal	18.7	[106]
Activated carbon from industrial solid waste (sago waste)	16.2	[107]
Orange peel	14.3	[105]
Coir pith	2.6	[108]

5.2.3. Adsorption kinetic

The kinetic of the adsorption of RhB on MNPs coated with CM-β-CD were studied at the optimum pH adsorption (pH 5) with an initial RhB concentration of 250 mg/L and three different temperatures, 298, 313 and 328 K. The analysis of the liquid phase concentration was carried out within 3 hours in short intervals. Two kinetic models, namely, Lagergren pseudo-first-order and Ho and McKay pseudo-second-order models were explored to represent the experimental data and further to determine what mechanism controls or rate-limiting steps of the adsorption for examples adsorption surface, mass transfer and external diffusion.

Figure 5-7 shows the uptake of RhB adsorbed onto magnetic nanoparticles coated with CM-β-CD. The initial concentration generated the driving force required to overcome the

mass transfer resistance between the aqueous and solid phases [109]. At first few minutes, the adsorption process increases rapidly because no dye molecules are initially attached by nano-sized adsorbent particles, therefore the driving force is highest at the initial period. For all temperatures, approximately more than 50% of the adsorption took place during the rapid rate period and then follow by a gradual increase in the adsorption process. It was possibly caused the adsorption was carried out in the polymer network [16]. After that, it is almost constant at the equilibrium. It was possibly caused by the decreasing of the driving force as it approaches to equilibrium.

At various temperatures, the maximum amounts of dye adsorbed (with an initial concentration of 250 mg/L) decreases with increasing temperature. The decrease of the dye adsorbed is possibly due to a decrease in surface affinities of the active sites of adsorbent as temperature increases from 298 to 328 K. At a higher temperature, the equilibrium is attained in a longer time and the amount of the dye adsorbed onto CMCD-MNPs decreases, so, the dye adsorption is more effective at room temperature (298 K). In addition, this adsorption process might be considered as a fast adsorption since the equilibrium condition was attained less than an hour for all different adsorption temperatures. The rapid removal of RhB from aqueous solution is of significant practical importance to facilitate the use of small adsorbent volumes to ensure efficiency and economy. Therefore, the finding reflects that CMCD-MNPs can be considered as a potential adsorbent to remove RhB from aqueous solution.

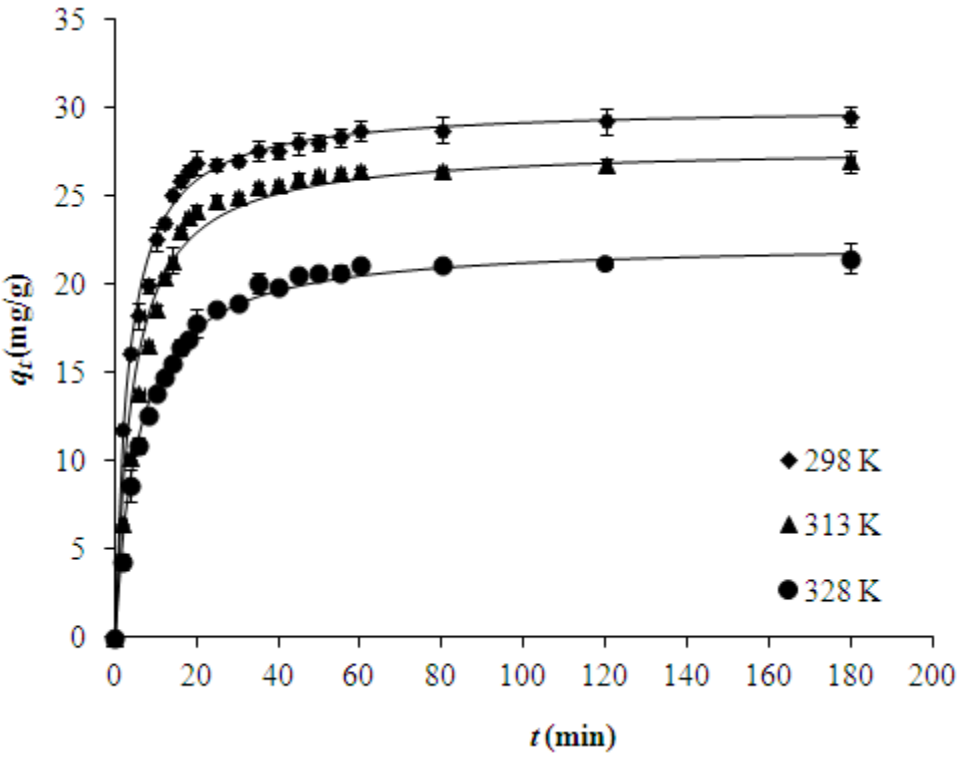

Figure 5-7 The uptake of RhB onto CM-β-CD coated on MNPs versus time at three different temperatures (condition: initial concentration = 250 mg/L, adsorbent mass = ~120 mg, pH 5, volume = 10 ml, agitation speed = 200 rpm, temperatures 298, 313 and 328 K)

Figures 5-8 and 5-9 display pseudo-first-order and pseudo-second-order kinetic models, respectively. From pseudo-first-order kinetic model, plots of (q_e-q_t) versus t only yielded straight lines at fast adsorption stages or before the system reached saturation. After reaching equilibrium, experimental data deviated from linearity. It shows that experimental data obey Lagergren model at rapid adsorption period which is depicted by high values of the linear regression coefficient (R^2>0.9). However, for all experimental data, they were not represented well with the pseudo-first-order kinetic model or the uptake of AB25 by adsorption onto the CM-β-CD modified magnetic nanoparticles does not follow pseudo-first-order model.

Figure 5-9 shows that the experimental data at various temperatures are following pseudo-second-order kinetic model closely with higher correlation coefficients compare to the other kinetic model. The adsorption of RhB is probably carried out via surface exchange reaction until the surface functional sites are fully occupied. It then follows by diffusion of adsorbate molecules through the polymer network takes place by the formation of inclusion complex or hydrophobic interaction [9].

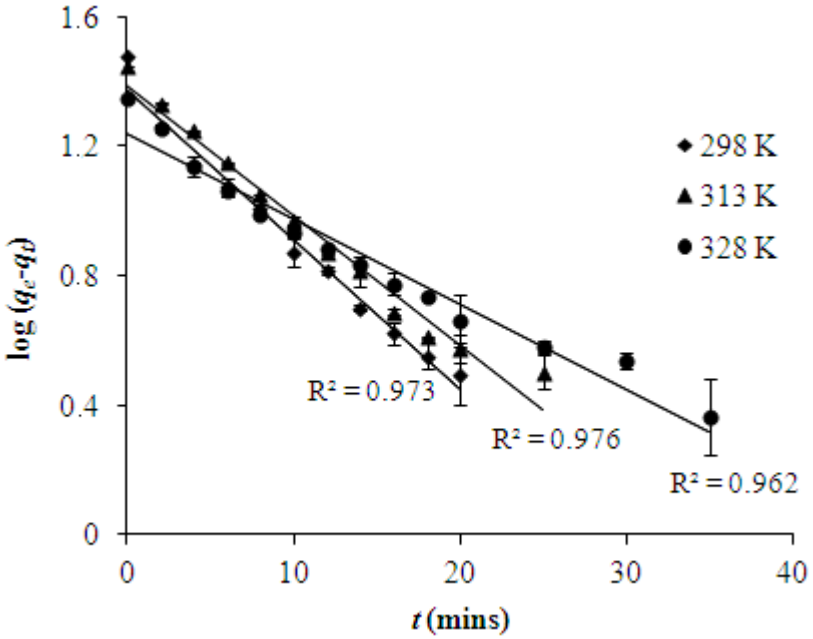

Figure 5-8 Pseudo-first-order kinetic plots of the adsorption of RhB onto CMCD-MNPs at three different temperatures (condition: initial concentration = 250 mg/L, adsorbent mass = ~120 mg, pH 5, volume = 10 ml, agitation speed = 200 rpm, temperatures 298, 313 and 328 K)

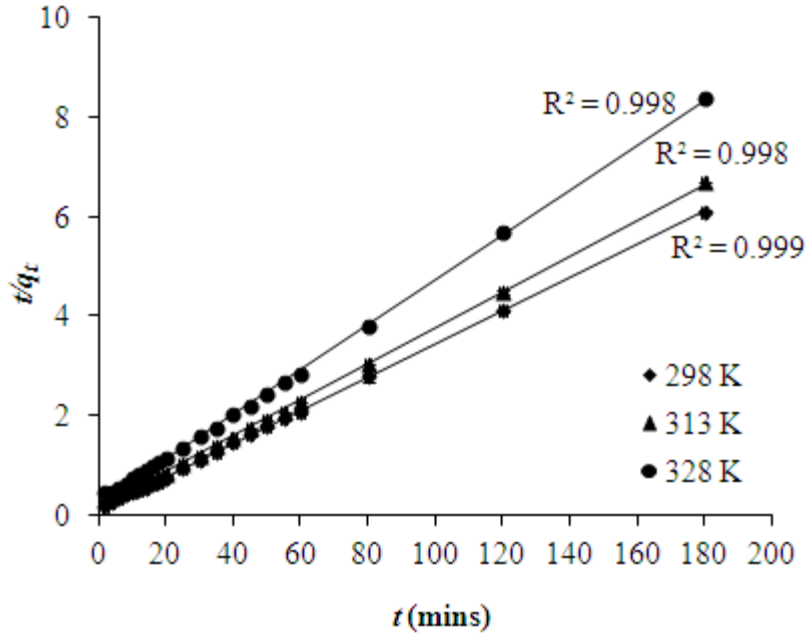

Figure 5-9 Pseudo-second-order kinetic plots of the adsorption of RhB onto CMCD-MNPs at three different temperatures (condition: initial concentration = 250 mg/L, adsorbent mass = ~120 mg, pH 5, volume = 10 ml, agitation speed = 200 rpm, temperatures 298, 313 and 328 K)

Table 5-4 Adsorption kinetic parameters of RhB adsorbed on the surface of CM-β-CD modified on magnetic nanoparticles adsorbent. Conditions: initial concentration 250 mg/L, pH 5, temperatures 298, 313 and 328 K

Kinetic model	Parameters	CMCD-MNPs		
		298 K	313 K	328 K
Pseudo-first-order (before saturated)	k_1, min^{-1}	$0.094\pm2.4\times10^{-4}$	$0.093\pm1.4\times10^{-4}$	$0.070\pm1.8\times10^{-4}$
	$q_{e\,(cal)}$, mg/g	21.55±0.05	25.07±0.04	18.92±0.05
	R^2	0.973	0.976	0.962
	Error (F_{obj})	0.702	0.438	1.162
Pseudo-first-order	k_2, g/(mg min)	$0.010\pm9.5\times10^{-6}$	$0.008\pm2.1\times10^{-5}$	$0.008\pm1.9\times10^{-5}$
	$q_{e\,(cal)}$, mg/g	30.03±0.03	27.86±0.07	22.37±0.05
	$q_{e\,(exp)}$, mg/g	29.56±0.03	26.95±0.06	21.47±0.05
	R^2	0.999	0.998	0.998
	Error (F_{obj})	0.018	0.319	0.192

The kinetic parameters of the adsorption of RhB using CMCD-MNPs are tabulated in Table 5-4. The calculated adsorption capacities ($q_{e,cal}$) obtained using pseudo-second-order kinetic model, at 298, 313 and 328 K, are 30.03, 27.86 and 22.37 mg/g,

respectively. They are consistent with those obtained from kinetic experiments after adsorption RhB reached saturated values at 298, 313 and 328 K, 29.56, 26.95 and 21.47 mg/g, respectively.

5.2.4. Adsorption mechanism

FTIR analysis is used to obtain information on interaction mechanism between RhB and CMCD-MNPs nano-adsorbent.

Figure 5-10 shows the IR spectra of CMCD-MNPs, adsorbed RhB and free RhB. It can be seen from Figure 5-10 (a), the broad peak at 3387 cm^{-1} are due to highly -OH stretch vibration on the CMCD-MNPs adsorbent, while the other peaks at 1026 and 1150 cm^{-1} are due to C-O-C and C-OH groups of CD moieties, respectively [2]. Before adsorption, the assignments for the RhB are presented in Figure 5-10 (c). Based on the literature [110, 111], the bands at 3408, 2974 and 2930 cm^{-1} are due to -OH, $-CH_2$ and $C-CH_3$ stretch vibrations, respectively. The prominent peaks at 1589 cm^{-1} associate with aromatic ring vibrations, and peaks at 1646 cm^{-1} correspond to the C-N bond. Those at 1344 cm^{-1} are assigned to C-aryl bond vibration. The C=O groups vibration are found at 1720 cm^{-1}. After adsorption took place, the main peaks in the spectra of CMCD-MNPs at 900-1100 cm^{-1} shift which demonstrates the possibility of the interaction of these functional groups with RhB. An increase of the absorption band at 3387 cm^{-1} to 3389 cm^{-1} is attributed to the disappearance of water molecules from the CD cavity which is similar to the case of true inclusion complexes [112]. Some peaks related to the attachment of the RhB onto CMCD-MNPs are shown at 1597 cm^{-1} corresponded to

aromatic ring vibration, 1341 and 1641 cm^{-1} attributed to the C-aryl bond and C-N bond vibrations, respectively. Several weak absorption bands at 1718, 2972 and 2924 are caused by C=O, $-CH_2$ and $C-CH_3$ stretch vibrations, respectively. Thus, the results from FTIR analysis show the mechanism of interaction between RhB and CMCD-MNPs nanoadsorbent.

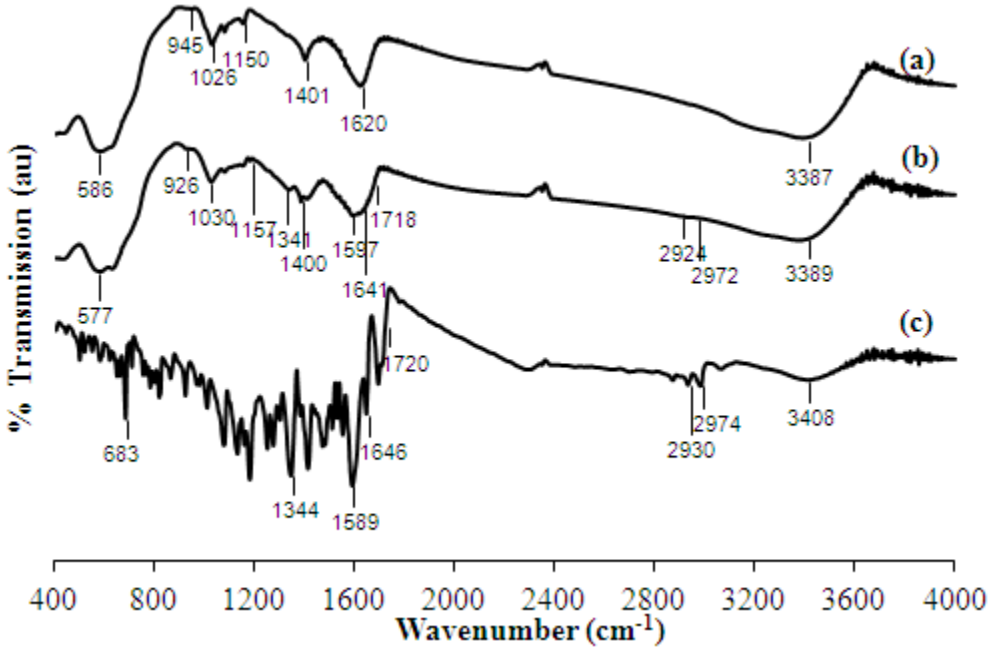

Figure 5-10 FTIR spectra of (a) CMCD-MNPs before adsorption, (b) after adsorption with Rhodamine B and (c) Rhodamine B. FTIR spectra of the samples were analyzed using Bio-Rad spectrometer at 64 scans at 4.0 cm^{-1} resolution in the range of 400 to 4000 cm^{-1}

5.2.5. Desorption and regeneration experiments

Desorption experiment helps to understand adsorption mechanism and recyclability of the adsorbent used. In this work, the detachment of RhB adsorbed on magnetic nanoparticles coated with CM-β-CD was investigated at the optimum pH 5 with an initial RhB concentration of 250 mg/L. After adsorption equilibrium had been attained, a 5 ml of

desorbing agent was mixed directly with supernatant for each sample. The system was agitated for 5 hours to make sure that desorption equilibrium was achieved. The absorbance of the liquid phase was measured using UV/vis spectrophotometer (Shimadzu UV-1601). The experimental concentrations of the supernatants were obtained through converting the absorbance data to the standard curve of concentration. The percentage of dye desorbed was calculated using equations [3-2] to [3-4]. The result of desorption experiment are tabulated in Table 5-5.

Table 5-5 Percentage of RhB removed from the CMCD-MNPs adsorbent using different desorbing agents

Desorbing agent	% Removal
Methanol 100%	90.4±0.65 %
Acetic acid in methanol (5% v/v)	84.4±0.25 %
Hydrochloric acid 0.4 M	78.5±0.41 %
Alkaline water pH 8	74.3±0.24 %
Ethanol 100%	58.2±0.53 %

Table 5-5 shows the percentage of RhB desorbed from CMCD-MNPs adsorbent. Desorption with acetic acid in methanol (5% v/v) solubilised 84% of RhB from the nano-sized magnetic adsorbent. It indicates that the affinity of the RhB on the CMCD-MNPs is not so strong [113] and it is possible that the dye molecules agglomerated on the surface of the adsorbent [114]. Methanol was also used as a chemical for desorption experiment due to the fact that organic dyes are generally soluble in organic solvents like methanol and ethanol. The use of pure methanol could desorb around 90% of RhB from the adsorbent surface. The application of the organic solvent might break the aggregation of the dye and then diffuse into the adsorbent. Desorption study was also carried out with alkaline aqueous solutions, due to the least adsorption capacities at the pH 8 as

demonstrated in Figure 5-1. It was assumed that the alkaline solutions might facilitate the dissociation of the dye from the adsorbent. It obtained an approximately desorption efficiency as high as 74%. Acidic solution was also used as a chemical for desorption experiment due to low adsorption capacity at low pH. The finding shows that hydrochloric acid solution 0.4 M could desorp around 79% of RhB from adsorbent. However, in the adsorption of RhB onto the surface of CMCD-MNPs nano-sized adsorbent, methanol was better to be applied as a desorbent since the dye is soluble in methanol [115]. Moreover, since the interaction between the guest molecules and the adsorbent was driven mainly by inclusion complexes, organic solvents such as methanol could be good candidates as desorbing agents in order to regenerate the adsorbent [116].

Based on the findings of desorption study as shown in Table 5-5, the best chemical used for desorbing RhB from CMCD-MNPs was pure methanol. After that, recovery experiment was studied. Since long term stability and regeneration of the adsorbent are key factors for an advanced adsorbent, recovery study is important. The study of adsorbent's recyclability is further associated with the cost analysis. The cost of the adsorbent can be less if an adsorbent possesses high reproducibility of adsorption and desorption properties. For adsorbent regeneration study, adsorption and desorption experiments are carried out for several cycles. The concentration of the supernatant samples after adsorption and desorption experiments were analyzed, and then the equilibrium adsorption capacity of the dye was calculated. The result of recovery experiment is depicted in Figure 5-11.

Figure 5-11 shows the performance of CMCD-MNPs adsorbent within three cycles. After used for three cycles of adsorption, the adsorption capacity values changed. However, the change is not more than 10%. This indicates the chemical stability of the adsorbent and reproducibility of the adsorption capacity values.

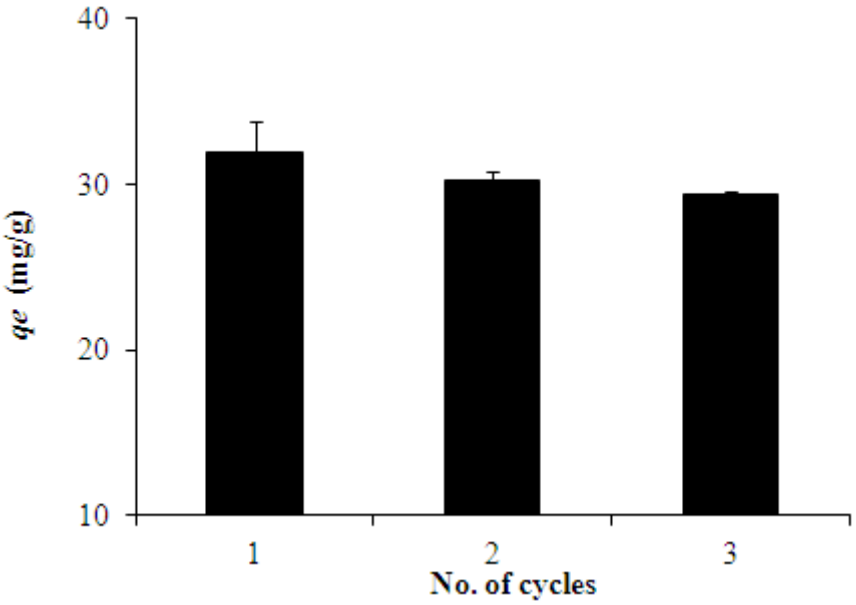

Figure 5-11 Performance of CMCD-MNPs adsorbent for the adsorption of RhB after three cycles of regeneration (conditions: initial concentration = 250 mg/L, adsorbent mass = ~120 mg, pH 5, volume = 10 ml, agitation speed = 200 rpm, temperature 298 K)

The stability of the adsorbent can be seen from the FTIR results obtained from CMCD-MNPs before and after adsorption of RhB, after desorption with pure methanol and after three times recycled as shown in Figure 5-12 and Table 5-6. After desorption and used for several times, the important peaks of the adsorbent were still in their ranges. This indicates the stability of the adsorbent. However, after being used three times for RhB adsorption, the performance of the adsorbent decreased that was reflected by their structural changes, which can be seen in Figure 5-12. Moreover, the shifted of the adsorption bands of CMCD-MNPs are summarized in Table 5-6.

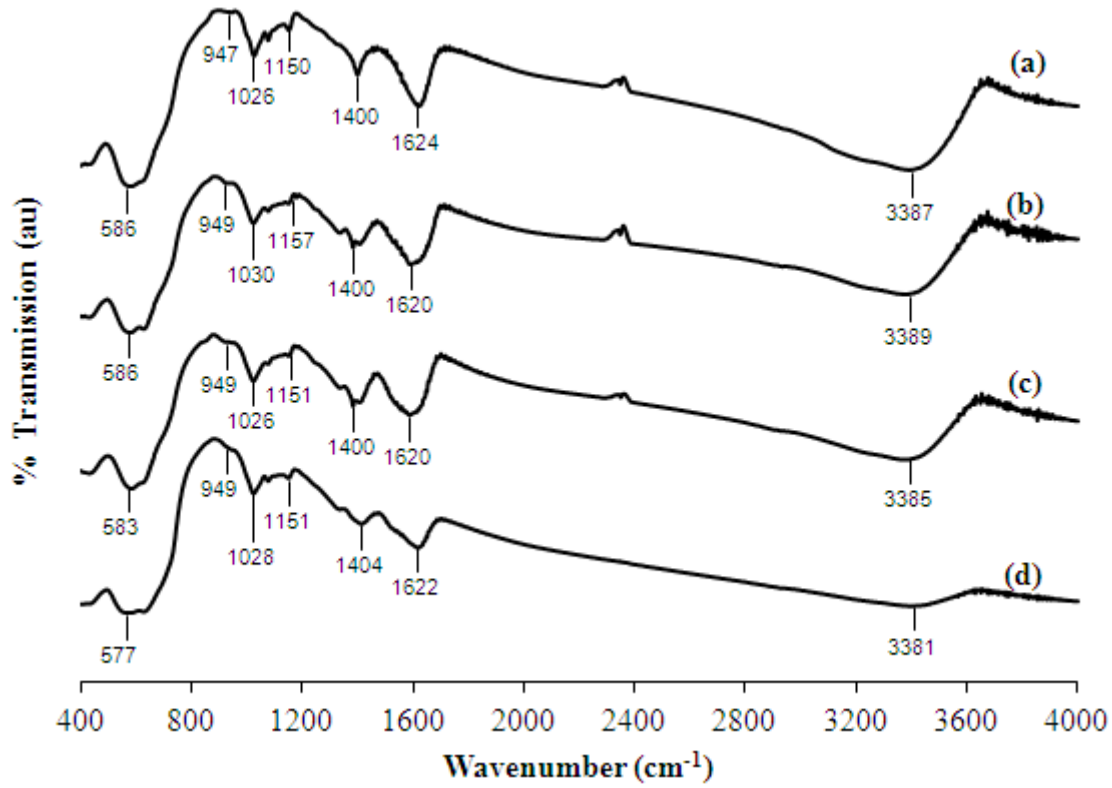

Figure 5-12 FTIR spectra of CMCD-MNPs (a) and (b) before and after adsorption of RhB, (c) after desorption with pure methanol and (d) after three times recycled

Table 5-6 The spectra of CMCD-MNPs before and after RhB adsorption, after desorption with methanol and after three times recycled

Characteristic	CMCD-MNPs				
	Before adsorption (cm^{-1})	After adsorption (cm^{-1})	After desorption (cm^{-1})	After recycle (cm^{-1})	Range (cm^{-1}) [2, 88, 111]
Fe-O in the tetrahedral site	586	586	583	577	558-630
-OH stretching vibration	3387	3389	3385	3381	3140-3680
R-1,4-bond skeleton vibration of β-CD	947	949	949	949	940-950
Antisymmetric glycosidic ν_a (C-O-C) vibrations	1026	1030	1026	1028	960-1200
Coupled ν (C-C/C-O) stretching vibrations	1150	1157	1151	1151	
COOM (M=metal) (the COOH groups of CM-β-CD were reacted with OH groups of Fe_3O_4 to form Fe-carboxylates	1400 and 1624	1400 and 1620	1400 and 1622	1404 and 1620	~1400 and ~1620

5.3. Conclusions

Adsorption of a cationic dye, RhB, on CM-β-CD coated magnetic nanoparticles was carried out at different pH and temperatures. It was found that the maximum adsorption capacity was obtained at pH 5. At various temperatures ranging from 298 to 328 K, room temperature (298 K) performs better adsorption. Increasing temperature will raise the dye's solubility. Consequently, dye molecules will attach to the solution stronger than the adsorbent. At high temperatures, the surface activities of the sites of the adsorbent also decrease so less targeted molecules are attached to the adsorbent. Langmuir isotherm model can represent well the adsorption equilibrium of RhB using uncoated and CM-β-CD functionalized on MNPs, whereas Ho and McKay pseudo-second-order kinetic model can describe well the kinetic data of RhB adsorption using CMCD-MNPs. The adsorption mechanism of RhB to CMCD-MNPs was confirmed by FTIR analysis. Desorption of RhB adsorbed onto the surface of CMCD-MNPs adsorbent were observed using various chemicals such as organic solvents like methanol and ethanol, acetic acid in methanol, as well as acidic and alkaline solutions. It is found that methanol can desorb approximately 90% of RhB from the adsorbent. Moreover, recovery experiment shows that CMCD-MNPs adsorbent can be reused for three times RhB adsorption with a little decrease of its performance which is also strengthened by the structural changes of CMCD-MNPs investigated with FTIR. As a conclusion, the application of CM-β-CD modified on MNPs adsorbent for dye removal and recovery experiment, shows a simple, but feasible, versatile and unique tool for wastewater treatment.

Chapter 6 Adsorption, desorption and regeneration experiments of an acid dye (Acid Blue 25) using CMCD-MNPs

6.1. Introduction

In chapter 5, adsorption of a cationic dye, Rhodamine B, using carboxymethyl-beta-cyclodextrin coated on the surface of nano magnetic particle adsorbent was carried out. Adsorption, desorption and recovery studies were conducted at the previous chapter. For the adsorption of targeted molecules, the common driving forces are ion exchange, electrostatic interaction, hydrophobic interaction, intramolecular forces interaction [9, 16, 65, 107]. However, CDs exhibit an ability to form microencapsulation or inclusion complex. This ability makes CDs have different sorption mechanism from the other adsorbents. The formation of these complexes has been attributed to weak interactions such as hydrophobic effect which induce the apolar group of a molecule to preferentially enter the CD cavity, Van der Waals interactions, hydrogen bonding between guest molecule and hydroxyl groups at the rim of the cavity, solvent and steric effects [13, 26, 27]. Among these factors, hydrophobic interactions had been mainly considered as the major factor in complexation.

For adsorption of RhB, nano-sized magnetic particles coated with CM-β-CD enhance the adsorption capacity compared to uncoated ones. Moreover, pH of solution affects the amount of the uptake by changing its structure and temperature also had significant effects. Therefore, in this chapter, both types of nano-sized magnetic particles were further used for the removal of an anionic dye, Acid Blue 25.

AB25 (C.I. number 62055) is one class of anthraquinone dyes, the most significant group of synthetic dyes. It is also the second most important class of commercial dyes after azo-compounds [75]. It is applied widely in wool, nylon, silk, other protein fibers, paper, ink, aluminium, detergent, wood, fur, cosmetics, and biological stain [76]. In this work, AB25 was taken as a model guest solute due to its strong adsorption onto solids [24], its representative as the common compound for removing anthraquinonic dyes from aqueous solutions [76], and its carcinogenic effect [77, 86]. When dissolved in water, the sulfonate groups (SO_3^-) of AB25 dissociate and the dye is converted into anionic dye ions [24].

Besides extending the application of magnetic particles for the removal of another class of dye, the other basic considerations of this project are to distinguish several characteristics in the uptake of different dyes, determine the possibility of the recovery of the adsorbent for acid dye removal, confirm the effectiveness of the magnetic separation technique using different targeted molecules and compare the enhancement of coating MNPs with CM-β-CD to bare MNPs in term of adsorption capacity.

Thus, in this chapter, both magnetic nanoparticles, uncoated and coated with CM-β-CD, were used as adsorbents for uptaking AB25 in aqueous solution in different adsorption conditions such as pH and temperature. The comparison of the enhancement of coating strategy in dye adsorption to uncoated MNPs was also carried out at room temperature, optimum pH and under other similar conditions. The attachment of the dye onto CMCD-

MNPs adsorbent was analyzed using FTIR. The similarities between theoretical and experimental adsorption capacities are determined by error analysis. Desorption of AB25 was performed to give information of adsorption mechanism and the possibility of adsorbent's recycle. Desorption study was conducted as a function of different desorbing agents such as organic solvents (methanol and ethanol) and alkaline solution (NaOH in water). An evaluation of conformational changes of AB25 in adsorption, desorption as well as adsorbent recovery processes was also investigated by FTIR.

6.2. Results and discussion

6.2.1. Adsorption at different pHs

The effect of pH on the adsorption of AB25 was investigated in batch adsorption run at pHs 2 to 11 using different dye concentrations for each pH. Here, adsorption equilibriums were run at specific pHs. The solutions were agitated at least 5 hours at room temperature to attain equilibrium condition. Here, the pH of the aqueous solution also has a significant effect for the adsorption of AB25 by CMCD-MNPs as depicted in Figure 6-1.

As can be seen in Figure 6-1, the maximum uptake was obtained at pH 3 and the least removal was at pH 11. In the case of AB25 adsorbed by CM-β-CD modified on MNPs, the adsorption is controlled by surface charged interactions. At lower pHs, there are more hydrogen ions (protons) which make the surface of the adsorbent positive, so the adsorption increases. The positive charged of the adsorbent assists electrostatic interaction with the negatively charged sulfonate groups (SO_3^-) of the dye [25] since in aqueous solutions, AB25 is first dissolved and its sulfonate groups dissociate, finally the

dye becomes anionic dye ions. However, at pHs lower than 2, the excess hydrogen ions competes with the adsorbent to bind the dye molecules. Therefore, the amount of dye taken by the adsorbent diminishes. When pH rises, the amount of hydroxyl ions (OH^-) is numerous and they create a competition with COO^- groups of the adsorbent in binding dye molecules. In addition, at high pHs, both the dye and the adsorbent have same charges (negative charges), so the electrostatic repulsion of the similar charges in solution lead to a inhibition of dye removal [117]. For each experiment, after adsorption, the pH of solution increased not more than 0.7 units. This indicates an ion-exchange mechanism also participated in the adsorption of AB25 with magnetic nanoparticles adsorbent [24].

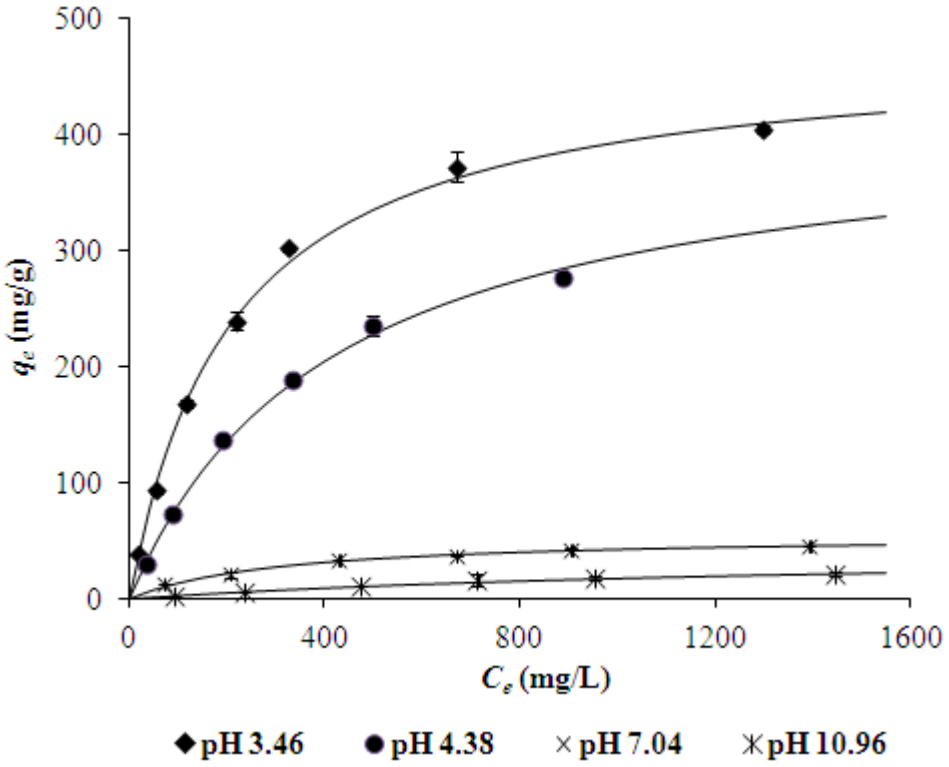

Figure 6-1 AB25 adsorption on CMCD-MNPs at different pHs (condition: initial concentrations = 100 to 1500 mg/L, adsorbent mass = ~120 mg, pH 2 to 11, agitation time = 5 hours, volume = 10 ml, agitation speed = 200 rpm and room temperature)

6.2.2. Adsorption equilibrium

The adsorption isotherms of AB25 adsorbed onto uncoated MNPs and CMCD-MNPs were studied at pH 3 with initial dye concentrations ranging from 100 to 3000 mg/L. The AB25 adsorbed onto CMCD-MNPs was also explored at different temperatures from 298 to 328 K. Figure 6-2 demonstrates the equilibrium isotherm for the adsorption of AB25 on uncoated and CM-β-CD coated on MNPs adsorbents. It demonstrates that for adsorption with CMCD-MNPs at temperatures from 298 to 328 K and also with uncoated MNPs at 298 K, the equilibrium adsorption capacities increased with increasing AB25 concentration from 100 to 1500 mg/L. However, with further increase in the dye concentration (>1500 mg/L), the equilibrium adsorption capacities did not change much and it reached an asymptotic value. Therefore, uncoated and CM-β-CD modified on MNPs adsorbent effectively removes this dye at low initial concentrations; at higher concentrations the isotherms reach a maximum capacity as presented by the plateau part.

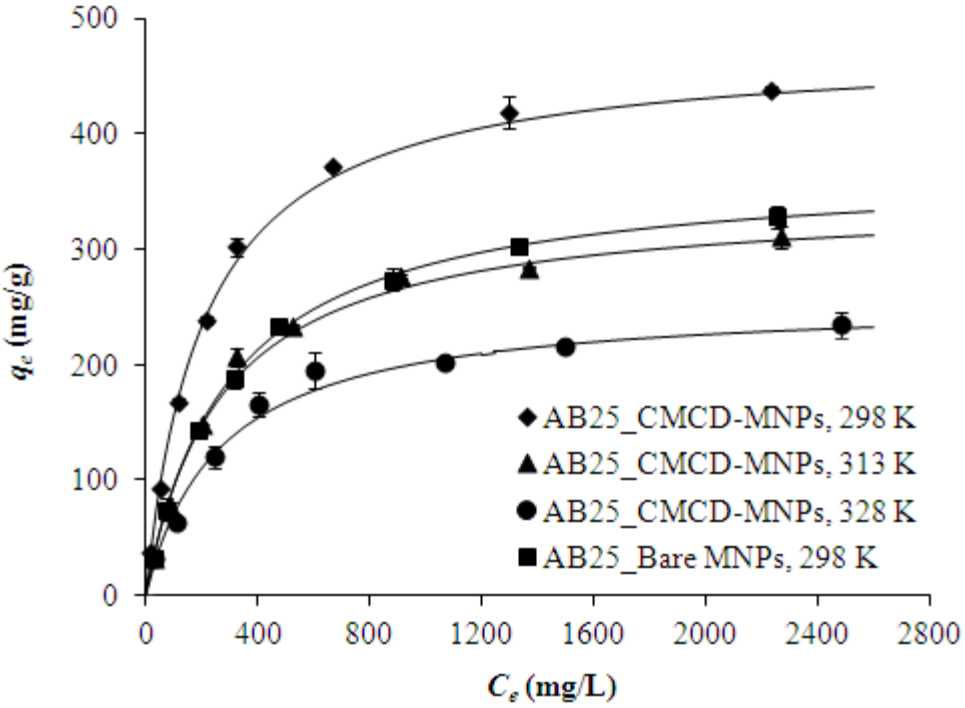

Figure 6-2 Equilibrium isotherm for the adsorption of AB25 onto CMCD-MNPs and uncoated MNPs at three different temperatures (conditions: initial concentrations = 100 to 3000 mg/L, adsorbent mass = ~120 mg, pH 3, agitation time = 5 hours, volume = 10 ml, agitation speed = 200 rpm, temperatures 298, 313 and 328 K)

Figures 6-3 to 6-5 demonstrate the fitting of isotherms based on Langmuir, Freundlich and Redlich-Peterson models, respectively. The fitting results, correlation coefficients (R^2) and the least square fittings (F_{obj}), are tabulated in Table 6-1. It can be seen that Langmuir isotherm model can describe better than the other two models. Furthermore, the values of β in Redlich-Peterson model for all temperatures are closed to unity; this indicates that Redlich-Peterson model is indeed similar to Langmuir model.

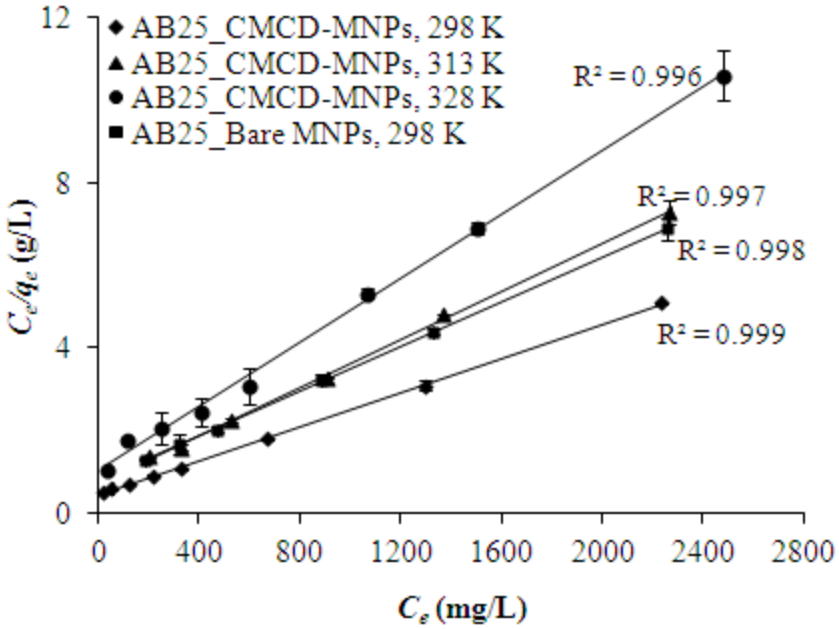

Figure 6-3 Langmuir isotherm plots for the adsorption of AB25 onto CMCD-MNPs and uncoated MNPs (conditions: initial concentrations = 100 to 3000 mg/L, adsorbent = ~120 mg, pH 3, agitation time = 5 hours, volume = 10 ml, agitation speed = 200 rpm, temperatures 298, 313 and 328 K)

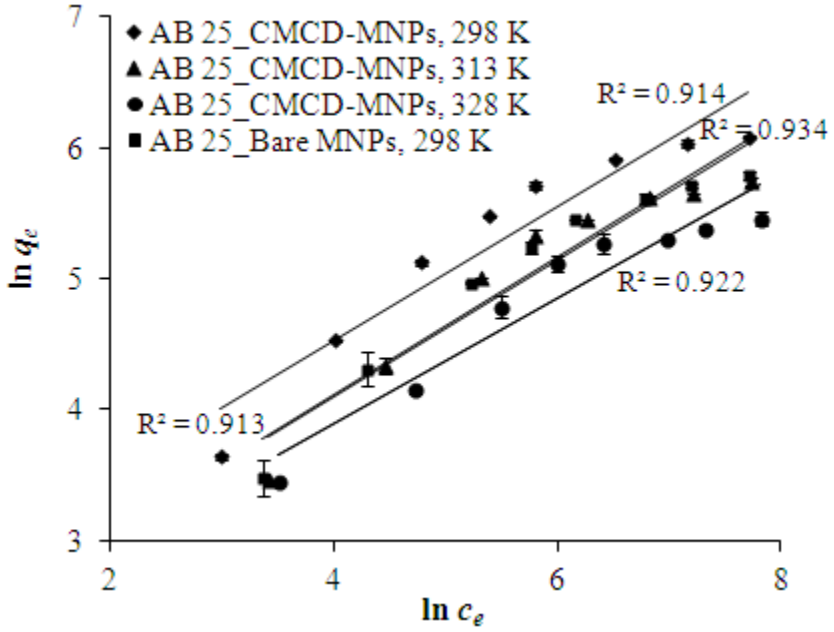

Figure 6-4 Freundlich isotherm plots for the adsorption of AB25 onto CMCD-MNPs and uncoated MNPs (conditions: initial concentrations = 100 to 3000 mg/L, adsorbent = ~120 mg, pH 3, agitation time = 5 hours, volume = 10 ml, agitation speed = 200 rpm, temperatures 298, 313 and 328 K)

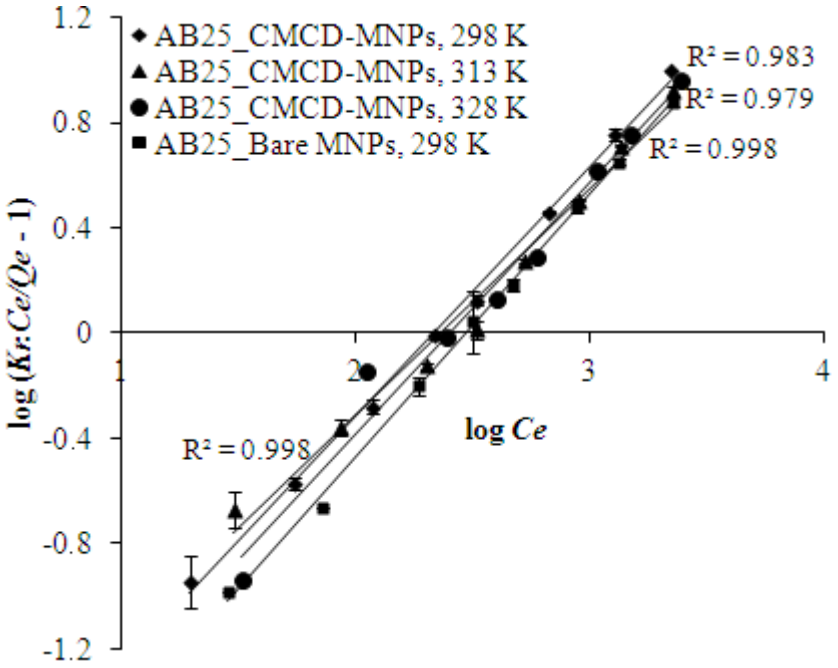

Figure 6-5 Redlich-Peterson isotherm plots for the adsorption of AB25 onto CMCD-MNPs and uncoated MNPs (conditions: initial concentrations = 100 to 3000 mg/L, adsorbent = 120 mg, pH 3, agitation time = 5 hours, volume = 10 ml, agitation speed = 200 rpm, temperatures 298, 313 and 328 K)

Table 6-1 Adsorption isotherm parameters for AB25 onto CMCD-MNPs and uncoated MNPs at pH 3, initial concentrations 100-3000 mg/L, agitation time 5 hours, and three different temperatures (298, 313 and 328 K)

Isotherm models	Parameters	CMCD MNPs			Uncoated MNPs (298 K)
		298 K	313 K	328 K	
Langmuir	q_m (mg/g)	476.19±0.95	344.83±1.07	256.41±2.23	370.37±0.96
	K_L (L/g)	$2.15\pm4.3\times10^{-3}$	$1.28\pm4.0\times10^{-3}$	$0.96\pm8.4\times10^{-3}$	$1.24\pm3.2\times10^{-3}$
	R^2	0.999	0.997	0.996	0.998
	R_L	0.07-0.69	0.08-0.73	0.08-0.73	0.09-0.75
	Error (F_{obj})	1.124	1.656	1.837	1.383
Freundlich	n_F	$1.96\pm9.8\times10^{-4}$	$1.91\pm7.6\times10^{-4}$	$2.08\pm3.7\times10^{-4}$	$1.90\pm3.2\times10^{-4}$
	K_F (mg/g)/L/g)^n	$12.04\pm6\times10^{-3}$	$7.35\pm2.9\times10^{-3}$	$7.18\pm1.3\times10^{-3}$	$7.47\pm1.3\times10^{-3}$
	R^2	0.914	0.913	0.922	0.934
	Error (F_{obj})	2.663	2.810	2.502	2.155
Redlich-Peterson	β	$0.95\pm1.4\times10^{-4}$	$0.90\pm2.6\times10^{-4}$	$0.96\pm2.4\times10^{-4}$	$1.00\pm2.3\times10^{-4}$
	R^2	0.998	0.979	0.983	0.998
	Error (F_{obj})	1.226	2.023	1.937	1.355

Table 6-1 shows that the maximum adsorption capacities of AB25 uptaken on CMCD-MNPs and uncoated MNPs adsorbents (both were performed at 298 K), are 476.19 and

370.37 mg/g, respectively. It confirms that modification the surface of the magnetic nanoparticles with CM-β-CD at pH 3 and room temperature could increase adsorption performance nearly 1.3 times, due to the amount of CM-β-CD coated on the surface of the magnetic nanoparticles adsorbent, approximately 12.8%. The adsorption favourability of AB25 which is measured in terms of separation factor (R_L) can also be seen in Table 6-1. The separation factors are all between 0 and 1 which indicate that the adsorptions of AB25 on MNPs are indeed favourable ones. Moreover, the value of Langmuir isotherm constant or K_L which relates to binding sites affinity is also shown in this table. For CMCD-MNPs used as adsorbent, the lower operating temperature performs better than the higher one.

Based on Table 6-1, all values of n_F (heterogeinity factor) for AB25 adsorption on CMCD-MNPs at different temperatures and uncoated MNPs are more than one. They also indicate favourable adsorption. Another parameter $1/n_F$ (a deviation from linearity of the adsorption mechanism which is related to adsorption intensity) for all experiments range is less than 1 because the first utilization of sites with the highest binding energies followed by lower binding energy sites [65].

The effect of temperature on dye adsorption on CMCD-MNPs can be seen by plotting the van't Hoff plot (ln Kp versus $1/T$) as shown in Figure 6-6.

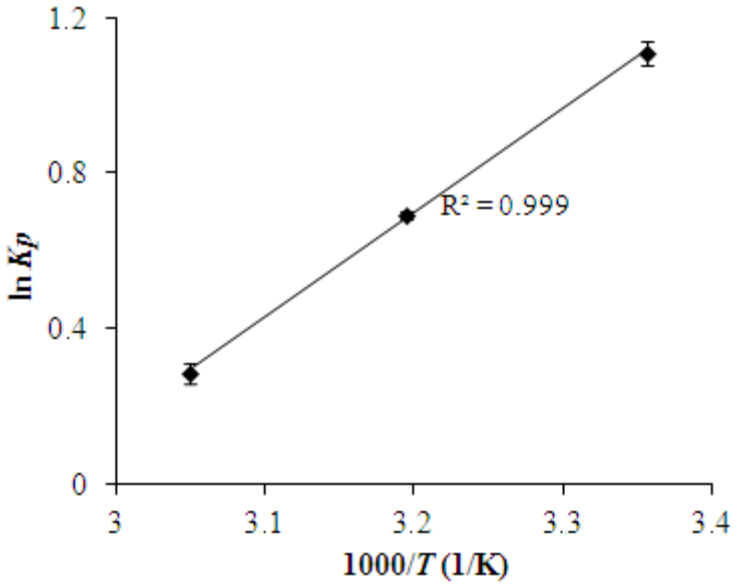

Figure 6-6 Van't Hoff plot for the adsorption of AB25 on CMCD-MNPs at pH 3 and three different temperatures (298 to 328 K)

The thermodynamic parameters for the adsorption of AB25 using CMCD-MNPs are presented in Table 6-2. They are obtained from equations [2-9] to [2-11]. The free energy change (*ΔG)* values for the uptake of AB25 by magnetic nanoparticles functionalized with CM-β-CD (CMCD-MNPs) at 298, 313 and 328 K were -2.75, -1.80 and -0.79 kJ/mol, respectively. All negative values confirmed the favourability and spontaneous nature of adsorption, and also demonstrated the affinity of the adsorbent for the dye molecules [2, 9]. Moreover, the magnitude of *ΔG* of the adsorption of AB25 onto CMCD-MNPs diminished with increasing the temperature. This phenomenon strengthened the exothermicity nature of the adsorption process of AB25 onto CMCD-MNPs adsorbent so the uptake of the dye would be higher at lower temperature. Generally, in adsorption with biopolymer, temperature has negative effect in the amount of guest molecules adsorbed. Temperature has several effects in the solubility of the dyes, the swelling capacity of the adsorbent and the equilibrium condition associated with the

exothermicity of the adsorption process [24, 118]. At high temperature, the solubility of the dye molecules increases, so molecules will attach stronger to the solution than to the adsorbent. Moreover, rising the temperature causes a decrease of surface activities of the sites of the adsorbent [100]. Consequently, the uptake of the dye becomes low.

From slope and intercept of the Van't Hoff plot, the values of ΔH and ΔS were -22.22 kJ/mol and -65.32 J/mol K, respectively. The negative value of the change of enthalpy depicted that the adsorption mechanism was exothermic in nature. The negative change of entropy (ΔS) showed a decrease randomness at the solid-solution interface and no significant changes occurred in the internal structure of the adsorbent through the adsorption of AB25 onto CM-β-CD coated nanoparticles magnetic adsorbent [101].

Table 6-2 Thermodynamic parameters for adsorption of AB25 onto CMCD-MNPs at pH 3 and temperatures from 298 to 328 K

Thermodynamic parameter	298 K	313 K	328 K
ΔG (kJ/mol)	$-2.75\pm5.5\times10^{-3}$	$-1.80\pm5.6\times10^{-3}$	$-0.79\pm6.8\times10^{-3}$
ΔH (kJ/mol)	-22.22±0.10		
ΔS (J/mol K)	-65.32±0.30		

The comparison of the maximum adsorption capacities found from published work is presented in Table 6-3. It shows that the adsorption capacity of AB25 on CMCD-MNPs found in this study is slightly higher than some of the functionalized nanoadsorbent. Therefore, the modification of CM-β-CD onto the surface of magnetic nanoparticles can be a potential adsorbent for removing acid dyes.

Table 6-3 Reported maximum adsorption capacities (q_{max} in $mg.g^{-1}$) in the literatures for AB25 obtained on some adsorbents

Adsorbent	Max. adsorbed amount, q_m (mg/g)	Reference
Treated cotton	589	[119]
Magnetic nanoparticle modified with CM-β-CD (CMCD-MNPs)	476.2	This study
Cationized sawdust	412	[118]
Ion-exchanger starch material	322	[24]
Chitosan beads	263.2	[120]
Cationic starch based material	249	[121]
Waste tea activated carbon (WTAC)	203.3	[25]
Chitosan-EGDE (ethylene glycol diglycidyl ether) beads	142.9	[120]
Chitosan/cyclodextrin composite	77.4	[122]
Ground hazelnut shell	60.2	[123]
Walnut wood sawdust	37	[123]
Cherry wood sawdust	32	[123]
Oak wood sawdust	27.9	[123]
Pitch-pine wood sawdust from	26.2	[123]

6.2.3. Adsorption kinetic

The kinetic of AB25 adsorbed on magnetic nanoparticles coated with CM-β-CD were studied at pH 3 with an initial dye concentration of 250 mg/L and three different temperatures, 298, 313 and 328 K. The analysis of the liquid phase concentration was carried out within 3 hours in short intervals. Two kinetic models, namely, Lagergren pseudo-first-order and Ho and McKay pseudo-second-order models were studied to represent the experimental data.

Figure 6-7 illustrates the uptake of AB25 adsorbed onto magnetic nanoparticles coated with CM-β-CD. The initial concentration generates the driving force required to overcome the mass transfer resistance between the aqueous and solid phases [109]. At first few minutes, the adsorption process increases rapidly because no dye molecules are

initially attached by nano-sized adsorbent particles, therefore the driving force is highest at the initial period. The phenomena are due to the availability of numerous active sites on the adsorbent. Fast adsorption during first minutes also demonstrates strong interaction between adsorbate and adsorbent. For all temperatures, almost all adsorption processes were carried out within 30 minutes. First, more than 50% of the adsorption took place during the rapid rate period. Second, the adsorption process increased gradually. Finally, it is almost constant at the equilibrium which was possibly caused by the decreasing of the driving force as it approaches to equilibrium.

At various temperatures, the maximum uptake of AB25 (with an initial concentration of 250 mg/L) decreases with increasing temperature. The decrease of the dye adsorbed is possibly due to a decrease in surface affinities of the active sites of adsorbent as temperature increases from 298 to 328 K. At a higher temperature, the equilibrium is attained in a longer time and the amount of the dye adsorbed onto CMCD-MNPs decreases, so, the dye adsorption is more effective at room temperature (298 K). In addition, this adsorption process might be considered as a fast adsorption since the equilibrium condition was attained less than half an hour for all different adsorption temperatures. Such a rapid adsorption process for the three temperatures also suggested that CMCD-MNPs can be considered as an effective adsorbent to remove AB25 from wastewater. The short duration of these experiments have significant practical importance, for example requiring smaller reactor volumes to facilitate efficiency and economy.

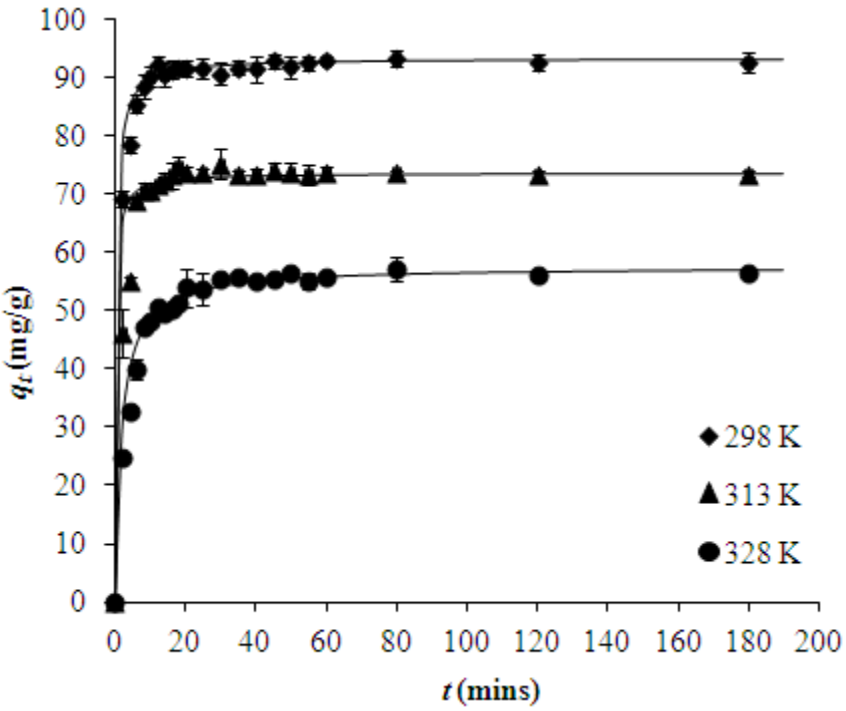

Figure 6-7 The amount of AB25 adsorbed onto CM-β-CD coated on MNPs versus time at three different temperatures (conditions: initial concentrations = 250 mg/L, adsorbent mass = ~120 mg, pH 3, volume = 10 ml, agitation speed = 200 rpm, temperatures 298, 313 and 328 K)

Figures 6-8 and 6-9 display pseudo-first-order and pseudo-second-order kinetic models, respectively. Based on pseudo-first-order kinetic model, at all temperatures and all range of experimental data, the straight lines could not be obtained. In other words, the value of the correlation coefficients for all experimental data, were very low and $q_{e,cal}$ largely deviated from $q_{e,exp}$. Plots of (q_e-q_t) versus time only yielded straight lines occurred at fast adsorption stages or before the system reached equilibrium. After reaching equilibrium, experimental data deviated from linearity. It shows that experimental data obey the Lagergren model at rapid adsorption period which is depicted by high values of the linear regression coefficient (R^2>0.9). However, for all experimental data, they were not represented well with pseudo-first-order kinetic model or the uptake of AB25 by

adsorption onto the CM-β-CD modified magnetic nanoparticles does not follow pseudo-first-order model.

Figure 6-9 shows that the experimental data at various temperatures are following pseudo-second-order kinetic model closely with higher correlation coefficients compare to pseudo-first-order kinetic model. The adsorption of AB25 is probably carried out via surface exchange reaction until the surface functional sites are fully occupied. Then, the diffusion of the adsorbate molecules to the polymer network takes place by the formation of inclusion complex or hydrophobic interaction [9].

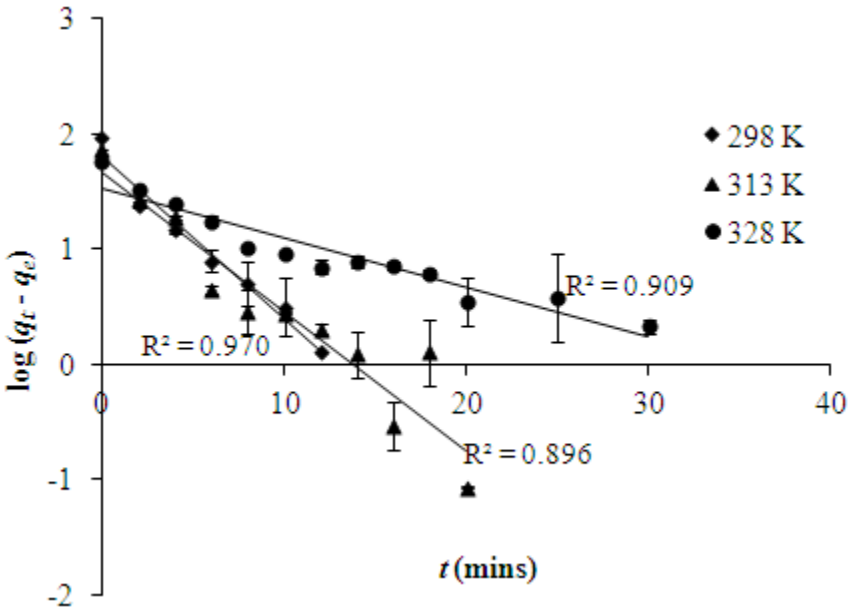

Figure 6-8 Pseudo-first-order kinetic plots of the adsorption of AB25 onto CMCD-MNPs at three different temperatures (conditions: initial concentrations = 250 mg/L, adsorbent mass = ~120 mg, pH 3, volume = 10 ml, agitation speed = 200 rpm, temperatures 298, 313 and 328 K)

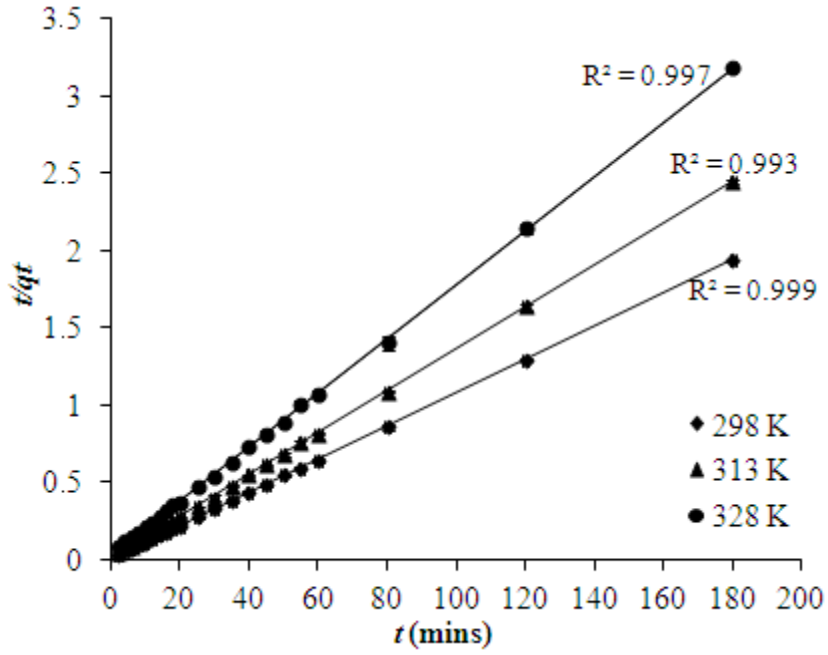

Figure 6-9 Pseudo-second-order kinetic plot of the adsorption of AB25 onto CMCD-MNPs at three different temperatures (conditions: initial concentrations = 250 mg/L, adsorbent mass = ~120 mg, pH 3, volume = 10 ml, agitation speed = 200 rpm, temperatures 298, 313 and 328 K)

Table 6-4 Adsorption kinetic parameters of AB25 on the surface of CM-β-CD modified on magnetic nanoparticles adsorbent (conditions: initial concentration 250 mg/L, pH 3, temperatures 298, 313 and 328 K)

Kinetic model	Parameters	CMCD-MNPs		
		298 K	313 K	328 K
Pseudo-first-order (before saturated)	k_1, min^{-1}	$0.384\pm2.8\times10^{-4}$	$0.280\pm2.9\times10^{-4}$	$0.099\pm9.7\times10^{-5}$
	$q_{e\,(cal)}$, mg/g	63.023±0.05	46.871±0.05	33.612±0.03
	R^2	0.970	0.896	0.909
	Error (F_{obj})	2.466	3.146	3.085
Pseudo-first-order	k_2, g/(mg min)	$0.0266\pm1.6\times10^{-5}$	$0.0514\pm6.2\times10^{-5}$	$0.0095\pm6.7\times10^{-6}$
	$q_{e\,(cal)}$, mg/g	93.458±0.06	73.529±0.09	57.471±0.04
	$q_{e\,(exp)}$, mg/g	92.673±0.06	73.476±0.09	56.541±0.04
	R^2	0.999	0.993	0.997
	Error (F_{obj})	0.023	0.232	0.105

The kinetic parameters of the adsorption of AB25 using CMCD-MNPs are tabulated in Table 6-4. The calculated adsorption capacities ($q_{e,cal}$) obtained using pseudo-second-

order kinetic model, at 298, 313 and 328 K, are 93.46, 73.53 and 57.47 mg/g, respectively. They are consistent with those obtained from kinetic experiments after AB25 adsorbed reached saturated value at 298, 313 and 328 K, 92.67, 73.48 and 56.54 mg/g, respectively.

6.2.4. Adsorption mechanism

The mechanism of adsorption AB25 onto the surface of CMCD-MNPs is confirmed using FTIR. Figure 6-10 shows the IR spectra of CMCD-MNPs, absorbed AB25 and free AB25. Figure 6-10 (a) demonstrates that the broad peak at 3387 cm^{-1} are due to highly -OH stretch vibration on the CMCD-MNPs adsorbent, while the other peaks at 1026 and 1150 cm^{-1} are due to C-O-C and C-OH groups of CD moieties, respectively [2]. Figure 6-10 (c) represents the assignment of AB25 before adsorption [113]. The absorption bands at 3425 cm^{-1} correspond to -OH stretch vibration while the significant peaks at 1591 and 1119 cm^{-1} are due to aromatic ring and sulfonate (SO_3^-) vibrations [111]. Weak bands at 1645 and 1701 cm^{-1} may be caused by -NH and C=O stretching vibrations respectively [111, 120]. The presence of -CH_3 deformation are presented at 1365 cm^{-1}. Several peaks between 1022 and 1044 cm^{-1} correspond to C-N bending vibrations. After adsorption occurred, the major peaks of CMCD-MNPs in the spectra of 900-1100 cm^{-1} shift which indicates that these functional groups may interact with AB25. An increase of the absorption band at 3387 to 3394 cm^{-1} is attributed to the disappearance of water molecules from the CD cavity which is similar to the case of true inclusion complexes [112]. The attachment of the adsorbent with the dye is also depicted by several peaks. For instance, two main absorption bands at 1590 and 1119 cm^{-1} which are caused by the

interaction with aromatic ring and sulfonate groups respectively, peaks at 1369 cm^{-1} attributes to -CH_3 deformation and those at 1570 cm^{-1} correspond to -NH stretching vibration.

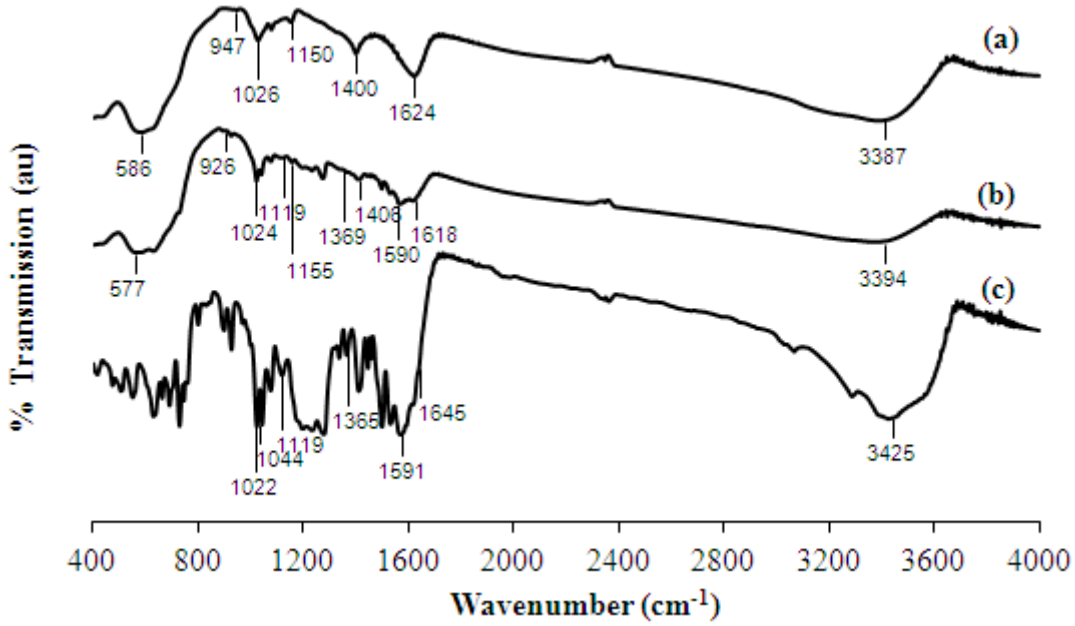

Figure 6-10 FTIR spectra of (a) CMCD-MNPs before adsorption, (b) after adsorption with Acid Blue 25 and (c) Acid Blue 25. FTIR spectra of the samples were analyzed using Bio-Rad spectrometer at 64 scans at 4.0 cm^{-1} resolution in the range of 400 to 4000 cm^{-1}

In general, the mechanism in dyes removal by adsorption may be summarized as the following: first, surface adsorption (physical adsorption and hydrogen bonding); second, diffusion into the polymer network; third, complexation because of the presence of sites in CD and finally ion exchange mechanism due to the presence of carboxylic groups [9]. CDs have ability to form inclusion complexes (microencapsulation) with wide variety of organic and inorganic compounds in its hydrophobic cavity through host-guest interactions to be a stable encapsulation without any covalent bonds [13, 26, 27]. The ability to form complexes makes cyclodextrin have different sorption mechanism from

the other adsorbents. The formation of these complexes has been attributed to weak interactions such as hydrophobic effect which induce the apolar group of a molecule to preferentially enter the CD cavity, Van der Waals interactions, hydrogen bonding between guest molecule and hydroxyl groups at the rim of the cavity (these contributions increase with polar molecules), solvent effects (release of high-energy water), and also steric effects [13, 26, 27]. Among the factors, hydrophobic interactions had been mainly considered as the major factor in complexation.

6.2.5. Desorption and regeneration experiments

Desorption experiment helps to understand adsorption mechanism and possibility of regeneration of the spent adsorbent. In this work, the removal of AB25 from on MNPs coated with CM-β-CD was investigated at the optimum pH 3 with an initial AB25 concentration of 250 mg/L. Before doing desorption study, adsorption equilibrium was carried out. After that, a 5 ml of desorbent were poured into supernatant and desorption equilibrium was performed in another 5 hours. The absorbance of the liquid phase was measured using UV/vis spectrophotometer (Shimadzu UV-1601). The experimental concentrations of the supernatants were obtained through converting the absorbance data to the standard curve of concentration. The percentage of dye desorbed was calculated using equations [3-2] to [3-4]. The result of desorption experiment are tabulated in Table 6-5.

Table 6-5 Percentage of AB25 removed from the CMCD-MNPs adsorbent using different desorbing agents

Desorbing agent	% Removal
Pure Methanol	98.91±1.09 %
Pure Ethanol	99.30±0.70 %
Ethanol 95% (v/v)	99.02±0.98 %
Ethanol 90% (v/v)	99.08±0.92 %
Ethanol 80% (v/v)	91.1±0.64 %
Ethanol 70% (v/v)	87.1±0.59 %
NaOH 0.4M	85±0.44 %
Methanol 95% (v/v)	51.5±0.62 %
Methanol 90% (v/v)	43.8±1.75 %
Methanol 80% (v/v)	28.5±1.05 %
Methanol 70% (v/v)	11.2±0.44 %

To investigate the mechanism of adsorption and recoverability of the adsorbent, several desorbing agents such as alkaline solution and organic solvents were used. Since the adsorption is low at high pH, NaOH 0.4 M is used as desorbing agent. Using this chemical, the amount of AB25 removed from the adsorbent was 85%. Desorption with organic solvents (pure methanol and ethanol) is due to the fact that organic dyes are generally soluble in organic solvents like methanol and ethanol, could remove all dye molecules from adsorbent. The usage of these organic solvents might break the aggregation of the dye and then diffuse into the adsorbent. However, in the case of AB25 removal, ethanol performed better in desorption than methanol. In ethanol-water 90% v/v, all dye molecules could be removed from adsorbent. In addition, because the interaction between the dye molecules and the adsorbent was driven mainly by inclusion complexes, organic solvents such as ethanol could be good candidates as desorbing agents in order to regenerate the adsorbent [116].

Based on the results of desorption study as shown in Table 6-5, the best chemical used for desorbing AB25 was ethanol in water (90% v/v). After that, recovery experiment was carried out because long term stability and recyclability of the adsorbent are important. These factors relate to the cost analysis as the cost of the adsorbent can be minimized if the adsorbent possesses high reproducibility of adsorption and desorption properties. For recycle study, adsorption and desorption experiments are conducted for several cycles. The concentration of the supernatant samples after adsorption and desorption experiments were analyzed, and then the equilibrium adsorption capacity of the dye was calculated. The result of recovery experiment is depicted in Figure 6-11.

Figure 6-11 shows the performance of CMCD-MNPs adsorbent within four cycles. After used for four cycles of adsorption, the adsorption capacity remained almost constant which can be confirmed by the adsorption capacity decreased less than 10% within four cycles of adsorption. This indicates the chemical stability of the adsorbent and reproducibility of the adsorption capacity values.

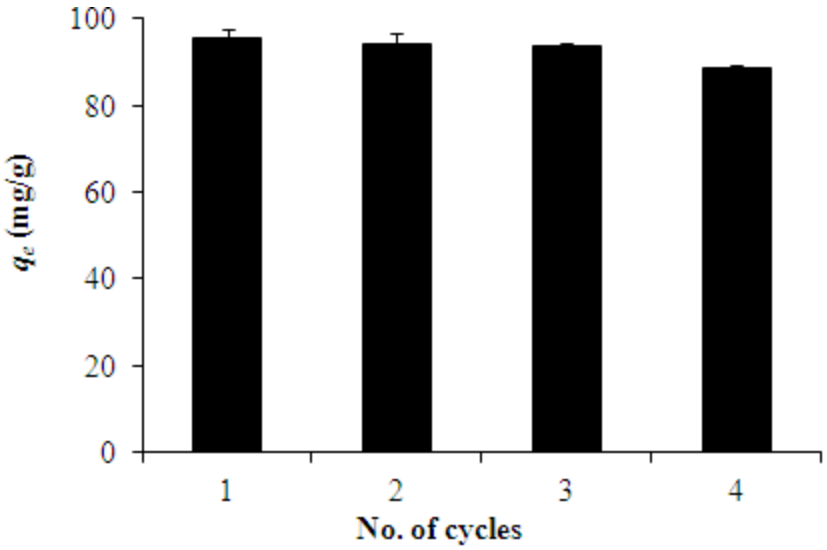

Figure 6-11 Performance of CMCD-MNPs for the adsorption of AB25 after four cycles of regeneration (conditions: initial concentrations = 250 mg/L, adsorbent mass = ~120 mg, pH 3, volume = 10 ml, agitation speed = 200 rpm, temperature 298 K)

The stability of the adsorbent can be seen from the FTIR results obtained from CMCD-MNPs before and after adsorption of AB25, after desorption with ethanol-water 90% and after four times recycled as shown in Figure 6-12 and Table 6-6. After desorption and used for several times, the important peaks of the adsorbent were still in their ranges. This indicates the stability of the adsorbent. However, after being used four times for AB25 adsorption, the performance of the adsorbent decreased that was reflected by their structural changes, which can be seen in Figure 6-12. Moreover, the shifted of the adsorption bands of CMCD-MNPs adsorbent are summarized in Table 6-6.

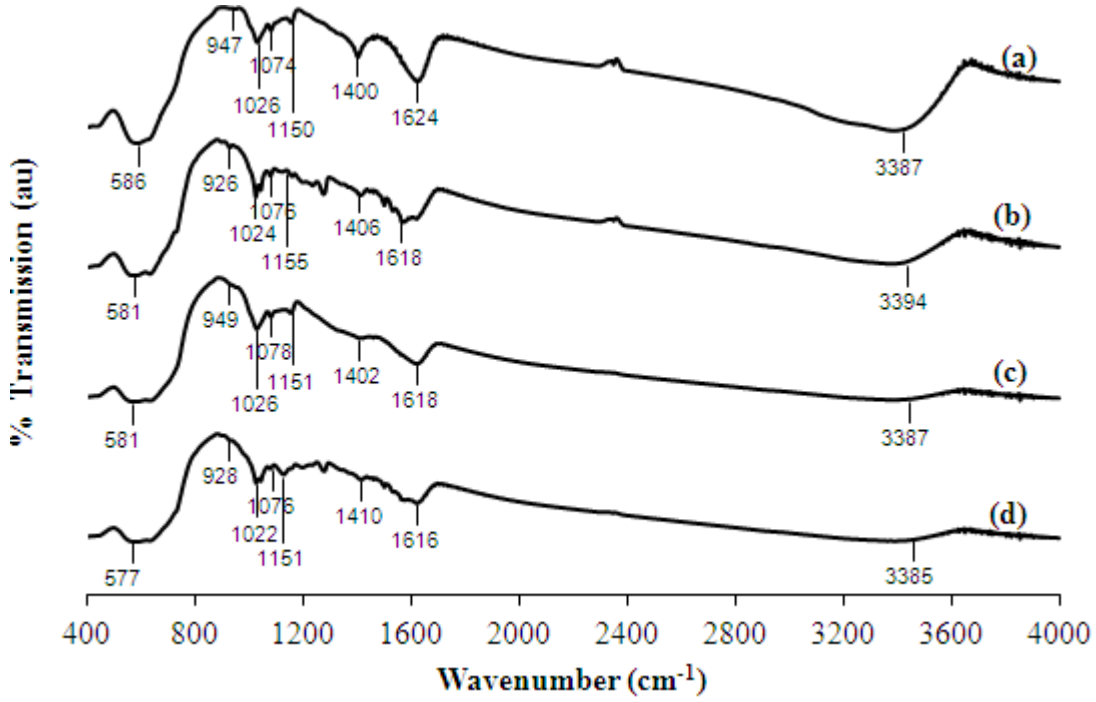

Figure 6-12 FTIR spectra of CMCD-MNPs (a) and (b) before and after AB25 adsorption, (c) after desorption with ethanol in water 90% (v/v) and (d) after four times recycled

Table 6-6 The spectra of CMCD-MNPs before and after AB25 adsorption, after desorption with ethanol-water (90% v/v) and after four times recycled

Characteristic	CMCD-MNPs				
	Before adsorption (cm^{-1})	After adsorption (cm^{-1})	After desorption (cm^{-1})	After recycle (cm^{-1})	Range (cm^{-1}) [2, 88, 111]
Fe-O in the tetrahedral site	586	581	581	577	558-630
-OH stretching vibration	3387	3389	3385	3381	3140-3680
R-1,4-bond skeleton vibration of β-CD	947	926	949	928	940-950
Antisymmetric glycosidic ν_a (C-O-C) vibrations	1026	1024	1026	1022	960-1200
Coupled ν (C-C/C-O) stretching vibrations	1150	1155	1151	1151	
COOM (M=metal) (the COOH groups of CM-β-CD were reacted with OH groups of Fe_3O_4 to form iron carboxylates	1400 and 1624	1406 and 1618	1402 and 1618	1410 and 1616	~1400 and ~1620

6.3. Conclusions

Results from experiments show that CMCD-MNPs can also be used for removal an acid dye, AB25. Similar to the cationic dye, the adsorption was carried out at different pHs and temperatures. The adsorption is controlled by electrostatic interaction between negatively surface charged of AB25 and positively charged of the adsorbent. It was found that the maximum adsorption capacity was obtained at pH 3. At various temperatures ranging from 298 to 328 K, room temperature (298 K) performs better adsorption. Langmuir isotherm model can represent well the adsorption equilibrium of AB25 using uncoated and CMCD-MNPs, whereas Ho and McKay pseudo-second-order kinetic model can describe well the kinetic adsorption data of AB25 using CMCD-MNPs. The binding mechanism of the dye on the adsorbent was also investigated by FTIR. The adsorption using adsorbent based on CDs exhibits different mechanism from other adsorbents as CDs are able to form complexes. In general, the adsorption mechanisms can be briefly summarized as first, surface adsorption (physical adsorption and hydrogen bonding); second, diffusion into the polymer network; third, complexation because of the presence of sites in CD and finally ion exchange mechanism due to the presence of carboxylic groups. Desorption of AB25 from the surface of CMCD-MNPs adsorbent were observed using various chemicals such as organic solvents like methanol and ethanol, and alkaline solutions. It is found that ethanol in water (90% v/v) is the best desorbing agent. In addition, recovery experiment shows that CMCD-MNPs adsorbent can be reused for four times AB25 adsorption with a little decrease of its performance which is also strengthened by the structural changes of CMCD-MNPs investigated with FTIR. Therefore, associated with decolorization process, nano-sized magnetic particles can be

very helpful since they can be easily modified with CM-β-CD to yield biocompatible adsorbent and provide the scalable, versatile and efficient separation of dyes from either diluted or concentrated aqueous solutions.

Chapter 7 Conclusions and Recommendations

The application of carboxymethyl-beta-cyclodextrin (CM-β-CD) coated on magnetic nanoparticles for the separation of anionic and cationic dyes from aqueous solution was studied in this thesis. The findings are presented as the characterizations of uncoated (bare MNPs) and CM-β-CD grafted on magnetic nanoparticles (CMCD-MNPs); adsorption, desorption and recovery experiments of Rhodamine B and Acid Blue 25 on CMCD-MNPs then compare the results with uncoated MNPs. All results are presented in three separated chapters. The conclusions for dye removal using magnetic nano-sized particles are summarized in sequence below. At the end of this chapter, the limitations of this work are discussed and some recommendations for future work are proposed.

7.1. Conclusions

Based on this project, the following conclusions can be drawn:

The first part of this experiment associates with synthesis and characterizations of magnetic nano-sized particles, bare and grafted with CM-β-CD. Nano-sized magnetic particles were successfully prepared via chemical precipitation method using Fe^{2+} and Fe^{3+} salts by maintaining a molar ratio of Fe^{2+} and Fe^{3+} at 1 to 2, under alkaline condition, rigorous mechanical stirring and inert environment through passing N_2 bubbling. With suitable mechanisms, the surfaces of MNPs were successfully functionalized with CM-β-CD. After preparing MNPs, characterization of their physical, chemical and magnetic properties were performed. XRD patterns indicated that the composition of magnetic particle is Fe_3O_4 with spinel structure showed by the characteristic peaks at 2θ of 30.1^0,

35.6^0, 43.3^0, 53.3^0, 57.1^0 and 62.9^0. Moreover, after surface functionalization with CM-β-CD, no other peak was detected proving that there was no impurities related and the phase of Fe_3O_4 did not change after coating. FTIR spectra showed that adsorption bands at 1620 and 1400 cm^{-1} are attributed to COOM (M is metal ions) groups which indicates that there was a reaction between COOH groups of CM-β-CD and OH groups of Fe_3O_4 to form iron-carboxylates. The FTIR analysis also agreed with XPS results. Based on the XPS results, the intensities of C1s were increased from 8,020 to 12,230 cps and so were those of O1s, from 27,880 to 36,170 cps; they are attributed to the attachment of carboxyl and hydroxyl groups to the metal ion. The TGA analysis showed that 13% of CM-β-CD grafted on the surface of MNPs confirmed by a sharp decrease in weight when the sample was heated from 20 to 700^0C. VSM results revealed that the prepared magnetic particles exhibit superparamagnetic property with the saturation magnetization values (Ms) of bare and CMCD coated MNPs were 75 emu g^{-1} and 54 emu g^{-1}, respectively. The existence of non-magnetic materials (CM-β-CD layer) on the surface of magnetic nanoparticles causes a formation of non-magnetic shell and thus decreases the saturation magnetization value. Zeta potential results also demonstrated that the value of isoelectric points shifted from 6.7 to 4.2 after coating process due to introduction of several functional groups containing oxygen. Thus surface coating of CM-β-CD onto the nano-sized magnetic particles adsorbent was successful. The size of the magnetic particles was measured with TEM and XRD analysis. TEM results showed that the synthesized magnetic particles were in nano-scale, with average diameters of about 10 nm and 11 nm for uncoated and CM-β-CD coated magnetic particles, respectively. The mean diameters calculated from XRD using Debye–Scherrer's equation also confirmed TEM results, 10 and 10.5 nm for

bare and CM-β-CD coated magnetic particles, respectively. The findings demonstrate that that the surface modification process did not result in aggregation and change in size of the nanoparticles, and also show that the magnetic particles with size less than 30 nm will exhibit superparamagnetism.

The application of CM-β-CD grafted on magnetic nano-sized particles for adsorption and desorption of Rhodamine B was studied. At room temperature (298 K), the performance of CMCD-MNPs was compared to uncoated ones. The adsorbent recovery study on CMCD-MNPs was also carried out. It was found that the adsorption of RhB onto CMCD-MNPs depends on pH and temperature. The maximum adsorption occurred at pH 5 since at neutral pHs (5 to 8), RhB molecules exist in zwitterionic/dimeric forms. Furthermore, the adsorption was better at room temperature because at higher temperature, the solubility of dye increases. Therefore, RhB molecules will attach to aqueous phase stronger than to solid adsorbent. Adsorption equilibrium data of RhB adsorbend on uncoated and CM-β-CD modified onto MNPs were represented well with Langmuir isotherm model, while the experimental kinetic data of the adsorption of RhB with CMCD-MNPs were fitted well with the Ho and McKay model (pseudo-second-order kinetic model). The adsorption mechanism of RhB molecules to the adsorbent was also confirmed by FTIR analysis showing that there were several important peaks which correspond to RhB attachment. Desorption was investigated using chemicals such as organic solvents, organic acid in methanol, acidic and alkaline solutions. Desorption study shows that pure methanol is the best desorbent. The changes of the important peaks of CMCD-MNPs after used three times for adsorption experiment were analyzed using

FTIR. The experimental results showed that after three cycles used as an adsorbent, CMCD-MNPs still exhibit stability and reproducibility of the adsorption capacity values which is confirmed by less decrease of its performance after the three cycles of adsorption as well as slight changes of their important peaks. However, the changes of their peaks were still in the range.

The CMCD-MNPs were further used to separate another type of dye, anionic dye. Acid Blue 25 was chosen as a model of guest solute. The uptake of AB25 is governed by electrostatic interactions between dye and adsorbent. Similar to RhB adsorption, the adsorption of AB25 is also pH and temperature dependant. Maximum amount of AB25 was adsorbed at pH 3 and room temperature. Moreover, Langmuir isotherm model can represent well the adsorption equilibrium of AB25 using uncoated and CM-β-CD coated on MNPs, whereas Ho and McKay pseudo-second-order kinetic model can describe well the kinetic data of AB25 adsorption using CMCD-MNPs. Desorption was studied using various desorbing agents like organic solvents and alkaline solution. The results shows that ethanol in water 90% (v/v) could remove all dye molecules from CMCD-MNPs adsorbent. The adsorbent can be reused for four times adsorption which indicates the stability of CMCD-MNPs. The attachment mechanism of AB25 to the adsorbent and the structural changes after desorption and recovery experiments were investigated by FTIR analysis.

In summary, magnetic nanoparticles prepared by chemical precipitation method are a promising tool for separation of dye contaminants in aqueous solution as they can be

synthesized easily and cost-effectively. Surface modification of magnetic nano-sized particles with CM-β-CD enhances colloidal stability, morphology and functionality. Nano-sized magnetic particles exhibit a large specific surface area to unit volume ratio, superparamagnetism, as well as unique physical and chemical properties. Furthermore, the results of adsorption, desorption and recovery experiments using CMCD-MNPs show that the adsorbent can be highly attractive used in many adsorptive separations of organic and biomolecules such as cationic and anionic dyes.

7.2. Limitations

The applications of CM-β-CD coated on nano-sized magnetic particles still have several limitations. First, beta-cyclodextrin particularly lacks mechanical strength and it may require cross-linking agents to increase resistance. Second, in general, iron oxides are stable in alkaline environment. They are prone to oxidation and dissolution under acidic conditions. As shown in the previous reaction, in acidic condition, Fe_3O_4 is not stable and will decompose to maghemite (Fe_2O_3 that is stable in acidic environment). Third, coating CM-β-CDs to MNPs have shown an enhancement compared to uncoated MNPs. However, CM-β-CDs used in the experiments are in normal forms (not polymer). Polymerization of CM-β-CDs using cross linkers will increase adsorption capacity more than normal ones. And fourth, although CMCD-MNPs are encouraging for dye removal, the experiments performed were batch adsorption system. In batch studies, the adsorption occurring at the solid/liquid interface causes a change in the concentration of the liquid solution. Adsorption data are obtained through measuring the concentration of adsorbate in the supernatant before and after adsorption, at predetermined adsorption parameters. In

general, batch operations are simple to be designed, operated and adjusted, but they usually required more time to reach equilibrium and to filtrate supernatant.

7.3. Recommendations for future work

This study has introduced a way to separate dye pollutants using surface modification of nano-sized magnetic particles and a comparison between bare and coated magnetic nanoparticles in term of the maximum amount of the dyes adsorbed by the two adsorbents. The advantage of using such method is that CMCD-MNPs are comparable to adsorb two different classes of dyes (anionic and cationic dyes) to other adsorbents, and coating the surface of MNPs increases their adsorption capacities. However, it should be noted that there are some limitations which show the need to develop further works, for instance:

1. The adsorption capacity can be greater if CM-β-CD polymers are used.

CDs consist of hydrophobic internal cavities which can form complexation with various inorganic and organic molecules, and hydrophilic surfaces with primary and secondary hydroxyl groups. The hydroxyl groups are able to form cross linking with coupling agents or cross linkers such as epichlorohydrin (EPI) and 3-aminpropyltriethoxysilane (APTES). Polymerization of CM-β-CD will increase adsorption capacity as many more CM-β-CD will be attached on iron oxides nanoparticles.

2. Results from experiments are based on batch adsorptions so it is required to design continuous separation system for wastewater treatment using magnetic separation.

Continuous separation can minimize time required for the adsorbent and aqueous phase to reach substantial equilibrium as well as time for filtration process. Moreover, for larger scale, the equipments such as agitated tanks and filter presses are also costly. Some recent developments in continuous magnetic separation system for wastewater treatment and environmental protection have been explored for removal heavy metals from steel mill wastewater by Hartikainen et al. [124]; and continuous High Gradient Magnetic Separation (HGMS) for removing soluble organics in water and treating composite wastewater from a food processing unit by Petruska and Perumpral [125].

3. This separations used two different classes of dye, so it is required to extend the applications of the adsorbent with more dyes as well as combinations between organic and inorganic contaminants

Further work with other types of dyes should be carried out to draw general conclusion and give deeper comprehension. Moreover, since this study was focused on single system, it is suggested to combine contaminants such as dye and organic pollutants or dye and inorganic pollutants, in order to make resemble to real wastewater. After that, an analytical comparison of enhancement in surface functionalization of MNPs is evaluated.

4. In preparation, synthesis and surface modification of magnetic nano-sized particles, conventional chemicals were used.

To reduce the toxic effects of chemical used, it is required to observe other friendly strategies for MNPs production such as biological routes with magneto-tactic bacteria as explored by Dunin-Borkowski et al. and Pan et al. [126,127] or the use of green solvents for synthesis MNPs as developed by Cao and Zhu, and Wang et al. [128,129]. These

alternative techniques provide low environmental impact compared to those with conventional solvents.

5. *In this work, a fixed quantity of CM-β-CD has been established for coating on the surfaces of MNPs.*

Study on the optimization of the concentration of CM-β-CD is required to obtain maximum efficiency in dye separation using MNPs modified with CM-β-CD.

References

[1] X. Zhao, J. Wang, F. Wu, T. Wang, Y. Cai, Y. Shi, G. Jiang, Removal of fluoride from aqueous media by Fe_3O_4@$Al(OH)_3$ magnetic nanoparticles, J. Hazard Mater. 179 (2010) 102-109.

[2] A.Z.M. Badruddoza, Goh Si Si Hazel, K. Hidajat, M.S. Uddin, Synthesis of carboxymethyl-β-cyclodextrin conjugated magnetic nano-adsorbent for removal of methylene blue, Colloids Surfaces A 367 (2010) 85-95.

[3] S.Y. Mak, D.H. Chen, Fast adsorption of methylene blue on polyacrylic acid-bound iron oxide magnetic nanoparticles, Dyes Pigments 61 (2004) 93-98.

[4] I. Safarik, M. Safarikova, Magnetic nanoparticles and biosciences, Monatsh Chem. 133 (2002) 737-759.

[5] Z.G. Peng, Separation of organic and biomolecules using nano-sized magnetic particles, Doctor of Phylosophy Thesis, NUS (2004).

[6] N. Shamim, L. Hong, K. Hidajat and M.S. Uddin, Thermosensitive polymer coated nanomagnetic particles for separation of bio-molecules, Sep. Purif. Technol. 53 (2007) 164-170.

[7] L.C.A. Oliveira, D.I. Petkowicz, A. Smaniotto, S.B.C. Pergher, Magnetic zeolites: a new adsorbent for removal of metallic contaminants from water, Water Res. 38 (2004) 3699-3704.

[8] L.C.A. Oliveira, R.V.R.A. Rios, J.D. Fabris, V. Garg, K. Sapag, R.M. Lago, Activated/carbon iron oxide magnetic composites for the adsorption of contaminants in water, Carbon 40 (2002) 2177-2183.

[9] G. Crini, Kinetic and equilibrium studies on removal of cationic dyes from aqueous solution by adsorption onto a cyclodextrin polymer, Dyes Pigments 77 (2008) 415-426.

[10] G. Crini, P.M. Badot, Application of chitosan, a natural aminopolysaccharide, for dye removal from aqueous solutions by adsorption processes using batch studies: A review of recent literature, Prog. Polym. Sci. 33 (2008) 399-447.

[11] G. Crini, H.N. Peindy, Adsorption of C.I. Basic blue 9 on cyclodextrin-based material containing carboxylic groups, Dyes Pigments 70 (2006) 204-211.

[12] J. Szejtli, Past, Present and Future of cyclodextrin research, Pure Appl. Chem. 76 (2004) 1825-1845.

[13] J. Szejtli, Introduction and General Overview of Cyclodextrin Chemistry, Chem. Rev. 98 (1998) 1743-1754.

[14] E.M. Martin Del Valle, Cyclodextrins and their uses: a review, Process Biochem. 39 (2004) 1033-1046.

[15] A.Z.M. Badruddoza, A.S.H. Tay, P.Y. Tan, K. Hidajat, M.S. Uddin, Carboxymethyl-beta-cyclodextrin conjugated magnetic nanoparticles as nano-adsorbents for removal of copper ions: Synthesis and adsorption studies, J. Hazard. Mater. 185 (2011) 1177-1186.

[16] G. Crini, H.N. Peindy, F. Gimbert, C. Robert, Removal of C.I. Basic Green 4 (Malachite Green) from aqueous solutions by adsorption using cyclodextrin-based adsorbent: kinetic and equilibrium studies, Sep. Purif. Technol. 53 (2007) 97-110.

[17] B.A. Veen, J.C.M. Uitdehaag, B.W. Dijkstra, L. Dijkhuizen, Engineering of cyclodextrin glycosyltransferase reaction and product specificity, Biochim. Biophys. Acta 1543 (2000) 336-360.

[18] G. Sudipa, A.Z.M. Badruddoza, M.S. Uddin, K. Hidajat, Adsorption of chiral aromatic amino acids onto carboxymethyl-β-cyclodextrin bonded Fe_3O_4/SiO_2 core-shell nanoparticles, J. Colloid Interface Sci. 354 (2011) 483-492.

[19] R. Azman, Use of Nano-Magnetic Particles for Wastewater Treatment, Final year thesis for the degree of Bachelor of Technology Programme, Department of Chemical and Biomolecular Engineering, NUS (2011).

[20] Y. Ji, X. Liu, M. Guan, C. Zhao, H. Huang, H. Zhang, C. Wang, Preparation of functionalized magnetic nanoparticulate sorbents for rapid extraction of biphenolic pollutants from environmental samples, J. Sep. Sci. 32 (2009) 2139-2145.

[21] J.H.P. Watson, D.C. Ellwood, Biomagnetic Separation and Extraction Process for Heavy-Metals from Solution, Miner. Eng. 7 (1994) 1017-1028.

[22] S. Arivoli, M. Thenkuzhali, Kinetic, Mechanistic, Thermodynamic and Equilibrium Studies on the Adsorption of Rhodamine B by Acid Activated Low Cost Carbon, E-J. Chem. 5 (2008) 187-200.

[23] Y.P. Guo, J.Z. Zhao, H. Zhang, S.F. Yang, Z.C. Wang, H.D. Xu, Use of rice husk-based porous carbon for adsorption of Rhodamine B from aqueous solutions, Dyes Pigments 66 (2005) 123-128.

[24] F. Renault, M.C. Nadia, F. Gimbert, P.M. Badot, G. Crini, Cationized starch-based material as a new ion-exchanger adsorbent for the removal of C.I. Acid Blue 25 from aqueous solutions, Bioresour. Technol. 99 (2008) 7573-7586.

[25] M. Auta, B.H. Hameed, Preparation of waste tea activated carbon using potassium acetate as an activating agent for adsorption of Acid Blue 25 dye, Chem. Eng. J. 171 (2011) 502-509.

[26] G. Crini, M. Morcellet, Synthesis and applications of adsorbents containing cyclodextrins, J. Sep. Sci. 25 (2002) 789-813.

[27] G. Mocanu, D. Vizitiu, A. Carpov, Cyclodextrin polymers, J. Bioact. Compat. Pol. 16 (2001) 315-342.

[28] S. Lewin, Displacement of water and its control of biochemical reactions, London, New York Acad. Press 367 (1974).

[29] A.B. Ellis, M.J. Geselbracht, B.J. Johnson, G.C. Lisensky, W.R. Robinson, Teaching General Chemistry: A Materials Science Companion, Am. Chem. Soc., Washington, DC (1993).

[30] I. Safarik, M. Safarikova, Magnetic particles for egg research. In: Bioactive egg compounds, characterization and application (R. Huopalahti, R. Lopez-Fandino, M. Anton, R. Schade, Eds.), Springer-Verlag (2007) 275-285.

[31] R.M. Cornell, U. Schwertmann, The iron oxide: Structure, Properties, Reaction, Occurrences and use, Wiley-VCH gmbh & Co. Kgaa, 2nd edition (2003) 694.

[32] T.K.T. Nguyen, Surface functionalization of nano-magnetic particle with beta cyclodextrin and its use In bio-molecule refolding process, M.Eng Thesis, NUS (2007).

[33] U.O. Häfeli, W. Schütt, J. Teller, et al. (Eds), Scientific and Clinical Applications of magnetic Cariers, New York (1997).

[34] B. Li, D. Jia, Y. Zhou, Q. Hu, W. Cai, In situ hybridization to chitosan magnetite nanocomposite induced by the magnetic field, J. Magn. Magn. Mater. 306 (2006) 223-227.

[35] B.M. Moskowitz, The Hitchhiker's Guide to Magnetism, Environmental Magnetism Workshop at the Institute for Rock Magnetism (1991).

[36] U. Schwertmann, R.M. Cornell, Iron oxides in the laboratory: Preparation and characterization, Weinheim, Cambridge, VCH (1991).

[37] G.H. Kwei, R.B. Von Dreele, A. Williams, J.A. Goldstone, A.C. Lawson II, W.K. Warburton, Structure and valence from complementary anomalous X-ray and neutron powder diffraction, J. Mol. Struct. 223 (1990) 383-406.

[38] E. Blums, A. Cebers, M.M. Maiorov, Magnetic fluids, Berlin: Walter de Gruyter (1996) 416.

[39] Z. Ma, H. Liu, Synthesis and surface modification of magnetic particles for application in biotechnology and biomedicine, China Particuology 5 (2007) 1-10.

[40] I.I. Yaacob, A.C. Nunes, A. Bose, D.O. Shah, Synthesis and characterization of magnetic nanoparticles in spontaneously generated vesicles, J. Colloid Interface Sci. 168 (1994) 289-301.

[41] S.E. Khalafalla, G.W. Reimers, Preparation of dilution-stable aqueous magnetic fluids, IEEE Trans. Magn. 16 (1980) 178-183.

[42] W.C. Elmore, Ferromagnetic Colloid for Studying Magnetic Structures, J. Phys. Rev. 54 (1938) 309-310.

[43] N. Shamim, Thermosensitive Nanomagnetic Particles for Bio-Separation, Doctor of Phylosophy Thesis, NUS (2007).

[44] M.A. Lopez-Quintela, J. Rivas, Chemical reactions in microemulsions: A powerful method to obtain ultrafine particles, J. Colloid Interface Sci. 158 (1993) 446-451.

[45] J. Rockenberger, E.C. Scher, A.P. Alivisatos, A new nonhydrolytic single-precursor approach to surfactant-capped nanocrystals of transition metal oxides, J. Am. Chem. Soc. 121 (1999) 11595-11596.

[46] A.K. Gupta, M. Gupta, Synthesis and surface engineering of iron oxide nanoparticles for biomedical applications, Biomaterials 26 (2005) 3995-4021.

[47] A.M.G.C. Dias, A. Hussain, A.S. Marcos, A.C.A. Roque, A biotechnological perspective on the application of iron oxide magnetic colloids modified with polysaccharides, Biotechnol. Adv. 29 (2011) 142-155.

[48] M. Takafuji, S. Ide, H. Ihara, Z. Xu, Preparation of poly(1-vinylimidazole)-grafted magnetic nanoparticles and their application for removal of metal ions, J. Mater. Chem. 16 (2004) 1977-1983.

[49] C. Fang, M. Zhang, Multifunctional magnetic nanoparticles for medical imaging applications, J. Mater. Chem. 19 (2009) 6258-6266.

[50] L. Laconte, N. Nitin, G. Bao, Magnetic nanoparticle probes, Nanotoday 3 (2005) 32-38.

[51] E. Eren, Removal of lead ions by Unye (Turkey) bentonite in iron and magnesium oxide-coated forms, J. Hazard. Mater. 165 (2009) 63-70.

[52] A.A. Atia, A.M. Donia, W.A. Al-Amrani, Adsorption/desorption behavior of acid orange 10 on magnetic silica modified with amine groups, Chem. Eng. J. 150 (1) (2009) 55-62.

[53] S.R. Shirsath, A.P. Hage, M. Zhou, S.H. Sonawane, M. Ashokkumar, Ultrasound assisted preparation of nanoclay Bentonite-FeCo nanocomposite hybrid hydrogel: A potential responsive sorbent for removal of organic pollutant from water, Desalination 281 (2011) 429-437.

[54] S. Qu, F. Huang, S. Yu, G. Chen, J. Kong, Magnetic removal of dyes from aqueous solution using multi-walled carbon nanotubes filled with Fe_2O_3 particles, J. Hazard. Mater. 160 (2008) 643-647.

[55] A. Afkhami, M.S. Tehrani, H. Bagheri, Modified maghemite nanoparticles as an efficient adsorbent for removing some cationic dyes from aqueous solution, Desalination 263 (2010) 240-248.

[56] A.R. Mahdavian, M.A.S. Mirrahimi, Efficient separation of heavy metal cations by anchoring polyacrylic acid on superparamagnetic magnetite nanoparticles through surface modification, Chem. Eng. J. 159 (2010) 264-271

[57] G.D. Moeser, K.A. Roach, W.H. Green, P.E. Laibinis, T.A. Hatton, Water based magnetic fluids as extractants for synthetic organic compounds, Ind. Eng. Chem. Res. 41 (2002) 4739-4749.

[58] B.S. Inbaraj, B.H. Chen, Dye adsorption characteristics of magnetite nanoparticles coated with a biopolymer poly(γ-glutamic acid), Bioresour. Technol. 102 (2011) 8868-8876.

[59] H.Y. Zhu, R. Jiang, L. Xiao, W. Li, A novel magnetically separable γ-Fe_2O_3/crosslinked chitosan adsorbent: Preparation, characterization and adsorption application for removal of hazardous azo dye, J. Hazard. Mater. 179 (2010) 251-257.

[60] D.H. Kim, K.N. Kim, K.M. Kim, Y.K. Lee, Targeting to carcinoma cells with chitosan- and starch-coated magnetic nanoparticles for magnetic hyperthermia, J. Biomed. Mater. Res. A. 88 (2008) 1-11.

[61] A. Kaushik, R. Khan, P.R. Solanki, P. Pandey, J. Alam, S. Ahmad, Iron oxide nanoparticles-chitosan composite based glucose biosensor, Biosens. Bioelectron. 24 (2008) 676-683.

[62] I. Safarik, M. Safarikova, Magnetic nano- and microparticles in biotechnology, Chem. Pap. 5 (2009) 497-505.

[63] Q. Peng, Y. Liu, G. Zeng, W. Xu, C. Yang, J. Zhang, Biosorption of copper (II) by immobilizing Saccharomyces cerevisiae on the surface of chitosan-coated magnetic nanoparticles from aqueous solution, J. Hazard. Mater. 177 (2010) 676-682.

[64] A. Zouboulis, I.A. Katsoyannis, Arsenic removal using iron oxide loaded alginate beads, Ind. Eng. Chem. Res. 41 (2002) 6149-6155.

[65] E.N.E. Qada, S.J. Allen, G.M. Walker, Adsorption of basic dyes from aqueous polution onto activated carbons, Chem. Eng. J. 135 (2008) 174-184.

[66] R.D. Ambashta, M. Sillanpää, Water purification using magnetic assistance: a review, J. Hazard. Mater. 180 (2010) 38-49.

[67] C. Shen, Y. Shen, Y. Wen, H. Wang, W. Liu, Fast and highly efficient removal of dyes under alkaline conditions using magnetic chitosan-Fe (III) hydrogel, Water Res. 45 (2011) 5200-5210.

[68] L. Liu, Q.X. Guo, The Driving Forces in the Inclusion Complexation of Cyclodextrins, J. Incl. Phenom. Macrocycl. Chem. 42 (2002) 1-14.

[69] J. Szejtli and T. Osa (Eds.), Comprehensive Supramolecular Chemistry, Vol. 3: Cyclodextrins, Pergamon, Oxford (1996) 693.

[70] S.V. Jorgensen, Environmental management in the 21st century, Environ. Sci. Technol. 33 (1999) 376-379.

[71] G. McKay, Adsorption of dyestuffs from aqueous solutions with activated carbon. Part I. Equilibrium and batch contact-time studies, J. Chem. Technol. Biotechnol. 32 (1982) 759-772.

[72] X. Wang, M. Song, Y.C. Long, Synthesis, Characterization, and Crystal Structure of the Lactone Form of Rhodamine B, J. Solid State Chem. 156 (2001) 325-330.

[73] P. Suwannawong, S. Khammuang, R. Sarnthima, Decolorization of Rhodamine B and congo red by partial purified laccase from Lentinus polychrous Lév, J. Biochem. Technol. 3(2) (2010) 182-186.

[74] M.H.G. Hamdi, A. Ashraf, El-Sayed, Activated carbon from agricultural by-products for the removal of Rhodamine-B from aqueous solution, J. Hazard. Mater. 168 (2009) 1070-1081.

[75] I. Bouzaida, C. Ferronato, J.M. Chovelon, M.E. Rammah, J.M. Herrmann, Heterogeneous photocatalytic degradation of the anthraquinonic dye, Acid Blue 25 (AB25): a kinetic approach, J. Photoch. Photobio. A: Chemistry 168 (2004) 23-30.

[76] H. Ghodbane, O. Hamdaoui, Decolorization of antraquinonic dye, C.I. Acid Blue 25, in aqueous solution by direct UV irradiation, UV/H_2O_2 and UV/Fe(II) processes, Chem. Eng. J. 160 (2010) 226-231.

[77] L.E. Sendelbach, A review of the toxicity and carcinogenicity of anthraquinone derivatives, Toxicology 57 (1989) 227-240.

[78] O. Redlich, D.L. Peterson, A useful adsorption isotherm, J. Phys. Chem. 63 (1959) 1024-1026.

[79] T. Weber, R. Chakravorti, Pore and solid diffusion models for fixed bed adsorbent. J. Am. Inst. Chem. Eng. 2 (1974) 228-238.

[80] J. Wu, H.Q. Yu, Biosorption of 2,4-dichlorophenol from aqueous solution by Phanerochaete chrysosporium biomass: isotherms, kinetics and thermodynamics, J. Hazard. Mater. 137 (2006) 498-508.

[81] Y.S. Ho, G. McKay, A comparison of chemisorption kinetic models applied to pollutant removal on various sorbents, Process Saf. Environ. 76 (1998) 332-340.

[82] Y. Ho, G. McKay, Pseudo-second order model for sorption processes, Process Biochem. 34 (1999) 451-465.

[83] A. Wooding, M. Kilner, D.B. Lambrick, Studies of the double surfactant layer stabilization of water-based magnetic fluids, J. Colloid Interface Sci. 144 (1991) 236-242.

[84] L.F. Shen, P.E. Laibinis and T.A. Hatton, Bilayer surfactant stabilized magnetic fluids: Synthesis and interactions at interfaces, Langmuir 15 (1999) 447-453.

[85] K. Kumar, S. Sivanesan, Comparison of linear and non-linear method in estimation the sorption isotherm parameters for safranin onto activated carbon, J. Hazard. Mater. B. 123 (2006) 288-292.

[86] V.H. Montoya, D.I.M. Castillo, A.B. Petriciolet, M.A.M. Moran, M.A.P. Cruz, Role of the pericarp of Carya illinoinensis as biosorbent and as precursor of activated carbon for the removal of lead and acid blue 25 in aqueous solutions, J. Anal. Appl. Pyrol. 92 (2011) 143-151.

[87] J. Popplewell, L. Sakhnini, The Dependence of the Physical and Magnetic-Properties of Magnetic Fluids on Particle-Size, J. Magn. Magn. Mater. 149 (1995) 72-78.

[89] W. Zhang, L. Zhuang, H. Shen, M. Xie, Z. Hu, H. He, Controlled synthesis and properties of carboxymethyl chitosan-bound magnetic nanoparticles, J. Sci. Conf. Proc. 1 (2009) 211-214

[89] Z.G. Peng, K. Hidajat, M.S. Uddin, Extraction of 2-Hydroxyphenol by Surfactant Coated Nanosized Magnetic Particles, Korean J. Chem. Eng. 20 (2003) 896-901.

[90] V.S. Zaitsev, D.S. Filimonov, I.A. Presnyakov, R.J. Gambino, B. Chu, Physical and chemical properties of magnetite and magnetite-polymer nanoparticles and their colloidal dispersions, J. Colloid Interface Sci. 212 (1999) 49-57.

[91] Z.G. Peng, K. Hidajat, M.S. Uddin, Adsorption and desorption of lysozyme on nano-sized magnetic particles and its conformational changes, Colloids Surface B 35 (2004) 169-174.

[92] N. Shamim, L. Hong, K. Hidajat, M.S. Uddin, Thermosensitive polymer (N-isopropylacrylamide) coated nano magnetic particles: preparation and characterization, Colloids Surface B 55 (2007) 51-58.

[93] B. Smith, T. Koonce, S. Hudson, Decolorizing dye wastewater using chitosan, Am. Dyestuff Rep. 82 (1993) 18-36.

[94] S. Qadri, A. Ganoe, Y. Haik, Removal and recovery of acridine orange from solutions by use of magnetic nanoparticles, J. Hazard. Mater. 169 (1-3) (2009) 318-323.

[95] R. Anliker, G. D¨urig, D. Steinle, E.J. Moriconi, List of colorants to be classified as toxic, JSDC 104 (1988) 223-225.

[96] G. Crini, Non-conventional low-cost adsorbents for dye removal: a review, Bioresour. Technol. 97 (2006) 1061-1085

[97] A.A. Attia, W.E. Rashwan, S.A. Khedr, Capacity of activated carbon in the removal of acid dyes subsequent to its thermal treatment, Dyes Pigments 69 (2006) 128-136.

[98] G. Gupta, S. Shukla, An inexpensive adsorption technique for the treatment of carpet effluents by low cost materials, Adsorpt. Sci. Technol. 13 (1995) 15-26.

[99] A. Ghanadzadeh, M.A. Zanjanchi, R. Tirbandpay, The role of host environment on the aggregative properties of some ionic dye materials, J. Mol. Struct. 616 (1-3) (2002) 167-174.

[100] Z. Aksu, S. Tezer, Equilibrium and kinetic modelling of biosorption of Remazol Black B by Rhizopus arrhizus in a batch system: effect of Temperature, Process Biochem. 36 (2000) 431-439.

[101] L.C. Juang, C.C. Wang, C.K. Lee, Adsorption of basic dyes onto MCM-41, Chemosphere 64 (2006) 1920-1928.

[102] M. Hema, S. Arivoli, Rhodamine B adsorption by activated carbon: Kinetic and equilibrium study, Indian J. Chem. Techn. 16 (2004) 38-45.

[103] P.S. Kunwar, S. Guptaa, K.S. Arun, S. Sinhab, Experimental design and response surface modeling for optimization of Rhodamine B removal from water by magnetic nanocomposite, Chem. Eng. J. 165 (2010) 151-160.

[104] N. Ahalya, T.V. Ramachandra, R.D. Kanamadi, Low cost biosorbents for dye removal, CES Technical Report 113 (2006) 59-110.

[105] G. Annadurai, R.S. Juang, D.J. Lee, Use of cellulose-based wastes for adsorption of dyes from aqueous solutions, J. Hazard. Mater. B. 92 (2002) 263-274.

[106] Sumanjit, T.P.S. Walia, I. Kansal, Removal of Rhodamine-B by Adsorption on Walnut Shell Charcoal, J. Surface Sci. Technol. 24 (2008) 179-193.

[107] K. Kadirvelu, C. Karthika, N. Vennilamani, S. Pattabhi, Activated carbon from industrial solid waste as an adsorbent for the removal of Rhodamine-B from aqueous solution: Kinetic and equilibrium studies, Chemosphere 60 (2005) 1009-1017.

[108] C. Namasivayam and K. Kadirvelu, Coir pith, an agricultural waste by-product for the treatment of dyeing wastewater. Bioresour. Technol. 38 (1994) 79-81.

[109] S. Karagöz, T. Tay, S. Ucar, M. Erdem, Activated carbons from waste biomass by sulfuric acid activation and their use on methylene blue adsorption, Bioresour. Technol. 99 (2008) 6214-6222.

[110] J. Li, W. Ma, P.X. Lei, J.C. Zhao, Detection of intermediates in the TiO_2-assisted photodegradation of Rhodamine B under visible light irradiation, J. Environ. Sci. 19 (2007) 892-896.

[111] D.L. Pavia, G.M. Lampman, G.S. Kriz, Introduction to Spectroscopy (Saunders Golden Sunburst Series) (2000).

[112] O. Egyed, V. Weiszfeiler, Structure determination of copper(II)-β-cyclodextrin complex by Fourier transform infrared spectroscopy, Vib. Spectrosc. 7 (1994) 73-77.

[113] B.S. Inbaraj, N. Sulochana, Use of jackfruit peel carbon (JPC) for adsorption of Rhodamine B, a basic dye from aqueous solution, Indian J. Chem. Techn. 13 (2006) 17-23.

[114] F. Perineau, J. Molinier, A. Gaset, Adsorption of ionic dyes onto charred plant-material, J. Chem. Technol. Biotechnol. 32 (1982) 749–758.

[115] R.C. Ellis, Reagent and Dye Solubility Chart, IHC WORLD, LLC (2003-2011).

[116] G. Crini, Studies on adsorption of dyes on beta-cyclodextrin polymer, Bioresour. Technol. 90 (2003) 193-198.

[117] R. Klimaviciute, A. Riauka, A. Zemaitaitis, The binding of anionic dyes by cross-linked cationic starches, J. Polym. Res. 14 (2007) 67-73.

[118] M.H.V. Baouab, R. Gauthier, H. Gauthier, M.E.B. Rammah, Cationized sawdust as ion exchanger for anionic residual dyes, J. Appl. Polym. Sci. 82 (2001) 31-37.

[119] Bouzaida, M.B. Rammah, Adsorption of acid dyes on treated cotton in a continuous system, Mater. Sci. Eng. C. 21 (2002) 151-155.

[120] A. Kamari, W.S.W. Ngah, L.K. Liew, Chitosan and chemically modified chitosan beads for acid dyes sorption, J. Environ. Sci. 21(2009) 296-302.

[121] F. Delval, G. Crini, N. Morin, J. Vebrel, S. Bertini, G. Torri, The sorption of several types of dye on crosslinked polysaccharides derivatives, Dyes Pigments 53 (2002) 79-92.

[122] B. Martel, M. Devassine, G. Crini, M. Weltrowski, M. Bourdonneau, M. Morcellet, Preparation and sorption properties of a betacyclodextrin-linked chitosan derivative, J. Polym. Sci. Pol. Chem. 39 (2001) 169-176.

[123] F. Ferrero, Dye removal by low cost adsorbents: Hazelnut shells in comparison with wood sawdust, J. Hazard. Mater. 142 (2007) 144-152.

[124] T. Hartikainen, J.P. Nikkanen, R. Mikkonen, Magnetic separation of industrial wastewaters as an environmental application of superconductivity, IEEE Trans. Appl. Supercond. 15 (2) (2005) 2336-2339.

[125] J.A. Petruska, J.V. Perumpral, Magnetic Separation of Soluble Organic Pollutants from Water, Virginia Water Resour. Res. Center, Buletin 108 (1977).

[126] R.E.D. Borkowski, M.R. McCartney, R.B. Frankel, D.A. Bazylinski, M. Posfai, P.R. Buseck, Magnetic Microstructure of Magnetotactic Bacteria by Electron Holography, Science 282 (1998) 1868-1870.

[127] Y. Pan, W. Lin, J. Li, W. Wu, L. Tian, C. Deng et al., Reduced efficiency of magnetotaxis in magnetotactic coccoid bacteria in higher than geomagnetic fields, Biophys. J. 97 (2009) 986-991.

[128] S.W. Cao, Y.J. Zhu, Iron oxide hollow spheres: microwave–hydrothermal ionic liquid preparation, formation mechanism, crystal phase and morphology control and properties, Acta Mater. 57 (2009) 2154-2165.

[129] Y. Wang, S. Maksimuk, R. Shen, H. Yang, Synthesis of iron oxide nanoparticles using a freshly-made or recycled imidazolium-based ionic liquid, Green Chem. 9 (2007) 1051-1056.